Applied Energy 377 (2025) 124645

Contents lists available at ScienceDirect

Applied Energy

journal homepage: www.elsevier.com/locate/apenergy

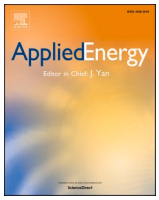

On the importance of degradation modeling for the robust design of hybrid energy systems including renewables and storage

Francesco Superchi [a], Antonis Moustakis [b], George Pechlivanoglou [b], Alessandro Bianchini [a,*]

[a] Università degli Studi di Firenze, Department of Industrial Engineering, Via di Santa Marta 3, 50139 Firenze, Italy
[b] Eunice Energy Group, 29, Vas. Sofias Ave, 10674, Athens, Greece

HIGHLIGHTS

- Stochastic optimization framework to reduce costs in the sizing phase of hybrid energy systems comprising storage devices.
- Innovative simulation method able of accounting for performance degradation in time maintaining low computational cost.
- Complete description of component models for alkaline electrolyzer, PEM fuel cell, Li-Ion battery, and hydrogen compressor.
- In-depth literature and market review to estimate average prices of all considered components.
- Comparison between the proposed method and a simplified one to estimate the error when neglecting the components' degradation.

GRAPHICAL ABSTRACT

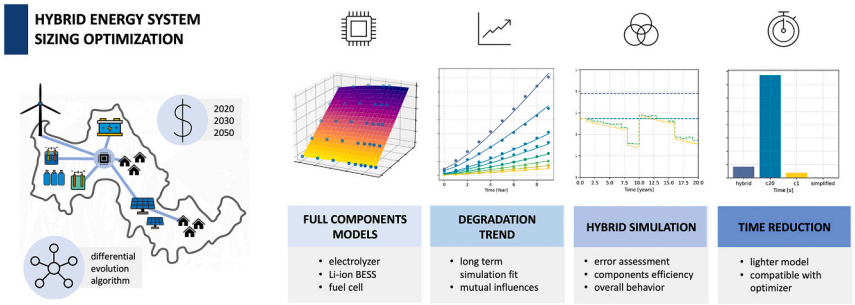

ABSTRACT

Due to additional complexity and computational cost, most of the techno-economic analyses presented to date on hybrid energy systems overlooked the long-term performance decay of components. This study introduces a novel simulation approach that accounts for degradation effects while maintaining a reasonable computational cost, achieving a 88.5 % time reduction in comparison to complete physics-based models, while introducing only a 0.015 % error in estimating long-term impacts. The proposed approach is tested against standard simulation methods using a real-world case study, i.e., the upgrade of the hybrid energy system on the island of Tilos to achieve full energy self-sufficiency through photovoltaic and wind power, supported by a combination of Lithium-Ion batteries and a hydrogen chain (electrolyzer, compressor, tank, and fuel cell). The novel simulation approach was integrated into a stochastic optimization framework aimed at minimizing the cost of supplying the entire energy request from the island. The economic analysis is also supported by an in-depth market review of average prices for RES and storage components. First, and most importantly, the study demonstrates that accounting for components' degradation is an absolute requirement to get robust and sustainable energy systems capable of meeting the long-term demands of renewable energy systems. The proposed approach is shown to perfectly fit this scope. Results on then selected case study indicate that incorporating a hydrogen chain as seasonal storage leads to more cost-effective solutions, reducing the cost by 17.5 %. The comparison with a *simplified* method reveals that ignoring degradation can lead to substantial errors in estimating the energy cost (by an average of 10.2 %) and undersized designs: 103.1 % on average for the electrolyzer, 31.5 % for the H_2 tank, 59.6 % for the battery, and up to 7.7 % for the fuel cell.

* Corresponding author.
E-mail address: alessandro.bianchini@unifi.it (A. Bianchini).

https://doi.org/10.1016/j.apenergy.2024.124645
Received 25 June 2024; Received in revised form 5 September 2024; Accepted 2 October 2024
Available online 25 October 2024

Nomenclature

Symbols

C	Capacity[MWh]
d	Daily damage [−]
D	Damage [−]
E	Energy [kWh]
I	Current [A]
P	Pressure [bar]
r	Interest rate [%]
T	Temperature [°C]
V	Voltage [V]
η	Efficiency [%]
φ	Conversion factor [kg/MWh]
t	Time [s] [min] [year]
m	mass [kg]
c	specific hear [J/kgK]
β	compression ratio [−]
k	ratio of specific heats [−]

Subscripts

1	final value at the end of the first year of operation
avg	average
comp	compressor
el	electrolyzer
eq	equivalent
ext	external
fc	fuel cell
gw	glass wool
id	ideal
int	internal
isen	isentropic
op	operating
spec	specific
t	tank
T_nom	nominal temperature
th	thermoneutral
Thermal,deg	temperature cooling related degradation
time,deg	time related degradation
work	actual working hours

Acronyms

ALK	Alkaline
BESS	Battery Energy Storage System
c1	one-year simulation using complete models of components
c20	twenty-year simulation using complete models of components
CAPEX	Capital expenditures
DOD	Depth Of Discharge
EES	Energy Storage System
EL	Electrolyzer
EOL	End Of Life
FC	Fuel Cell
HES	Hybrid Energy System
HPS	Hybrid Power Station
LCOE	Levelized Cost of Electricity
LCOH	Levelized Cost of Hydrogen
LCORE	Levelized Cost of Required Storage
NIIs	Non-Interconnected Islands
NPV	Net Present Value
O&M	Operation and Maintenance
OPEX	Operating expenditures
P2G2P	Power to Gas to Power
PEM	Proton Exchange Membrane
PV	Photovoltaic
RES	Renewable Energy Sources
SCADA	Supervisory Control And Data Acquisition
SOC	State Of Charge
SOC	State Of Charge
SOEC	Solid Oxide Electrolysis Cell
SOH	State OF Health
SSd	Self-Sufficiency degree
WT	Wind Turbine

1. Introduction

Hybrid energy systems (HESs) can integrate the most promising renewable generation technologies (wind and photovoltaics [1]) with energy storage systems (ESS) to enable the stand-alone operation of fully-decarbonized grids [2]. In this context, lithium-ion batteries are the most common technology for Battery Energy Storage Systems (BESS). In some cases, the mismatch between production and request can be on a seasonal basis. Hydrogen technologies, with the power-to-gas-to-power (P2G2P) or "hydrogen chain" paradigm, are one possibility for addressing this issue. Using an electrolyzer (EL), the power excess from renewables can be converted into green hydrogen (power-to-gas) [3–6]. This green hydrogen can be then converted back to electricity by a fuel cell (FC) when an energy deficit takes place (gas-to-power) [7]. The feasibility and profitability of hydrogen production, especially from renewable sources, were widely investigated in literature in the past years [8–19].

Integrating different RES and different energy storage technologies that involve several separate components can be a complex task and advanced computational methods may be required to define the best combination of generators and storage. Optimization algorithms are suited to fulfill this task: these tools can outline the best strategy to reach a specific target by evaluating the techno-economic outcome of different combinations of components and varying their sizes in defined ranges. To evaluate the outcome of a configuration, the optimization framework must comprehend a simulation framework able to estimate how the system would behave in a certain time frame [20].

The most common cost metrics to evaluate the performance of energy systems are the Net Present Value (NPV) [21–32], the Levelized Cost of Energy (LCOE) [33–40] or Levelized Cost of Storage [41–45]. All of those metrics consider the entire lifetime of the plant to evaluate the overall techno-economic outcome of an energy system (20–25 years on average [46–48]). This long-term horizon means that an optimization framework that aims to minimize those cost metrics should either simulate the system behavior during the entire lifetime or, as it often happens [49], assume that the performance related to a narrower time window can be attributed to the rest of the expected lifetime.

Storage devices and, especially, electrochemical cells (e.g., battery modules, electrolyzer stacks, or fuel cell stacks) are affected by the degradation of their performance over time. This degradation depends on the technology, the size, and the application type and the amount of working hours in a year [50–52]. An accurate assessment of the degradation of components is key for correctly estimating the techno-economic outcome of an energy system: according to the type of usage, a component may last longer or require a premature substitution [53,54]. Consequently, a performance drop in one or more components of an energy system affects not only the overall technical behavior but also maintenance and replacement costs.

Even if often neglected [55–58], techno-economic optimizations that aim to minimize LCOE/LCOS or maximize NPV should consider the

effect of performance decay, since the metric that they aim to optimize is directly influenced by degradation effects [59,60]. If this effect is not considered, results from economic optimizations can be misleading, as shown in Section 4. This study proposes a novel simulation approach, able to account for the long-term performance decay of storage components in HESs, crucial for the correct estimation of cost metrics. The method also aims at maintaining a limited computational cost, making the approach compatible with stochastic optimization algorithms.

1.1. Degradation of performance in sizing optimization of HESs

HESs comprising hydrogen chains are getting increasing attention. In their systematic review of renewable HESs with hydrogen storage, Modu et al. [61] highlighted the recent advancements in the sizing and management of hybrid RES. However, the literature lacks studies that propose methods to optimize the sizing of hybrid systems that consider the actual performance of components. In another review of renewable HESs, Basnet et al. [62] highlighted that only a few research works consider the effect of intermittency on the electrolyzer for the production of hydrogen. Moreover, the performance degradation of electrochemical cells is often neglected and only a few studies tried to address the problem of considering the drop in performance of different components in the sizing optimization of energy systems.

The long-term effect of storage systems degradation on the overall performance of hybrid energy systems has been proven to be a key issue by previous studies. Ceran et al. [63] proposed a novel approach to evaluate the performance of a PV system with H_2 storage including aging. The authors evaluated the long-term performance of case studies using parametric components models for the PV, FC, electrolyzer, and hydrogen tank. They found that the system performance decline is nonlinear since the performance decay of one component affects also the other devices. Results from this study clearly show that not considering aging will generate a significant error in any analysis. Ceran and Orlowska [64] found similar implications of component degradation in a study that considered PV, WT, and fuel cells. Jurasz et al. [65] proved that the reliability of a PV-BESS system should be determined in the long horizon due to the performance decay of the generator and capacity fade of the storage system. The analysis proposed here confirms the potential error caused by neglecting the degradation and presents a way to account for its long-term effect by keeping computational costs limited and compatible with sizing optimization algorithms.

The effect of performance decay has a deep impact also in the management of HESs. Degradation models have been also introduced for the scheduling optimization of energy systems. One possible application is the optimization of system operating conditions of hydrogen technologies. Parhizkar and Hafeznezami [66] proposed a degradation-based model to optimize the operation of a SOFC. Bordin et al. [67] considered the effect of battery degradation in a linear programming approach to optimize the management of off-grid systems. Maluenda et al. [11] included a degradation model in the optimal operation scheduling of a hybrid system involving PV, BESS, and an electrolyzer. Qin et al. [68] proposed an online lifecycle operating costs minimization strategy for fuel cell buses considering power source degradation. The state of health estimation was incorporated into the objective function to reduce battery and fuel cell degradation. Abdelghany et al. [69] proposed a sophisticated hybrid energy storage system dynamic model to optimize the economical schedule of wind-solar microgrids with hybrid energy storage systems considering the effect of degradation. Shen et al. [70] considered degradation for the optimization of a dispatch method for an integrated energy system with hybrid energy storage. The effect of PEM electrolyzer degradation was considered in the device design and implementation by Liu et al. [71]. Concerning control and schedule optimizations of vehicles, Huang et al. [72] proposed the coupling between design and EMS optimization for a hybrid propulsion system including Li-ion batteries and supercapacitors considering the effect of the battery degradation. Fan et al. [73] developed a comprehensive degradation model to accurately calculate the degradation costs of a fuel cell to minimize the operation cost of a ship microgrid. The platinum catalyst degradation in PEM fuel cells was included in the optimal management strategy also by Sheng et al. [74]. He et al. [75] proposed the quantification of fuel cell degradation and a techno-economic analysis for fuel-cell-powered vehicles. In their analysis, the total fuel cell degradation was 3.6 % per vehicle within one year. In [76–79], the degradation effect was also considered to develop health-conscious EMS for fuel-cell hybrid electric vehicles.

Methods used to include the effect of degradation in the management optimization of HESs can be applied also to sizing problems. However, sizing and management problems differ in simulation horizon, computational requirements and many other aspects. This work indeed focuses on sizing optimization problems and robust design of HESs.

To the best of the authors' knowledge, the problem of considering the performance degradation of components in the optimum sizing of renewable HESs was first considered by Erdinc and Uzunogl [55]. These authors multiplied the output power capacity of each hybrid system with a performance degradation constant to provide results from the worst-case scenario.

The BESS is the most considered component in studies that account for storage degradation in the sizing optimization of microgrids. Amni et al. [80] considered capacity degradation and replacement year for the optimal sizing of battery energy storage in a microgrid. They proposed a linear model to use Mixed Integer Linear Programming (MILP) to investigate the long-term effect of the BESS capacity degradation on performance and microgrid total cost. In studies from Terlouw et al. [81] and Shmidt et al. [82], authors included Li-ion battery degradation as a constraint in the analysis of energy systems. Wang et al. [83] optimized the system configuration and working modes of a vehicle-to-micro-grid network considering the battery degradation of electric vehicles. Sufyan et al. [56] tried to reduce the operating cost of isolated microgrids by economic scheduling considering the optimal size of the battery. The authors modeled the real battery operation cost considering the depth of discharge that shortens the lifetime of the BESS. Rehman et al. [84] proposed another MILP optimization for the sizing of battery energy storage and PV systems considering uncertainties and battery degradation. Their modeling approach accounts for the cycle-life degradation of the Li-ion based BESS to ensure that the BESS will not be replaced during the lifetime of the project. Fioriti et al. [85] developed a rainflow-based model of storage degradation to optimize the sizing of residential BESS. They modeled the PV degraded capacity and proposed a multi-year sizing methodology where the complete lifetime of batteries is simulated at a 15-min time resolution until complete degradation. They adopted a three-loop nested methodology, where they simulated the BESS operation in the inner loop, estimated the BESS degradation in the middle loop, and tested multiple BESS configurations in the external loop to select the most profitable one. Shin and Roh [86] proposed a framework for calculating the capacity of the energy storage supplementing PV that considers the effect of the size and operation on battery degradation while maximizing profits. They also introduced an iterative algorithm that finds a solution by accessing battery degradation and optimizing profitability. Liu et al. [87] presented an operating cost model for the sizing of an energy system involving wind and BESS that considers capacity fading. They also proved that the global optimization method of dynamic programming can reduce significantly capacity degradation and operation costs. Mielcarek et al. [49] highlighted the importance of long-term simulations considering the degradation of components when simulating independent systems including PV and BESS. Castillejo-Cuberos et al. [88] proved that assuming a constant battery degradation can result in an underestimation of LCOE. Liu et al. [89] included the annual degradation PV and an electric vehicle BESS in the energy design and optimization for a net-zero energy building. On the other hand, this study considers a more complex system that combines RES generation with P2G2P, other than a BESS. The presence of multiple components makes it mandatory to study the effect that the

degradation of each component has on the average performance of the other components.

Several attempts have been made to include the effect of storage degradation in sizing and management optimization of hybrid power trains: fuel cells and BESS combinations have indeed a wide application range for vehicles and the transportation sector. The degradation effect on hybrid Li-ion and PEMFC has been explored by works from Dall'Armi et al. [90,91] and Pivetta et al. [92]. The authors proposed a multi-objective optimization aiming at minimizing PEMFC degradation while reaching other techno-economic objectives. Results have shown that, due to this inclusion in the objective function, is possible to reduce degradation by up to 65 %, highlighting the importance of including the degradation factor. Those studies aim at solving MILP problems, thus using linearized models of components. The effect of degradation was included in other studies that propose MILP optimization with linearized component models. One example is a study by Zhang et al. [93] that included degradation costs for batteries and fuel cells in a MILP optimization problem to identify the optimal fuel alternative for a ship. Differently, the current study proposes a method to extrapolate the long-term evolution of average performance indicators starting from a one-year simulation that may use also non-linear components models. Moreover, this study focuses on the introduction of a hydrogen chain for stationary applications in which daily cycles, typical of transport applications, are much less dominant. The selected case study shows results related to an application in which hydrogen works mainly as seasonal storage. The methodology proposed here also aims to account for the mutual interaction of degradation processes affecting different components and highlights implications on computational requirements.

Some studies have included a fixed degradation rate for components of the hydrogen chain in their analyses. Rezaei et al. [94] evaluated the levelized cost of hydrogen produced by water electrolysis fed by solar and wind energy. The authors considered the effect of performance decay but they assumed a fixed plant degradation rate of 0.5 %/year, as in [95]. Liu et al. [96] evaluated the short and long-duration energy storage requirements in solar-wind hybrid systems. They also introduced a fixed degradation rate of 0.2 % per year for the estimation of the LCOE from [97]. The findings of the present studies have shown that this hypothesis can lead to inaccurate results.

Zhang and Yuan [98] proposed an optimization and economic evaluation of a PEM system subjected to variable power operations considering its degradation. The authors propose three improved algorithms to solve this optimization problem. Roshandel et Parhizkar [99] developed a degradation-based optimization to consider the degradation effect when optimizing the profit of a SOFC power plant. However, these case studies were limited to a single component, while the current study aims to propose a framework capable of considering the long-term interaction between several components that may compose a hybrid energy system.

Pu et al. [57] proposed a two-level optimal sizing method to analyze energy systems that combine power-hydrogen-heat-cooling cogeneration. They considered the degradation of the battery using a semi-empirical model that estimates the SOH trend starting from the power released or absorbed by the component. They also considered time degradation and degradation due to start-and-stop operation for the PEM fuel cell and the PEM electrolyzer. However, since the focus of their study was the application of a MILP optimizer, all degradation constraints were linearized, and they used simplified component models to optimize the operation on typical days. Authors simulated selected time windows in the considered system lifetime and then they estimated the remaining life of components with a linear fit of the obtained yearly degradation trend. Results presented in the current work show that the linear degradation hypothesis can lead to errors in estimating the long-term performance of the system.

Guinot et al. [100] investigated an HES including batteries and a hydrogen chain (electrolyzer, gas storages, and fuel cell i.e., P2G2P) for an off-grid application. Authors considered the impact of performance aging: linear voltage time degradation of +10 μV/h for the electrolyzer and -5 μV/h the fuel cell, cyclic, and calendar aging for the BESS. They minimized simultaneously the LCOE and the Maximum Daily Power Failure Time using the Strength Pareto Evolutionary Algorithm 2. Their results proved that not considering the degradation of performance over time can lead to errors in the sizing of hybrid energy systems.

Li et al. [101] considered MILP optimization to determine the best operating strategy for a stand-alone microgrid considering electric power, cooling/heating, and hydrogen consumption and a genetic algorithm to search for the best size of each component. They considered the influence of several factors on sizing results, including degradation of fuel cell, electrolyzer, and battery. However, they only used 12 days as input data to obtain the optimal sizing results. Moreover, the 1-h resolution that they used to simulate 365 days and test the validity of sizing results can be inappropriate to accurately assess the cyclic degradation of the battery and the average performance of the electrolyzer or the fuel cell.

Li et al. [102] investigated the planning and optimization for electricity-hydrogen integrated energy systems considering the degradation of storage devices to minimize life cycle costs. The authors proposed tools to evaluate the voltage degradation of a PEMFC and a Li-ion BESS, but the mutual influence of performance degradation of components on each other in the long term is not considered.

Le et al. [103] presented the design and operation optimization of a hybrid ESS comprising hydrogen and batteries, in which they also considered components' degradation and energy cost volatility. This work proposed a Multi-Objective Modified Firefly Algorithm (MOMFA) to optimize the size of a system involving PV, battery storage, and hydrogen storage. Results found that, when the penetration of renewables is higher than 80 %, storage systems that involve hydrogen become more effective. The battery was modeled using a fixed efficiency and assumed a constant degradation rate of 2.9 % per year. They assumed a linear degradation also for the electrolyzer (+10 μV/h) and the fuel cell (-5 μV/h). Again, the linear hypothesis may potentially lead to misleading results.

1.2. Design of 100 % self-sufficient HESs

Many studies have addressed the problem of reaching 100 % self-sufficiency on HESs only using RES. Most of them have conducted techno-economic optimizations to understand the best combination of RES and storage to install, or to optimally size them.

One of the most interesting test cases for the introduction of renewable HESs that aim to reach full self-sufficiency is represented by small-to-medium islands, which have always been affected by some sort of energy struggle. Several previous analyses considered case studies in the non-interconnected islands (NIIs) cluster, in Greece. According to the status of electricity generation in the NIIs for the Aegean Sea Region from Tzanes et al. [104], the RES share in the area has stagnated in the range between 15 and 18 % since 2010 due to existing technical limitations. On the other hand, the current thermal power stations are characterized by low capacity factors and high specific fuel consumption that result in high operating costs and LCOE higher than 600 €/MWh. The paradigm of the smart energy solution and battery-based HPS is proposed as one of the methods to address the current situation. Skopetou et al. [105] examined short (2030) and mid-term (2050) implementations of novel technologies in NIIs and demonstrated that a NII can realistically abolish the use of fossil fuels and enhance energy self-sufficiency using the local RES. Results from Żołądek et al. [106] show that the payback period for a self-sufficient microgrid in this area is 11–15 years. Kougias et al. [107] investigated whether the development of renewable energy sources could lead to sustainable systems in islands in the Aegean Sea. Results show that the RES additions to cover the demand represent a more cost-effective option than traditional fossil fuels.

The current study presents the application of the proposed methodology for the robust design of a HESs targeted to sustain a small island part of the NIIs, i.e., the island of Tilos. Results on this study case allowed comparing different simulation approaches, assessing the accuracy of the new proposed method, and evaluating the potential error coming from the application of simulation techniques that neglect degradation. Beyond contributing to the body of literature on 100 % self-sufficient grids, by proposing a novel simulation approach, this study underlines the possible issues in all analyses that consider the long-term performance of renewable systems that include storage devices.

1.3. Aims of the present study and novelty

The in-depth literature analysis has shown that the effect of performance decay of components must be considered for correctly estimating the long-term performance of HESs [65]. Moreover, several analyses started accounting for degradation in optimization problems related to control, scheduling, and sizing. However, many studies only included the effects of time degradation in linearized problems or impose fixed degradation rates to components.

This study proposes a simulation method able to account not only for the linear time degradation of components, but also for the mutual impact that the degradation of a device has on the yearly average performance of other components. Mutual impact assessment is crucial when studying multi-component systems that involve hybrid storage technologies such as the combination of batteries and hydrogen chains. Long-term simulations that employ complete components models, as proposed in some studies (e.g., [63,64]), can provide insights into the mutual effects of degradation on other components and the overall system behavior. On the other hand, computational cost rises with complexity of models and with the length of the time-horizon of simulations. Consequently, those simulation approaches are not compatible with sizing optimization algorithms that require several iterations to reach the global optimum when the number of variables rises. Differently, the present work proposes a novel approach still able to consider the long-term performance decay of while limiting the computational costs and becoming compatible with stochastic optimizers.

First, trends of the long-term degradation of performance of BESS, electrolyzer, and fuel cell were studied. Those trends are obtained from the results of a complete simulation that uses complete component models to simulate the system behavior over 20 years of operation (*c20*). Then, this work introduces a novel *hybrid* simulation method able to predict the long-term trend of the degradation, in a given simulation, by exploiting results of only one year of simulation. The proposed method can indeed be used to set up a set of accurate simplified simulations starting from partial results coming from every kind of model. The reduction of computational time can thus be achieved also starting from non-linear models, commercial tools or empirical data. This hybrid approach, which combines complex simulations with simplified ones, is tailored for techno-economic optimizations, in which the tradeoff between the accuracy of results and computational times is key.

The proposed optimization framework is tested using a real case study: the HPS of the island of Tilos. This work continues the analysis started with [108], again considering the case study of the HESs installed on the island of Tilos, comprising a wind turbine and a PV field. The introduction of P2G2P, as well as an upgrade of the PV field and the substitution of the ZEBRA battery with a larger lithium-ion battery, was already discussed in the previous analyses. However, previous studies employed simplified component models and neglected a key aspect highlighted in the current work: the long-term performance decay of storage components. Differently, the present study proposes an optimization framework for the sizing of renewable HESs that addresses the problem of considering degradation. Moreover, a sensitivity analysis on PV size shows how results vary when constraints are applied to the maximum generation capacity.

The present work goes beyond the state of the art and contributes to literature from several perspectives. More specifically, the study:

- presents an innovative simulation framework capable of considering the performance degradation in time and accurately estimating the lifetime of components while reducing computational costs.
- applies the innovative simulation method to a real case study to highlight the potential error in component sizing and cost evaluation when neglecting the long-term component degradation.
- presents and describes in detail parametric components models to simulate the behavior of an alkaline electrolyzer, a PEM fuel cell, and a Li-ion battery.

Contents are organized as follows. Section 2 describes the reference case study of Tilos. Section 3 outlines the methodology of this study and introduces the four considered simulation methods: three based on standard approaches (labelled in the following as "*simplified*", "*c1*", and "*c20*") and the novel one ("*hybrid*"). Section 3.1 explains the activation logic of the proposed hybrid ESS comprising batteries and hydrogen, while Section 3.2 describes in detail how the electrolyzer, the fuel cell, the compressor, hydrogen tanks, and the lithium-ion battery are modeled for complete simulations. Section 3.3 explains how components models can be simplified to reduce computational costs. Then, Section 3.4 presents the *hybrid* simulation method and how degradation trends of different devices were obtained. Section 3.5 presents the proposed optimization framework and explains the reason behind using the differential evolution algorithm to find the minimum LCORE. Section 3.6 presents the results of the market review that lead to the price values considered in the economic analysis. Section 4 presents the results from the proposed analyses. Section 4.1 first compares the outcome from different simulation methods to assess the accuracy of the novel approach. Then, Section 4.2 presents the results of a sizing optimization carried out by using the novel approach. Results were compared to those obtained using standard simplified approaches to assess the magnitude of potential errors while neglecting degradation. Section 5 presents a discussion about the obtained results. Finally, the main conclusions of the study are outlined in Section 6.

2. Reference case study: The hybrid energy system of the island of Tilos

This work applies the novel methodology to optimize the design of a 100 % self-sustained HESs using a real case study. The economic analysis considering the degradation of components is used to evaluate the optimal upgrade of an actual microgrid based on renewables. The application to a real case study allowed also the comparison between different simulation methods, the evaluation of the accuracy of the proposed approach, and an analysis on how this technique compares with standard approaches.

Mediterranean islands have always struggled to achieve a reliable energy supply. On the other hand, the high availability of solar irradiance and sustained wind speeds make the installation of PV and wind turbines favorable and pushed the introduction of RES in the electricity mix of the area. In this context, the TILOS project [109] was born. Tilos is a Greek island, part of the Dodecanese group, between Kos and Rhodes. During that project, a Hybrid Power Station (HPS) comprising an 800-kW wind turbine, a 160-kWp PV field, and a 2.88-MWh sodium–nickel–chloride battery (ZEBRA) was installed on the island. The load (3 MWh) mainly comes from two villages: Megalo Chorio and Livadia. A more detailed description of the project and the current layout of the HES installed in Tilos can be found in other studies by the same authors [108,110].

The present study analyses the possibility of upgrading the current energy system installed on the island by expanding the power production capabilities and supporting this intermittent generation with two kinds of energy storage systems: lithium-ion batteries and P2G2P. This

upgrade aims to reach total energy independence on the island with clean and local energy production, remove the need to import fossil fuels or rely on external sources (Fig. 1).

One year of historical production from the wind turbine and the PV field and one year of request from the island of Tilos were harvested by the energy management system of the HPS. This dataset goes from November 29th, 2020, to October 29th, 2021. The method used for the reconstruction of the dataset is described in detail in [108].

Fig. 2 shows the overlap between the power production from the renewable generators and the power required from the island. The shape of the power request is characterized by an abrupt peak during the summer season, when tourists arrive. On the other hand, the average RES production is almost stable during the year and slightly higher during the winter season due to the predominance of wind production.

The consistent mismatch between the RES production and the load requires daily storage, to match the night power production with the daily one, and seasonal storage, to shift the winter energy excess towards the summer energy deficit. Therefore, this analysis considers the introduction of a hybrid ESS that combines lithium-ion batteries with the P2G2P. Open cells can decouple the nominal power with the energy storage capacity. Electrolyzers can be used to slowly produce a buffer of hydrogen by exploiting the power excess during winter. This hydrogen can be compressed and stored in tanks and later used by fuel cells to cover the demand during peaks of consumption. In this sense, the P2G2P acts as a backup generator that produces the required fuel with the excess from RES.

Even if the current energy excess (~ 1.08 GWh) is slightly higher than the current energy deficit (~ 1 GWh), an entire shift of the energy surplus towards the energy request would be economically unfeasible, since this action would require oversized storage capacities if compared to the load of the island and current generators. Moreover, a complete shift would require round-trip efficiency close to unity, a condition unfeasible with most current storage systems. Hence, this study also considers the possibility of expanding the PV production capabilities of the island to increase the load share that the RES generators can directly cover. Solar production, thanks to modularity and the higher matching degree with the summer deficit was selected as the best candidate for upscaling.

2.1. Wind turbine

The current main source of renewable energy production in Tilos is a 800 kW wind turbine, mounted in the northwest region of the island. The turbine model is an Enercon E-53 [111], with active pitch control. As stated in the manufacturer datasheet, the cut-in speed is 2 m/s, the nominal production is reached at 13 m/s, and the cut-out speed at 28 m/s.

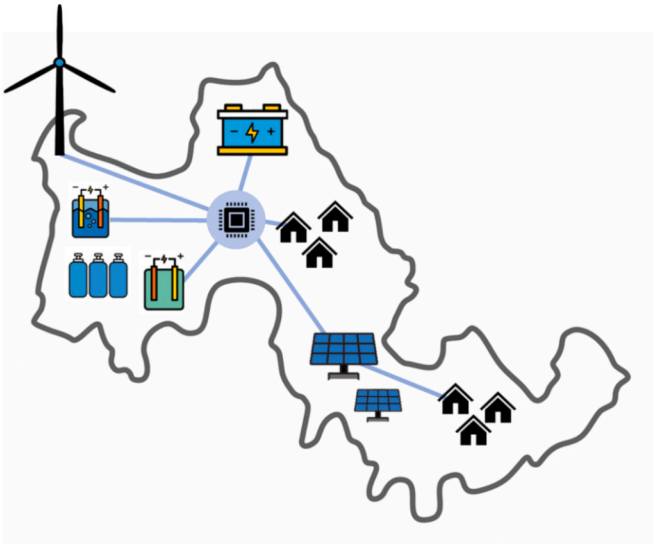

Fig. 1. Scheme of the proposed hybrid energy system to sustain the energy production of the island of Tilos.

The wind turbine production was reconstructed from the historical production dataset (one year of data, 1-min time resolution) while missing points were estimated starting with the wind speed dataset and the manufacturer's power curve.

2.2. PV field

The second source of renewable energy generation on Tilos is a 160 kWp PV field. The field is composed of JA SOLAR panels, mounted with a tilt angle of 30° towards the south and located in the central part of the island.

As for the wind turbine, the PV production was reconstructed from the historical dataset coming from the SCADA of the HPS (one year of data, 1-min time resolution). Due to modularity and high matching degree between the consumption peak because of tourists and higher PV production during summer, solar was the power generation source that the optimization framework was allowed to increase. The solar production is scaled according to the upgrade that the optimizer considers.

3. Methodology

As stated in the introduction section, techno-economic analyses of energy systems usually simulate only one year of operation. Then, the cost metric formula (NPV, LCOE, or LCOS) attributes the same energy production and the same performance of components to all the years of the lifespan of the system. However, this approach can lead to inaccurate results, especially when studying systems that involve a high number of components subject to deterioration. To account for long-term degradation of performance, the time horizon of simulations should match the expected lifetime of the system. However, computational costs may become unsustainable if complex components models are used to simulate twenty or more years of operation. Time for computation can be reduced by using simplified models, but the accuracy of the simulation would be greatly reduced as well.

This work proposes a novel hybrid simulation method to match the accuracy of a complete simulation across the while lifetime of a HESs but with much lighter computational costs, making the simulation framework compatible with the optimization tools required to obtain the best sizing of parts.

This section presents four simulation methods: the novel *hybrid* approach and three standard simulation systems (labelled as "*c1*", "*c20*", and "*simplified*") to evaluate results coming from standard approaches. The time resolution is the same for every approach (1 min), but the considered time frame and the models involved differ from each other. The main characteristics of the four approaches are as follows:

1) The first method (*simplified*) involves the simulation of a single year of operation using simplified models (described in Section 3.3). Differently from the models presented in the previous section, here the battery degradation and the consequent shrinking of the equivalent capacity is neglected. The fuel cell and the electrolyzer are modeled by considering only the nominal conversion factor and neglecting temperature and time effect. This is the simplest method and comes with the lowest computational cost.
2) The second method (*c1*) again involves simulating a single year of operation but uses complete models of components. In this case, the operation of the battery, the electrolyzer, and the fuel cell is modeled using the approach described in Sections 3.2.5, 3.2.1, and 3.2.2 respectively. This method is more advanced if compared to the previous approach and comes with a higher computational cost. However, *c1* still comes with the limitation of simulating only one

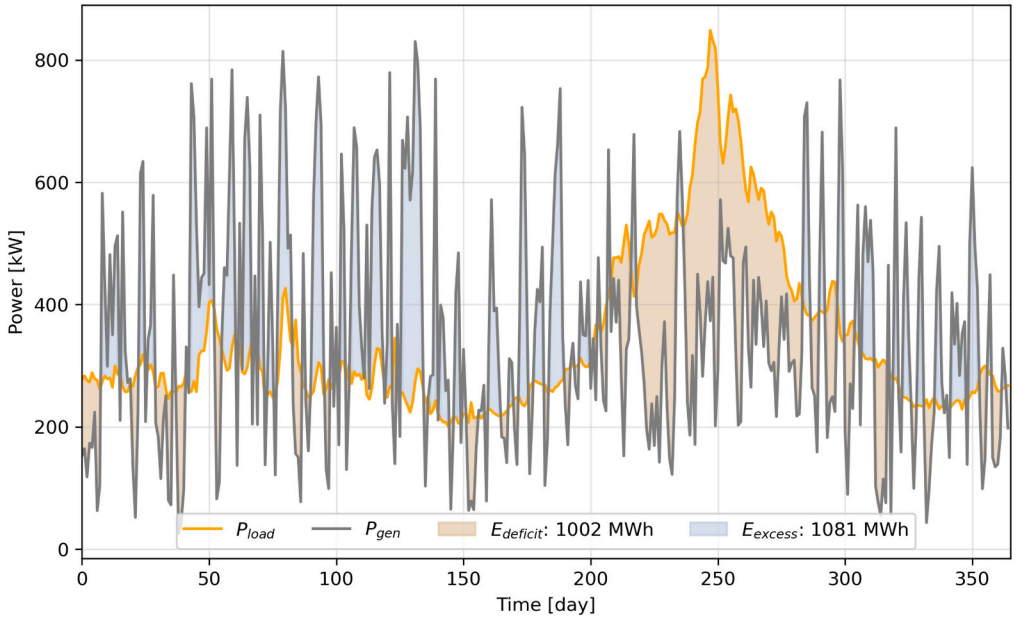

Fig. 2. The mismatch between RES production and load.

year of operation instead of the whole lifetime of the plant. The outcome of the first year is thus attributed to the remaining years of operation of the system.

3) The third method (*c20*) is the most accurate one. Instead of simulating only one year of operation, the complete models (Section 3.2) are used to simulate the behavior of the system during the entire lifetime of the plant (20 years in this case study). In this way, degradation models can be applied to estimate the decline in performance of all components and the impact on the overall system. This is the most accurate method and comes with the highest computational cost.
4) The fourth and final method (*hybrid*) follows the approach proposed in Section 3.4. It hybridizes the second method (one year of simulation with complete components models) with the first one (simulating the other years with simplified models) to obtain accurate results while maintaining a low computational cost. The *hybrid* approach simulates the whole lifetime of the plant (as *c20*) but uses complete models of components only for the first year.

Results from the first two approaches (*simplified* and *c1*) aim to show the error that usual analyses may encounter if following procedures that involve the simulation of a single year of operation. Results from the third method (*c20*, the most accurate one) are a benchmark to assess the accuracy of other simulation approaches. Results from the novel *hybrid* method are indeed compared with the outcome from the three standard simulation approaches in Section 4.1 and discussed in Section 5.

Section 3.1 describes the parametric activation logic of different components to explain the considered hierarchy for the management of a BESS in synergy with a hydrogen chain.

Section 3.2 describes the proposed models of components to simulate the behavior of storage systems under a long-term intermittent operation: electrolyzer, tanks, compressor, fuel cell, and Li-ion battery. Those models are used in *c1*, *c20*, and the first year of the *hybrid* simulation. Section 3.3 describes instead the simplified components models used for the *simplified* simulation and for the remaining years of the *hybrid* simulation. Section 3.4 presents the *hybrid* simulation approach and describes in detail how the set of simplified simulations can be tuned starting from the outcome of a single year of simulation using complete components models.

Section 3.5 presents the proposed optimization framework that uses the newly proposed *hybrid* simulation to optimize the sizing of the proposed system via a stochastic simulation approach.

Section 3.6 presents the list of component prices obtained from an extensive literature and market review.

3.1. Components activation logic

This paper proposes the synergy between BESS and P2G2P since the two storage systems have complementary characteristics. Alkaline electrolyzers need over 20 % of their rated power to start hydrogen production. Consequently, if the excess energy from renewable generators is lower than this threshold, the electrolyzer cannot absorb the surplus. This limitation makes the hydrogen chain based on alkaline electrolyzers unfeasible for managing low energy excesses. In contrast, batteries can absorb all power levels, provided that technical constraints on capacity and power variation are met. Batteries are also characterized by high round trip-efficiencies (generally higher than 90 % [112]). Compressed hydrogen systems can, however, compensate for some of the drawbacks of batteries. As mentioned by [113], batteries have a high volume and weight, their capacity degrades over time and have material limitations making them less suitable for long-term energy storage [114].

A hierarchical control was developed to simulate the activation logic of the different energy storage devices. The energy flows from the renewable generators towards the load, after being modulated by the BESS and the P2G2P. Models of components estimate the actual performance of devices, while storage models track the state of charge (SOC) of storage devices. The proposed control scheme (flowchart in Fig. 3) is used for all the four proposed simulation methods.

The activation logic works as follows:

1) Power produced from renewable generators feeds the load.
2) The battery is the first storage component to be activated. BESS charges when there is an energy excess and discharges when there is a deficit.
3) The P2G2P block is activated to manage the hydrogen production or consumption:
   a. The fuel cell model activates in presence of a residual energy deficit after the battery action.

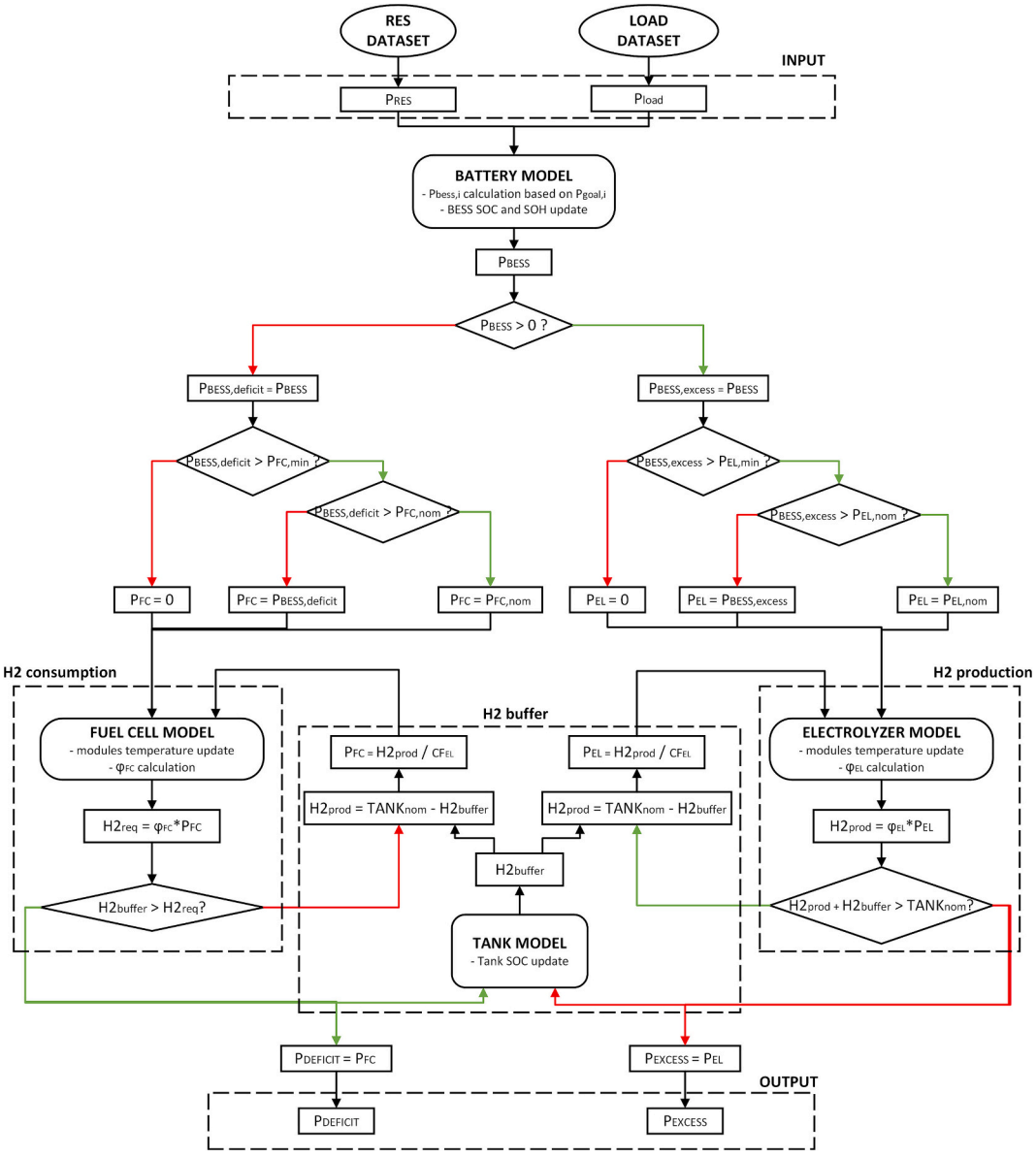

Fig. 3. Flowchart of the control strategy applied in the simulation framework.

i. According to the FC cell temperature and number of working hours, the conversion factor of the FC is updated. This factor allows the calculation of the required hydrogen.
ii. The tank model checks if there is enough hydrogen to produce the required power. If not, the power production from the FC is corrected according to the maximum hydrogen available.
iii. The quantity of consumed hydrogen updates the SOC of the H_2 tank.

b. The electrolyzer model activates in presence of a residual energy excess after the battery action.
i. According to the EL cell temperature and number of working hours, the conversion factor of the EL is updated. This factor allows the calculation of producible hydrogen.
ii. The tank model checks if there is enough room for the hydrogen that can be produced by processing the excess power. If not, the hydrogen production from the EL is corrected accordingly.
iii. The quantity of produced hydrogen updates the SOC of the H_2 tank.

4) The power excess or deficit of the timestep is saved.

3.2. Complete components models

This section describes in detail the complete models of components used in simulation approaches that involve the complete simulation of one year of operation (*c1*), the complete simulation of twenty years of operation (*c20*), and the first year of the *hybrid* simulation approach.

3.2.1. Electrolyzer

An electrolyzer uses electrical power to split water molecules into oxygen and hydrogen [115]. The most commonly used technologies for hydrogen production from water electrolysis are: alkaline electrolyzers (ALK), proton exchange membrane electrolyzers (PEM), and solid oxide electrolysis cell (SOEC) [116]. Alkaline is the most mature technology, has an electric efficiency of up to 70 % [117], a competitive cost [118] and works from 1 to 30 bar [119]. Moreover, those devices have a simple structure, do not require precious materials as catalysts, and, consequently, have the highest market share in the electrolysis field [120]. Because of these reasons, this study proposes the modeling of an ALK electrolyzer.

The ALK electrolyzer model used in this work was developed by some

of the authors and described in depth in [117]. The model is based on a high-current commercial model: electrolyzer cells work at a nominal current of 5 kA. Considering a nominal operating voltage of 1.89 V, the power absorption from each cell at nominal conditions is 9.45 kW. The model considers the cell always operating at ideal current levels, while the voltage is corrected according to time and temperature effects and computed as in Eq. 1.

$$V_{op,el} = V_{ideal} + \Delta V_{time,deg} \cdot h_{work} + \Delta V_{temp,deg} \cdot (T_{rated} - T_{el}) \quad (1)$$

where the time degradation of the voltage $\Delta V_{time,deg}$ is set to 3 μV per working hour, while the thermal degradation $\Delta V_{temp,deg}$ is 5 mV per degree of cool down.

The temperature variation is computed through a thermal model. Heat is generated during hydrogen production by the difference between the operating voltage of the cell and the thermoneutral voltage required for the water split reaction. On the other hand, heat is lost to the environment when the electrolyzer is off. The complete description of the geometry considered for the modeling of heat losses is detailed in [117].

The conversion factor of the electrolyzer stack (φ_{el}) is corrected according to the estimated voltage level and calculated as in Eq. 2. The nominal value of the electrolyzer conversion factor is 18 kg/MWh, corresponding to an electrical efficiency of around 60 %.

$$\varphi_{el} = \frac{H_{2,id}}{n_{cells} \cdot V_{op} \cdot I_{id}} \quad (2)$$

As in [121], the analysis considers a maximum lifetime of an electrolyzer stack of 10 years, and the replacement costs 0.45 times the costs of a new one. A premature substitution for the stack is required if the voltage increases by more than 20 % compared to the initial nominal value.

3.2.2. Fuel cell

Hydrogen can be converted back to electricity using a fuel cell [122]. Among the most widespread fuel cell technologies, the proton-exchange membrane (PEM) fuel cell and Solid Oxide fuel cell (SOFC) [123–125] have gained increasing attention. This study considers a PEM fuel cell, because of the advantage of operating at relatively low temperatures, the high efficiency, and the minimal noise production [126–128]. One single PEM cell has a voltage near 1 V at open circuit and around 0.6 V at rated conditions of power generation. Therefore, multiple cells must be connected in series to increase power production, thus forming a stack [129]. The PEM fuel cell stack used as a reference to develop this model is the NEDSTACK FCS 13-XXL [130]. Table 1 gives an overview of some important specifications of this stack.

At rated power (13.6 kW), the stack works at a current of 230 A and a voltage of 59 V. To analyze the performance of the fuel cell, the polarization curve for a fuel cell stack was modeled according to the datasheet of the stack (Table 2).

The polarization curve points in Table 2 refer to the nominal case. As for the alkaline electrolyzer, this condition changes during operation because of time and thermal degradation.

The voltage degradation of the fuel cell stack can be caused by several factors, such as dynamic operation, frequent on/off, and high loads [131]. Several methods have been proposed in the literature to predict the expected voltage variation and lifetime of a fuel cell [132,133]. This model follows a simplified approach that attributes a specific voltage increase per each working hour of the device. This value was extrapolated from the findings by Stropnik et al. [131]: results from this study show that the time degradation increases the voltage of each cell by 5 µV ($\Delta V_{time,deg}$) per working hour. This result is in line with the values used in the model by Fowler et al. [52] and their literature review.

Table 1
Specifications of fuel cell stack.

Specific	Value
Rated power	13.6 kW
Voltage range	58–94 V
Current range	0–230 A
Electrical efficiency	51 %
Conversion factor	59 kg/MWh
Size	580 × 196 × 288 mm
Weight	39 kg

Table 2
Stack polarization curve points in the datasheet.

Current (A)	0	40	80	120	160	200	230
Stack voltage (V)	94	78	73	69	66	62	59
Stack power (kW)	0.0	3.1	5.8	8.3	10.5	12.4	13.6

Usually, the maximum lifetime of the stack PEM FC is estimated at 10 years [134,135], but a premature substitution could be required if the performance of the cell goes below the required threshold. As for the electrolyzer, this analysis assumes a premature replacement of the fuel cell stack when the voltage drops by more than 20 % compared to the initial nominal value due to time degradation [102,136].

Since the stack predominantly consists of semiconductors, a rising temperature has a positive effect on the operation and performance of the fuel cell, resulting in an increase of conductivity and therefore a decrease in resistivity. Thermal degradation for cooling was estimated by the effects of temperature on the cell voltage loss as 0.51 mV per degree [137]. Fig. 4 shows that the stack voltage decreases over time, while a lower temperature also results in a lower voltage. Overall, the operating voltage is calculated according to Eq. 3.

$$V_{op,fc} = V_{ideal} - \Delta V_{time,deg} \cdot h_{work} - \Delta V_{temp,deg} \cdot (T_{rated} - T_{fc}) \quad (3)$$

where the rated temperature T_{rated} is equal to 60 °C.

Similarly to the mathematical formulation used for the electrolyzer, the conversion factor of the cell φ_{fc} represents a transfer function between the input hydrogen and power that can be delivered by oxidizing it. In Eq. 4, $H_{2,id}$ is the maximum hydrogen inlet flow rate, I_{id} the ideal current, while the voltage V_{op} is affected by time and thermal degradation.

$$\varphi_{fc} = \frac{H_{2,id}}{n_{cells} \cdot V_{op} \cdot I_{id}} \quad (4)$$

To track the stack temperature variation based on the hydrogen request, a thermal model was developed for the fuel cell. The geometry of the system is of importance since the shape of the device affects how heat is distributed and dissipated. A single fuel cell stack has a rated power of 13.6 kW, meaning that a connection of multiple stacks is needed to cover the load (up to 960 kW). A layout consisting of a three-by-two stacks arrangement was considered. Therefore, the length of the connection is one-sixth the number of connected stacks, times the length of one stack (580 mm). To calculate the heat losses from this rectangular shape, the equivalent diameter was calculated using the formula in Eq. 5,

$$d_{eq} = \frac{4S}{P} \quad (5)$$

where S is the cross-section and P is the perimeter [138]. Based on the datasheet and due to the arrangement considered, the cross-section has a width of 588 mm and a height of 576 mm. To prevent heat loss, the module would be placed inside a container.

Since the thermal conductivity of graphite (4180 W/mK) is significantly higher than other materials that are commonly used in PEM fuel cells like platinum (95 W/mK) and Nafion (0.18–0.27 W/mK) [139,140], the heat dissipation was modeled mainly considering the properties of the first material [141]. Assuming that one-fifth of the fuel

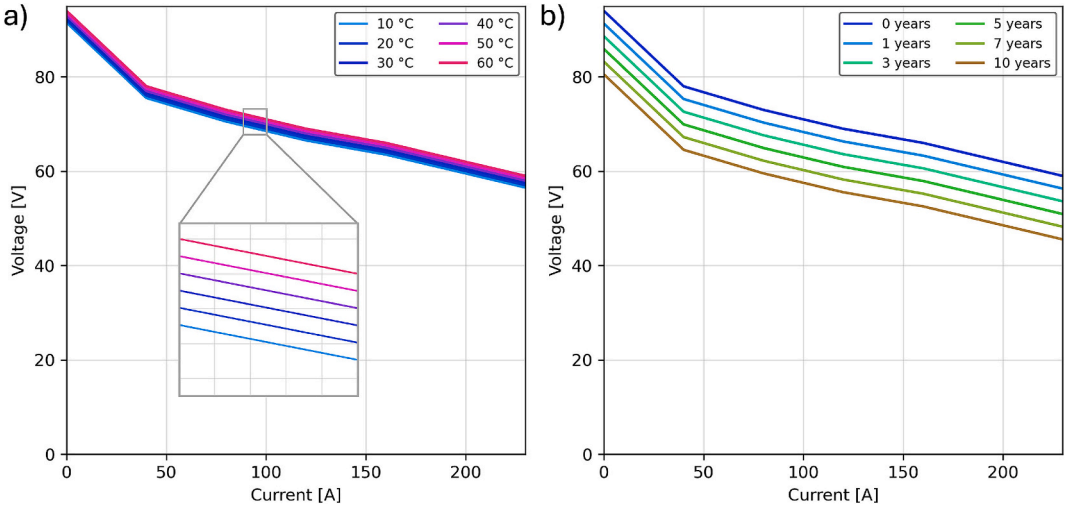

Fig. 4. a) Effect of temperature variation on the modeled polarization curve for a brand-new fuel cell stack b) Effect of working time on the modeled polarization curve at rated working temperature (60 °C), considering a capacity factor of 10 % (876 working hours per year).

cell stack consists of graphite, the equivalent mass of the fuel cell m_{fc} was calculated by multiplying the total volume of the module times the graphite density and dividing that value by five.

The temperature variation of the module during operation is then calculated using Eq. 7,

$$\Delta T = \frac{Q_{gain} - Q_{lost}}{m_{fc} \cdot c_{fc}} \tag{7}$$

where:

- Q_{gain}: Heat generation
- Q_{lost}: Heat loss
- m_{fc}: Equivalent mass of the fuel cell.
- c_{fc}: Heat capacity of the fuel cell, assumed equal to the heat capacity of graphite (710 J/kgK [141])

To prevent overheating while hydrogen is processed, the temperature is kept at a maximum of 60 °C by a cooling mechanism. In the context of the proposed parametric model, this component is neglected and the cooling action is assumed to be ideal.

To compute the heat generation (Q_{gain}), the mechanism responsible for heat generation is considered. The thermoneutral voltage V_{th} of the fuel cell is 1.48 V. The cell will operate at a voltage lower than this value and this voltage difference, multiplied by the operating current, corresponds to the power loss in the form of heat [142]. Therefore, Q_{gain} can be calculated as in Eq. 8.

$$Q_{gain} = \left(n_{stacks} \cdot V_{th} - V_{op}\right) \cdot I \tag{8}$$

The module will have thermal losses (Q_{lost}) to the surrounding environment, calculated accordingly to Eq. 9. Heat is transmitted across the following series of resistances: conduction of the container of the module itself, convection with the air between the container of the module and the external container, external container conduction, and eventually external air convection. Table 3 summarizes meaningful properties of the component geometry for the calculation of the temperature variation.

$$Q_{lost} = \frac{(T_{int} - T_{ext}) \cdot 2\pi L}{\frac{ln\left(\frac{R_{t,e}}{R_{t,i}}\right)}{k_t} + \frac{1}{h_1 \cdot R_{gw,i}} + \frac{ln\left(\frac{R_{gw,e}}{R_{gw,i}}\right)}{k_{gw}} + \frac{1}{h_2 \cdot R_{gw,e}}} \tag{9}$$

Once the heat gain and the heat loss are known, the stack temperature variation can be calculated using Eq. 7.

Fig. 5 (a) gives an example of temperature variation during one year of operation of the fuel cell. The temperature drops while the fuel cell is not active and loses heat towards the environment, while the temperature increases to 60 °C during active operation.

Fig. 5 (b) shows how the temperature variation affects the conversion factor φ_{FC}. When the temperature drops due to stand-by, the hydrogen request for the same power delivery increases. The effect of the time degradation is visible during the summer months when the module must cover the residual demand. Hour by hour, the φ_{FC} increases due to the voltage degradation. In terms of electrical efficiency, the performance of the fuel cell may drop from 51 % (59 kg/kWh) to 48 % (62 kg/kWh).

Table 3
Main characteristics and thermal parameters of different layers of the module.

Component	material	dimension	coefficient
Tank	steel	$R_{t,i} - R_{t,e} = 4$ mm	$k_t = 52$ W/mK
Gap	air	$R_{gw,i} = 1$ m	$h_1 = 10$ W/m^{2}K
Insulation	glass wool	$R_{gw,i} - R_{gw,e} = 200$ mm	$k_{gw} = 0.05$ W/mK
External air	air	–	$h_2 = 20$ W/m^{2}K

3.2.3. *High-pressure and low-pressure hydrogen tanks*

Hydrogen can be stored in gaseous or liquified form, or absorbed into materials [143]. Compressed hydrogen is a common way of storing hydrogen since this method requires less energy than liquefaction [144,145] and storing costs are usually contained [146,147].

This analysis assumes that the hydrogen is stored in compressed form inside tanks at low (LP) and high pressure (HP). Since the electrolyzer produces hydrogen at low and varying quantities, the compressor would have to start running multiple times for a short amount of time if there is no low-pressure storage. To avoid this intermittent operation, the hydrogen that is produced by the electrolyzer will first be stored in a low-pressure buffer tank. This first stage stores a small amount of hydrogen (10 kg) at the outlet pressure of the device (30 bar).

The hydrogen compression starts when this buffer tank is full, thus the compressor operates continuously at constant power. After compression, the hydrogen will be stored in high-pressure storage tanks for seasonal storage. The operating pressure of a high-pressure tank was selected accordingly most considered pressure levels for commercially available tanks and industry standards: 350 bar [148–152].

3.2.4. *Hydrogen compressor*

Hydrogen is produced at a pressure of 30 bar by the electrolyzer and

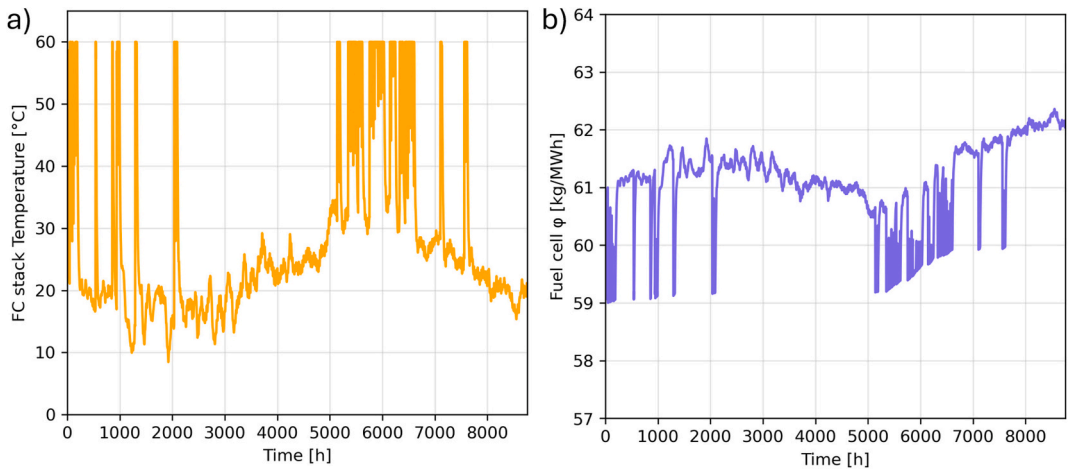

Fig. 5. Time variation of the fuel cell a) temperature and b) conversion factor (φ_{FC}).

stored in LP tanks. A compressor is used to increase the pressure of the gas to 350 bar and thus reducing the volume that is occupied for seasonal storage (HP tanks). The proposed analysis considers a variable operation for storage devices but always the same operation for the compressor. Consequently, the proposed model, tailored for this specific application, only aims at estimating a realistic energy absorption from a multi-stage reciprocating compressor (as in [153]).

The required specific energy ($\dot{E}_{adiabatic}$) to compress one kilogram of hydrogen from 30 bar to 350 bar was calculated using the formula for an adiabatic multistage compression (Eq. 10).

$$\dot{E}_{adiabatic} = N_{stages} \cdot \frac{k}{k-1} \cdot R_{spec} \cdot T \cdot \left(\beta^{\frac{k-1}{k}} - 1 \right) \tag{10}$$

where:

- N_{stages} is the number of stages. The minimum number of stages to manage a reasonable compression ratio (approximately 2.27 per stage) in each cylinder is 3.
- k is the ratio of specific heat under constant pressure to specific heat under constant volume. The average k value according to the temperature range that the hydrogen is going to face during the transformation was used. The value of this ratio (1.43) was calculated using CoolProp [154].
- R_{spec} is the universal gas constant divided by the molar mass of hydrogen, 3849 J/kgK.
- T is the initial temperature, assumed to be constant at 293.15 K
- β is the compression ratio, computed as in Eq. 11:

$$\beta = \left(\frac{P_{out}}{P_{in}} \right)^{\frac{1}{N_{stages}}} \tag{11}$$

- where $\frac{P_{out}}{P_{in}}$ is the fraction between outlet and inlet pressure.
- N_{stages} is the number of stages of compression.

Given these conditions, the $\dot{E}_{adiabatic}$ is equal to 0.89 kWh/kg. Considering an isentropic efficiency (η_{isen}) of 0.75, the actual required specific electrical energy per kilogram ($\dot{E}_{comp}$) is 1.18 kWh/kg (computed as in Eq. 12).

$$\dot{E}_{comp} = \frac{\dot{E}_{adiabatic}}{\eta_{isen}} \tag{12}$$

To calculate the power that the compressor absorbs, the hydrogen mass and the compression time are also needed. When the low-pressure tanks are full, the compression of the 10 kg hydrogen mass (m) contained starts. Given a compression time (t) of 10 min, the power absorbed by the compressor can be calculated as in Eq. 13.

$$P_{comp} = \frac{3600 \cdot \dot{E}_{comp} \cdot m}{t} \tag{13}$$

To avoid an additional burden on the electrical load during moments of low wind and solar production, the compressor starts working when the produced RES power is enough to cover the load, including the compressor. The battery supports compression in case the RES excess stops before the operation ends. The compression time was tuned via a preliminary analysis to find a tradeoff between exploiting sudden and short excesses of production from renewables without excessively increasing the electrical request. This choice is further discussed in Section 5. The required compression power is indeed almost 70 kW, and this power increases the total load of Tilos.

3.2.5. Battery

A BESS comprises electrochemical modules, inverters and containers. This study proposes the substitution of the current high-temperature battery used in Tilos with a larger BESS based on NMC lithium-ion modules. For safety reasons, the modules must be replaced when the SOH drops below 70 %, or after 10 years of operation [51,155]. The replacement cost of such modules was set at 80 % of the cost of a BESS new installation [156].

The proposed BESS model imposes limits to the maximum power that the component can absorb or release. Based on the same assumptions of [51], maximum C-rates are imposed during the charging and discharging phase. The BESS can be fully charged in 1 h (C-rate$_{max,charge}$ equal to 1C) and fully discharged in 20 min (C-rate$_{max,discharge}$ equal to 3C).

To avoid harmful cycles, the simulated control cannot completely discharge or charge the battery. Similar to what assumed in [51], the SOC is confined between 15 and 95 % of the maximum capacity.

At each timestep, the control logic allows the battery to satisfy the request of absorbing or releasing energy, as long as constraints on minimum and maximum SOC and C-rate are met.

Batteries are also characterized by charging and discharging efficiency. Both are influenced by SOC and C-rate. In this study, the efficiency function was modeled as a surface in a 3D space, considering the influence of both factors. The efficiency surfaces were obtained from a fit of points extrapolated from the model proposed by Gonzalez-Castellanos et al. [157] and they can be described by Eq. 14.

$$\eta = p_{00} + p_{01}y + p_{20}x^2 + p_{211}xy + p_{02}y^2 + p_{21}x^2y + p_{12}xy^2 + p_{03}y^3 \tag{14}$$

Where x is the SOC and y is the C-rate. Table 4 reports the fit coefficients for charge and discharge efficiency surfaces. Fig. 6 shows the efficiency surface considered during the charging phase, while Fig. 7 shows the surface considered during the discharging phase.

Table 4
Fit coefficients for charge and discharge efficiency surfaces.

	p_{00}	p_{10}	p_{01}	p_{20}	p_{11}	p_{02}	p_{21}	p_{12}	p_{03}
Charge	100.968	−0.259	−6.415	0.080	1.844	0.255	−0.563	−0.171	0.055
Disch.	100.147	0.100	−6.076	−0.244	0.151	0.043	0.879	−0.035	−0.003

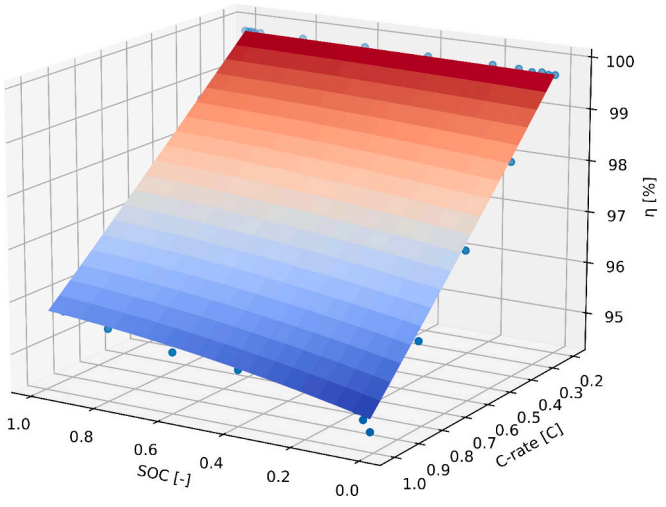

Fig. 6. Charging efficiency surface, fit from [157].

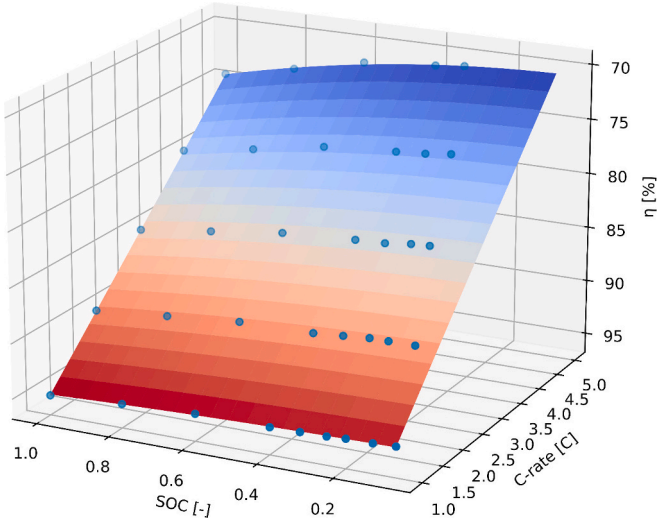

Fig. 7. Discharging efficiency surface, fit from [157].

A degradation model is used to estimate the capacity decline of the BESS and the actual lifetime of the battery modules. The analysis considers a precautionary maximum lifetime for Li-ion battery modules of 10 years. However, the decline in time of the State of Health (SOH) of modules shrinks the actual available capacity of the BESS and, if the SOH goes under a certain threshold (70 %), the modules will require a premature substitution [51,155].

As in [51,117,155], this model estimates the SOH from the degradation for cyclic operation, i.e., each time that the battery is charged and discharged, the component deteriorates. By means of a rainflow-counting algorithm, the number of cycles performed at a certain DOD ($cycles_i$) can be extracted from the trend in time of the SOC of the BESS in a certain time window [51]. The technique here applied compares the number of equivalent charge/discharge cycles performed at a certain depth of discharge (DOD), with the maximum number of cycles at that amplitude that the device can perform before the End of Life (EOL). This ratio corresponds to the damage to the battery in a certain time frame. This technique can be applied each day of operation to compute the daily damage (d_i), as in Eq. 15.

$$d_i = \sum_i \frac{cycles_i}{cycles\ to\ EoL_i} \tag{15}$$

Following the hypothesis of linear accumulation, the cumulative damage (D) can be calculated as the summation of daily damages (Eq. 16). The battery must be substituted when D arrives to 1.

$$D = \sum_i d_i \tag{16}$$

The maximum number of cycles at a certain DOD that the BESS can withstand ($cycles\ to\ EoL_i$) can be estimated from a degradation curve: a curve that links the number of cycles to EoL with the DOD performed by the device. In this study, the degradation curve used to assess the cyclic degradation (Fig. 8) was adapted from [50,51] and can be expressed using the following equation (Eq. 17):

$$cycles\ to\ EOL = a \cdot DOD^b \tag{17}$$

where a is 1512.45, and b is - 0.968423.

Considering that the battery failure happens at a SOH of 70 %, the SOH can be estimated from D as in Eq. 18.

$$SOH = 1 - (0.3 \cdot D) \tag{18}$$

This assessment allows the model to consider the progressive capacity fade of the BESS, computing the actual capacity as the product between the maximum one and the SOH (Eq. 19).

$$C_{actual} = SOH \cdot C_{max} \tag{19}$$

3.3. Simplified component models

The component models proposed in Section 3.2 can be simplified to reduce the complexity of the simulation and thus limit computational costs. Simplified components models neglect several factors described in the previous section:

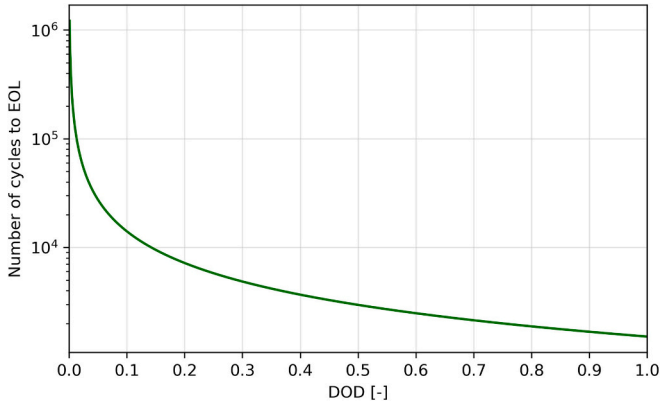

Fig. 8. Battery maximum number of cycles to the end of life (EoL) versus depth of discharge (DoD) curve, adapted from [50,51].

- the battery degradation, thus the capacity of the storage is fixed to a constant value.
- the variation of the conversion factor of the electrolyzer, fixed to a constant value.
- the variation of the conversion factor of the fuel cell, fixed to a constat value.

The present analysis makes use of simplified components' models to perform *simplified* simulation, a reference to understanding the order of magnitude of the evaluation error that may affect analyses that use this specific approach. This analysis considers the capacity of the battery fixed to the initial value ($C_{bess,\mathrm{nom}}$), the conversion factor of the electrolyzer fixed to the nominal value ($\varphi_{el,nom}$) and the conversion factor of the fuel cell again fixed to the nominal value ($\varphi_{fc,nom}$).

The *simplified* approach comes with the advantage of a light computational cost, even when the simulation uses the same inputs and the same time resolution (1-min). For this reason, the new proposed *hybrid* strategy also adopts simplified but specifically tuned component models to evaluate the long-term performance of system configurations.

3.4. Hybrid simulation approach

Due to degradation, the average performance of components varies during the lifetime of an energy system. The battery capacity declines, and the overvoltage that modifies the polarization curve of the electrolyzer and fuel cell varies with time. Moreover, the capacity factor of electrolyzer and fuel cell affects their average operating temperatures, again influencing their average performance. In addition, those effects have a mutual impact on each other: a smaller battery forces the system to rely more on the P2G2P, affecting the capacity factor of hydrogen production components with a consequent impact on the average conversion efficiency. All those effects can be considered in a long-term simulation using the components models described in Section 3.2 (*c20*). However, a simulation over the entire expected lifetime of a system comes with high computational requirements.

The *hybrid* approach is based on the concept of simulating only one year of operation using complete models (as in *c1*) and extracting key performance indicators to set up a set of simplified simulations of the remaining years of operation (nineteen in this specific case). Fig. 9 shows the scheme of the *hybrid* simulation approach. This approach leverages the fact that a simplified simulation, calibrated to specific parameters that characterize the unique combination of components, can yield results almost as accurate as the outcome of simulations using complete components models (*c20*). Section 4.1 presents results from this comparison and Section 5 discusses the implications.

A hybrid energy system that involves multiple storage devices subjected to specific degradation effects sees the average performance of components evolve in a non-linear way. Therefore, a reliable and tested method to predict the evolution of average performance of devices is required. This approach can be based on results of a specific combination during a single year of operation.

The simulation of the first year of operation using complete components models permits to accurately assess the trend of main components efficiency, conversion factors, and degradation. The output of this first year of simulation is not only an accurate assessment of the energy flows of the system, translated on the self-sufficiency degree that the analyzed combination can reach, but also the assessment of key parameters that allow tuning simplified simulations for the remaining years.

More specifically, results from a year of simulation with complete components models allow to extrapolate:

- **Average conversion factors of electrolyzer and fuel cell**: The trend of the conversion factors characterizing the fuel cell and the electrolyzer during their operation can be averaged to obtain fixed coefficients $\varphi_{fc,avg}$ and $\varphi_{el,avg}$. Those coefficients capture the behavior of P2G2P components in the combination under analysis. For example, a combination that considers a high-power electrolyzer will see the component often work at partial load or intermittently (lower capacity factors mean lower average performance), while a smaller electrolyzer would work for longer periods (higher capacity factors mean higher average performance).

  The complete simulation is able to capture the influence that such an operation would have on the conversion factor of the component.

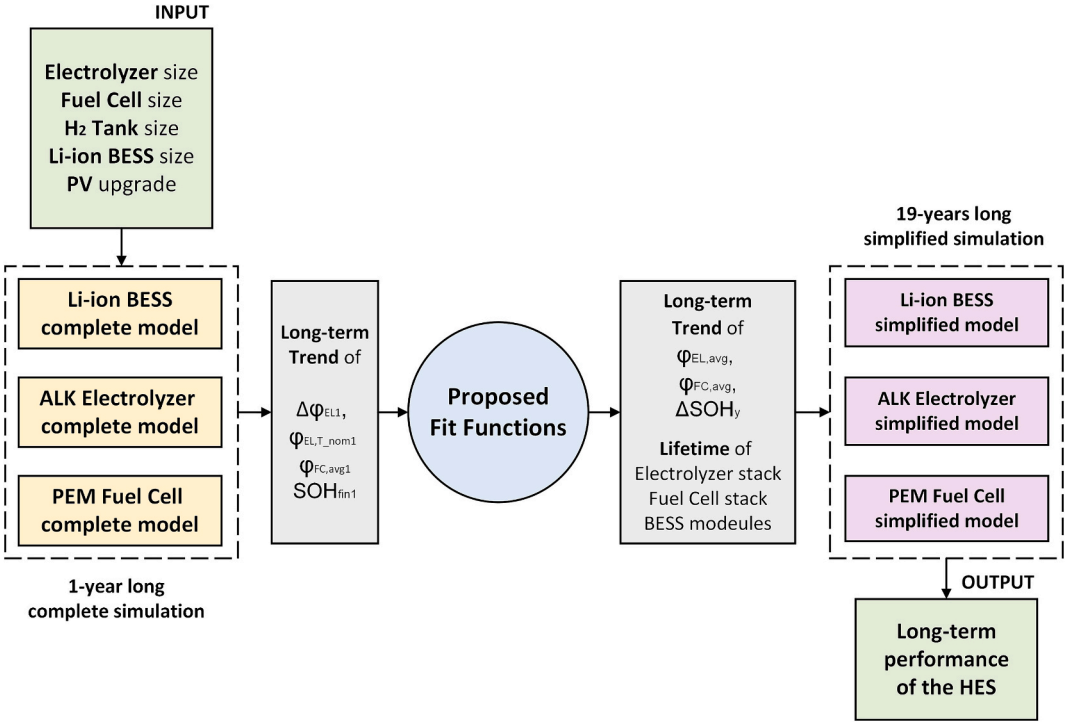

Fig. 9. Scheme of the *hybrid* simulation approach.

The average value of the variable $\varphi_{EL,avg}$ can be used to tune simplified simulations to model the remaining years. The expected decline in $\varphi_{FC,avg}$ and $\varphi_{EL,avg}$ can be estimated according to a method proposed in the following sections (3.4.2 and 3.4.3).

- **BESS capacity decline**: Due to degradation effects, the actual battery capacity "shrinks" in time with the cyclic operation. The battery model used in the complete simulation updates every day the capacity of the battery. At the end of the simulated year, the yearly degradation of battery capacity (SOH_{fin1}) can be estimated. According to the method proposed in the next section (3.4.1), this value can be used to estimate the decline of the BESS available capacity.
- **Components lifetime**: From the yearly degradation of the operating voltage of the electrolyzer and the fuel cell, and the degradation of the SOH of the battery, the expected lifetime of components can be estimated. This estimation allows to understand when the electrolyzer stack, fuel cell stack, and Li-ion battery modules must be substituted. Premature substitutions not only have a considerable impact on the economic outcome of the system, but also affect the technical operation: new stacks will be characterized by higher conversion factors and new BESS modules will have higher capacities.

Several complete simulations over 20 years of operation have been run using the *c20* approach to obtain data about the degradation of components and the trend of average performance indicators in time. Those trends have been studied and analyzed in depth to obtain functions that allow the estimation of the future evolution of key parameters only using results from a single year of complete simulation.

3.4.1. Battery SOH trend

Several configurations involving different battery sizes were tested by means of a complete simulation over 20 years of operation. Points in Fig. 10 are the scatter plots of the SOH at the end of each year simulated by a complete simulation (*c20*).

As described in Section 3.2.5, the battery activation in time produces a cyclic degradation that damages the component. The evolution of the SOH of the BESS can be expressed as a function of time (t). The obtained fit is close to the scatter of data coming from the complete simulation, meaning that the trend can be well described by a function as Eq. 22.

$$SOH = a \cdot t^{1.06} + 1 \tag{22}$$

where the parameter a depends on the battery size and the specific operation and can be obtained from the fit of the proposed curve (Eq. 22). A fit of this curve requires at least three points. A method for estimating the required three points using the final SOH at the end of the first year of complete simulation SOH_{fin1} was developed.

The first point describes the condition of a brand-new battery (year 0), while the second point describes the condition of the BESS at the end of the first year of operation (year 1). A third point can describe the condition after six months of operation (year 0.5).

To determine the third point without extrapolating the whole SOH evolution during the year, a correction (*corr*) must be computed as a function of the initial battery's capacity (C_{bess}). From results coming from 20 years of complete operation, the correction shows indeed a linear dependence from the C_{bess}. This line can be used to estimate *corr* in each case as in Eq. 23, whose parameters were also obtained from the study of results of complete simulations.

$$corr = \left(-5.42 \cdot 10^{-7}\right) \cdot C_{bess} + \left(7.63 \cdot 10^{-7}\right) \tag{23}$$

Table 5 reports the coordinates of the three points required for the curve fit. The lines in Fig. 10 show the extrapolated evolution that can be estimated by following the proposed method that only requires computing the SOH at the end of the first year of operation.

To summarize, the method proposed here to predict the evolution of the battery's SOH requires two inputs:

- The initial capacity of the battery (C_{bess})
- The SOH after one year of operation (SOH_{fin1}), available after the simulation of the first year using the complete simulation method.

The method outputs the list of nineteen SOH values that will characterize the operation during the nineteen remaining years. The trend of the average BESS capacity that the set of simplified simulations in the *hybrid* approach require as input is obtained by the SOH trend.

3.4.2. Electrolyzer conversion factor trend

As for the SOH of the BESS, the set of simplified simulations requires the average conversion factor of the electrolyzer ($\varphi_{el,avg}$) to estimate the average performance in converting electricity into hydrogen. The results from the 20 years of complete simulation (scatter data in Fig. 13) have shown that $\varphi_{el,avg}$ is characterized by a particular evolution in time, trivial to directly estimate. Therefore, this parameter must be analyzed by considering the two main factors influencing the variation of φ_{el}.

As reported in the description of the complete model of the electrolyzer, the efficiency of the device is affected by time and temperature degradation. The time degradation affects the conversion factor at the nominal temperature φ_{el,T_nom}. The $\varphi_{el,avg}$ can thus be obtained by subtracting from φ_{el,T_nom} a delta $\Delta\varphi_{el}$ that represents the effect of the average cool-down that the device faces during the operation (Eq. 24).

$$\varphi_{el,avg} = \varphi_{el,T\_nom} - \Delta\varphi_{el} \tag{24}$$

Points in Fig. 11 show the scatter of the φ_{el,T_nom} of the electrolyzer due to time degradation. Fig. 11 (a) considers a variation in the electrolyzer power, while Fig. 11 (b) considers a variation in the BESS size.

The evolution of the conversion factor at nominal temperature φ_{el,T_nom} depends on time degradation and, consequently, on the number of hours that the electrolyzer work during a year. A linear dependence on time (t) *has been hypothesized (Eq. 25).*

$$\varphi_{el,T\_nom} = m \cdot t + q \tag{25}$$

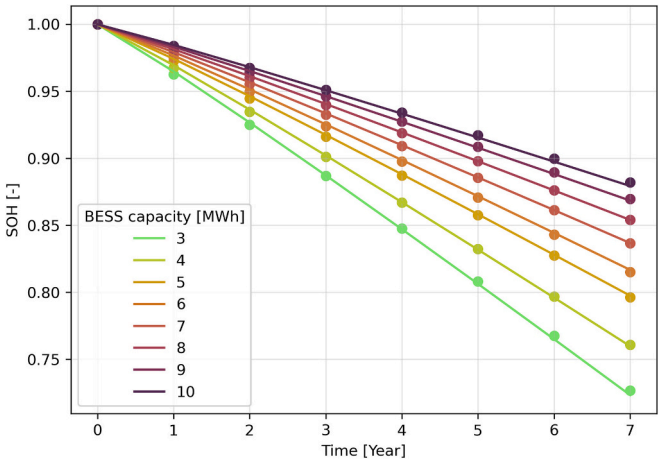

Fig. 10. Battery degradation trend. Points are the scatter plot of the SOH at the end of each year simulated by a complete simulation (*c20*), while lines represent the proposed fit.

Table 5
Required points for the SOH time evolution fit.

t [year]	SOH [−]
0	1
0.5	$\frac{1 + SOH_{fin1}}{2} + corr$
1	SOH_{fin1}

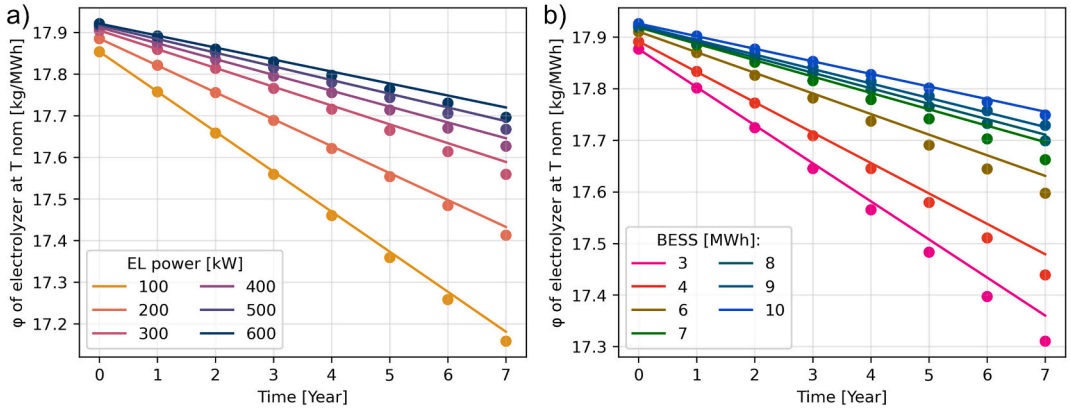

Fig. 11. A scatter of the resulting and plot of the estimated trend of the φ_{el,T_nom} of the electrolyzer due to time degradation. Variation considering a) different electrolyzer sizes and b) different BESS sizes.

Table 6
Required points for the φ_{el,T_nom} time evolution fit.

t [year]	SOH [−]
0	17.95
1	φ_{el,T_nom1}

The gradient (m) and the intercept (q) of this line can be obtained by the fit of Eq. 25 on the two points in Table 6. The first point refers to the new stack condition. The second point corresponds to the condition at the end of the first year of operation.

Lines in Fig. 11 show the obtained trend of the φ_{el,T_nom} of the electrolyzer from the proposed fit, on results from complete simulations that consider different electrolyzer sizes (a) and different battery sizes (b).

Points in Fig. 12 are the scatter of the $\Delta\varphi_{el}$ of the electrolyzer due to thermal degradation. Fig. 12 (a) considers a variation in the electrolyzer power, while Fig. 12 (b) considers a variation in the BESS size.

The analysis of results from the 20 years of complete simulation has shown that there is a correspondence between the $\Delta\varphi_{el}$ due to the average cooling of the electrolyzer and the SOH of the battery: with the decrease of SOH, the available battery capacity shrinks, and, to compensate, more energy must be fed to the electrolyzer for hydrogen production. This effect increases the utilization factor of the electrolyzer and mitigates the cool-down of the stack. Thus, the $\Delta\varphi_{el}$ to be subtracted from the φ_{el,T_nom} decreases with the SOH of the battery and slows down the decrease of the $\varphi_{el,avg}$.

A linear fit represents quite well the trend of the $\Delta\varphi_{el}$ with the SOH of the BESS. This line (Eq. 26) can be obtained by considering the state at the end of the complete simulation of the first year of operation ($\Delta\varphi_{el1}$ at $SOH_{fin,1}$).

$$\Delta\varphi_{el} = 1.1\cdot\left(SOH + SOH_{fin,1} \right) + \Delta\varphi_{el1} \tag{26}$$

The slope factor of 1.1 was again obtained by the fit of results from the complete simulations. The SOH trend is known after the application of the method proposed in the previous section.

Finally, lines in Fig. 13 compare the obtained trend for the $\varphi_{el,avg}$ with the scatter of points from the 20 years of complete simulation, considering different electrolyzer sizes (a) and different battery sizes (b). The comparison shows that the superposition of the considered effects and the proposed fits well describes the overall behavior of the electrolyzer.

The method proposed here can be used to estimate the evolution of the average conversion factor of the electrolyzer and requires estimating:

- The evolution of the SOH of the battery that supports the operation (previous method).
- The conversion factor at rated temperature after one year of operation ($\varphi_{el,T_{nom1}}$), available after the simulation of the first year using the complete simulation method.
- The difference between the $\varphi_{el,T_{nom1}}$ and the $\varphi_{el,avg}$ during the first year of operation ($\Delta\varphi_{el1}$), also available after the simulation of the first year using the complete simulation method.

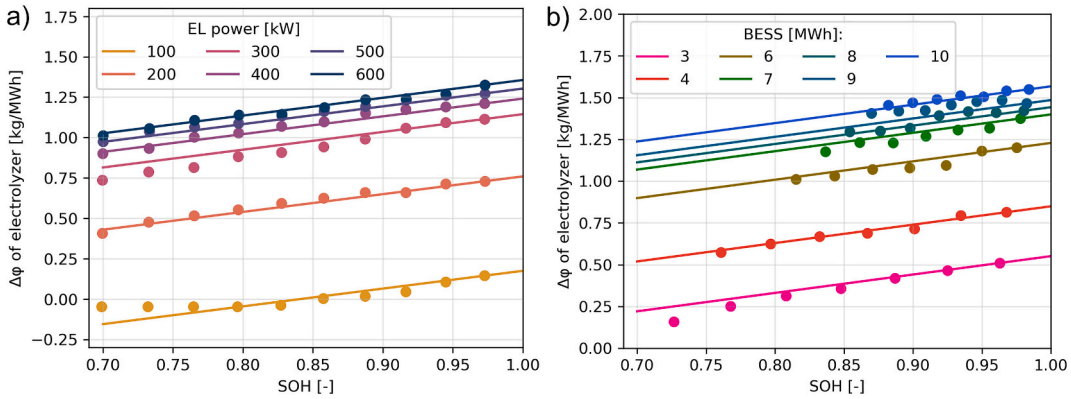

Fig. 12. A scatter of the resulting and plot of the estimated trend of the $\Delta\varphi$ of the electrolyzer due to temperature effects. Variation considering a) different electrolyzer sizes and b) different BESS sizes.

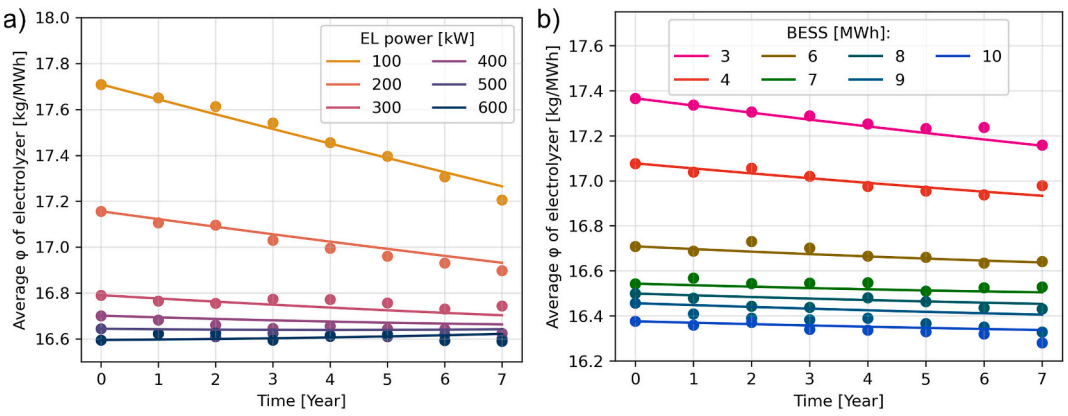

Fig. 13. The trend of the average φ of the electrolyzer due to time degradation and temperature effects. Variation considering a) different electrolyzer sizes and b) different BESS sizes.

3.4.3. *Fuel cell conversion factor trend*

The points in Fig. 14 show the scatter of the average φ of the fuel cell due to time degradation and temperature effects, varying the BESS size.

The $\varphi_{fc,avg}$ degrades with time and follows an exponential evolution (Eq. 27). The fit requires the computation of the average performance of the fuel cell during the first year of operation ($\varphi_{fc,avg1}$).

$$\varphi_{fc,avg} = k \cdot t^{1.25} + \varphi_{fc,avg1} \tag{27}$$

The analysis of results from the 20 years of operation has shown that the parameter k can be expressed as a function of the initial BESS capacity (C_{bess}), as in Eq. 28:

$$k = \frac{700 \cdot e^{-0.386 \cdot \frac{C_{bess}}{1000}}}{1000} \tag{28}$$

Curves in Fig. 14 compare the obtained trend with the scatter of the φ of the fuel cell. In this case, an accurate prediction of the $\varphi_{fc,avg}$ can be obtained by:

- knowing the capacity of the battery that supports the operation (C_{bess})
- computing the value of the conversion factor after the first year of operation ($\varphi_{fc,avg1}$), available after the simulation of the first year using the complete simulation method.

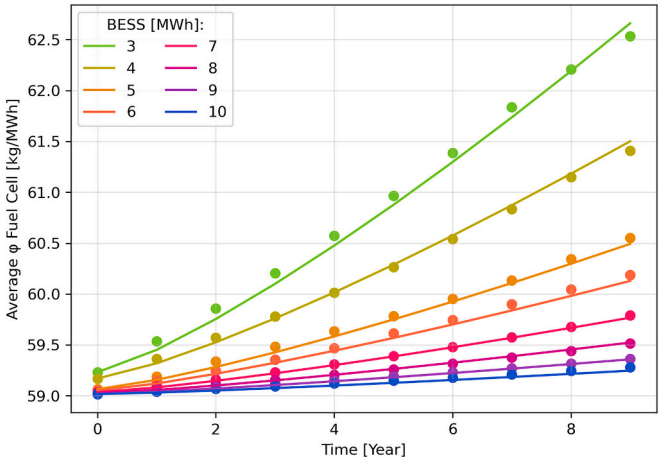

Fig. 14. The trend of the average φ of the fuel cell due to time degradation and temperature effects, varying the BESS size.

3.5. *Optimization framework*

The proposed optimization framework uses the *hybrid* simulation approach to simulate the long-term behavior of the system and to evaluate:

1. if the power generators and storage devices can satisfy the island load demand (E_{island}).
2. the degradation of components to understand if they must be prematurely substituted.
3. optimize the sizing of components to minimize the cost of providing energy to the island.

3.5.1. *Self-sufficiency degree*

The combinations of energy generation and storage considered in the current work must provide the island with all the energy required. In other words, the self-sufficiency degree (SSd - defined as in Eq. 21) must be 100 %.

$$SSd = \frac{E_{delivered}}{E_{requested}} \cdot 100 \tag{21}$$

During the optimization of sizes of components, it is key to consider the degradation of performance that the storage device has in time. Over the 20 years of operation, the SSd of the system can decrease when the battery capacity shrinks, or when the electrolyzer and the fuel cell become less efficient. At the time of substitution of stacks and modules, the performance parameters return to their initial value.

To ensure that the proposed solutions are able to maintain the full SSd for the whole lifetime of the system, a high price is attributed to residual deficit energy. In this way, the techno-economic optimization combinations unable to reach 100 % SSd.

3.5.2. *Levelized cost of required energy*

The optimization should consider only combinations able to cover the whole energy demand of the island (E_{isalnd}) and aims find the system configuration that minimizes the cost of each MWh that the HESs should deliver to the load, i.e., the SSd of all considered solutions must be 100 %. In this sense, the objective is to minimize a cost metric that expresses the cost of delivering the required energy at the instant of request.

A standard Levelized Cost Of Energy (LCOE) is not suitable for this purpose, since this cost metric considers the gross amount of energy produced from a generator, without accounting for the instant of production. Consequently, the Levelized Cost of Required Energy (LCORE), expressed as in Eq. 20, was introduced.

$$LCORE = \frac{\sum_{t=0}^{T} \frac{CAPEX + OPEX}{(1+r)^t}}{\sum_{t=0}^{T} \frac{E_{island}}{(1+r)^t}} \quad (20)$$

In the denominator, the LCORE considers only the energy fed to the load from the island, thus accounting for the time match between RES production and demand.

The economic analysis was performed considering average prices of components obtained by averaging several literature sources. Section 3.6 summarizes the main economic assumptions, while the complete market analysis is in Appendix A. CAPEX and OPEX of the various tested configurations were calculated considering the economic assumptions summarized in Table 7.

The capital expenditures (CAPEX) include the investment cost for the whole system (I_0), comprising the wind turbine, the PV field, the Li-ion BESS, the alkaline electrolyzer, the PEM fuel cell, the H_2 tanks, and the H_2 compressor. Moreover, the OPEX and the premature substitutions of parts of components were computed as a percentage of the initial investment of the corresponding component (I_0).

The considered time horizon for the investment (T) is set at 20 years. As depicted in the description of models of components (Section 3.2), the premature substitution of the stacks of the electrolyzer and the FC, and modules of the BESS are accounted for if precise operating conditions are reached during cyclic operation or time effects. Otherwise, replacement is forced after 10 years of operation based on industrial experience.

Renewable energy installations aiming at decarbonizing the energy supply of remote or rural areas may benefit from financial support from governments or supranational institutions. In their review of hybrid renewable mini-grids on non-interconnected small islands, Eras-Almeida and Egido-Aguilera [158] stated that incentives are required to reach the ambitious target of decarbonizing an island using RES. They compared projects developed all over the world and discovered that only islands in developed countries succeeded in the decarbonization process, while least developed islands must strengthen their regulatory framework and define suitable business models to reach the same targets. Consequently, this analysis considers a low-risk investment characterized by an interest rate r of 3 %.

3.5.3. Optimization algorithm

The shape of a function describing the techno-economic outcome of an HESs may present several local minima. A stochastic optimization algorithm was used to solve this issue. To achieve this goal, a differential evolution algorithm was implemented through the *differential_evolution* library [159] from the *SciPy* package on Python [160]. Among the various options, this optimization tool was chosen due to the ease of parallelizing the computation and enforcing integer constraints on the variables. Results from this algorithm were validated by comparison with the outcome from other optimization techniques such as the Particle Swarm Optimizer (PSO).

The differential evolution algorithm optimizes simultaneously five variables i.e., the sizes of the PV field, the Li-ion BESS, the ALK electrolyzer, the PEM fuel cell, and the high-pressure H_2 tank. Since those components cannot assume every possible value in the considered size range for commercial reasons, these variables were forced to assume integer values. The optimal combination of the five components is the configuration that minimizes the LCORE of the system, over 20 years of operation.

Due to computational reasons, it was unfeasible to include inside the optimization algorithm a simulation of 20 years of operation with a 1-min time resolution using the complete model of all considered components (*c20*). On the other hand, the proposed *hybrid* simulation framework (Section 3.4) is compatible with the stochastic optimization framework since the approach limits the required computational cost by combining a complete and complex simulation with simpler simulations. Fig. 15 shows the flowchart of the proposed optimization framework and the simulation logic based on the *hybrid* simulation framework that incorporates.

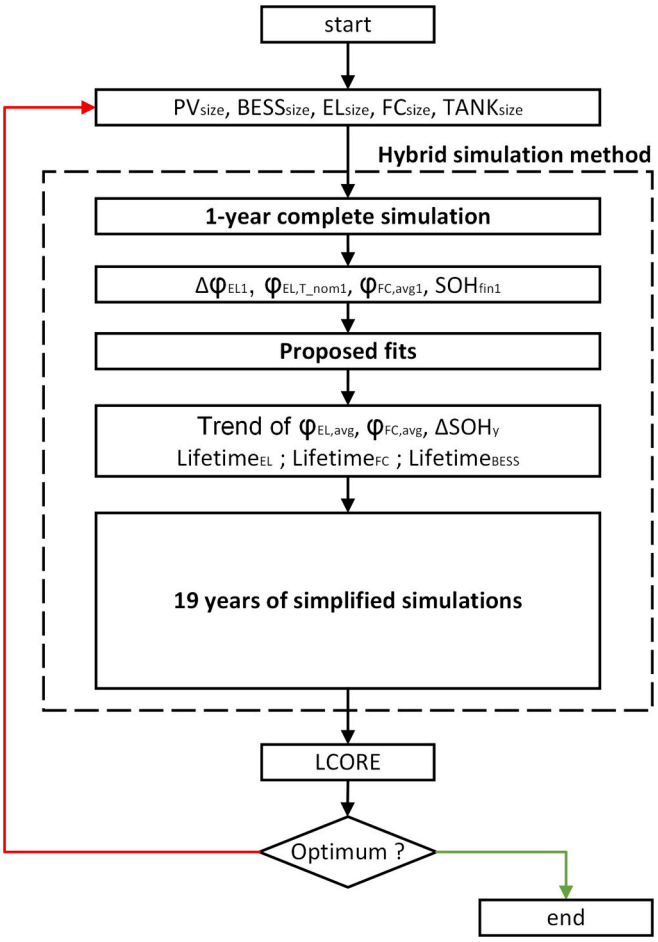

Fig. 15. Flowchart of the logic that the proposed optimization framework follows.

3.6. Components prices and economic assumptions

This analysis considers current generators and storage devices prices obtained after an extensive literature and market review. The complete list of sources considered for each component is reported in Appendix A.

The average prices, the OPEX, the substitution costs, and the maximum lifetime for each component are summarized in Table 7. Premature substitutions of the Li-ion BESS modules, fuel cell stack, or electrolyzer stack are considered if the thresholds outlined in the previous sections are reached before the end of life (Max Lifetime) of components.

Table 7
Main components costs.

Component	Specific cost	OPEX (% I_0)	Subst. cost (% I_0)	Max Lifetime
Wind Turbine	1509 €/kW	2.5 %	–	20 y
PV field	1080 €/kW	2.5 %	–	20 y
Li-ion BESS	298 €/kWh	2.5 %	80 %	10 y
ALK electrolyzer	883 €/kW	2.75 %	40 %	10 y
PEM FC	958 €/kW	2.75 %	40 %	10 y
H_2 compressor	1200 €/kW	2.5 %	–	20 y
H_2 Tanks	464 €/kg	1 %	–	20 y

4. Results

This section outlines the results coming from the application of the proposed novel method.

First, results from the comparison between three simulation methods based on standard approaches (*c1*, *c20*, and *simplified*) and the novel method (*hybrid*) are presented. Two possible configurations of the proposed HES were selected to perform a long-term analysis using the four considered simulation strategies. Then, results from the application of the new proposed *hybrid* method to the case study of the island of Tilos are reported. Those results enable the assessment of the computational cost and the accuracy of the method, and the impact of degradation while performing an actual sizing optimization.

The self-sufficiency degree that can be reached with only an increase in PV generation is analyzed to confirm the importance of including storage devices in the selected case study. Then, the effect that the introduction of a BESS has (first scenario) is presented. Finally, the hybrid storage that combines BESS with P2G2P is introduced and the results from the complete optimization framework (second scenario) are presented.

Global results outlined from the newly proposed simulation method are compared to results from the complete method (*c20*) to assess the accuracy of the proposed approach. Results from sensitivity analyses are also compared with results from the *simplified* method to highlight the error that two common simulation approaches may commit while evaluating the long-term performances of HESs. Insights about the potential impact of neglecting component degradation are detailed in Section 5.

4.1. Comparison between different simulation approaches

The long-term evolution of performance indicators resulting from the application of the *hybrid* simulation framework was compared with the outcome from the three standard methods presented in Section 3. Fig. 16 shows results from of the four methods when applied to simulate the same configuration involving a 300 kW electrolyzer, a 900 kW fuel cell, a 5 MWh BESS, a 2800 kg H_2 tank, and a PV power of 1760 kWp.

The trend outlined by *c20* serves as the reference and the accuracy of the other three methods is evaluated by comparing their result to this reference.

- Fig. 16 (a) shows the evolution of the yearly average conversion factor of the electrolyzer ($\varphi_{el,avg}$). The *simplified* simulation considers a constant φ equal to the nominal value. The *c1* simulation considers time and temperature effects and draws near to the actual behavior. The *hybrid* simulation considers the time degradation across the 20 years of operation, but slightly underestimates the performance. However, the absolute value of differences is negligible.
- Fig. 16 (b) shows the evolution of the yearly average conversion factor of the fuel cell ($\varphi_{FC,avg}$). Again, *c1* has an advantage over *simplified* simulation since this approach considers a higher φ due to time and temperature degradation. However, only the *hybrid* simulation can capture the increasing trend that characterizes the operation.
- Fig. 16 (c) shows the evolution of the yearly average capacity of the battery (C_{bess}). The outcome from different simulation approaches is

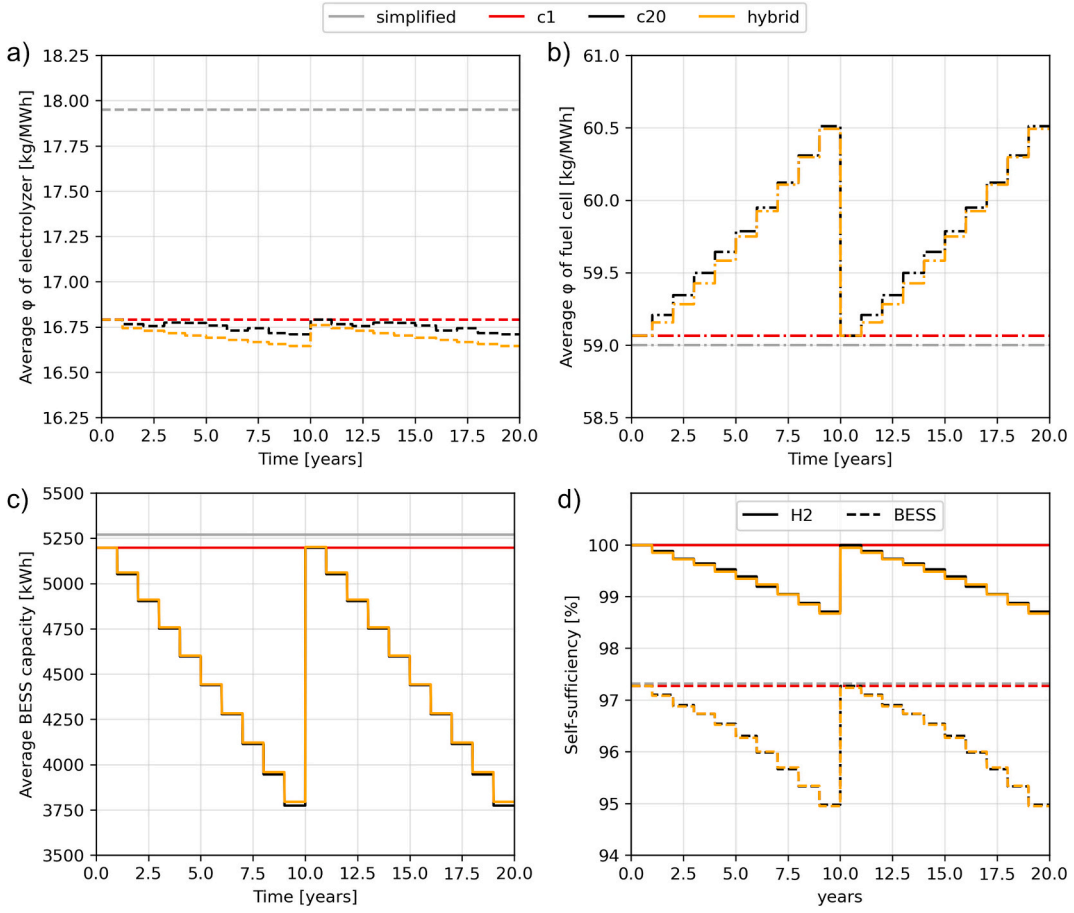

Fig. 16. Comparison between the time variation of a) average electrolyzer conversion factor, b) average fuel cell conversion factor, c) average BESS capacity, d) self-sufficiency due to battery effect and P2G2P effect.

similar to the previous case, even though the *hybrid* estimation is even closer to the actual one this time.

- Fig. 16 (d) shows the evolution of the self-sufficiency that the system can reach due to the BESS introduction (dashed lines) and P2G2P introduction (solid lines). This graph shows the result that the working parameters have on the general performance of the system. Only the *hybrid* approach can correctly estimate the actual drop in SSd.

Fig. 17 shows another comparison between the time variation of key performance indicators. In this case, the simulations were applied to the same configuration considered in Fig. 16 but with a smaller battery capacity (3 MWh). A smaller BESS causes a higher degradation of the component and a premature substitution of the modules. The *hybrid* simulation approach succeeded in capturing the degradation trend of the SOH (Fig. 17 (c)), and in estimating the correct lifetime of the modules, key in the correct assessment of the substitution cost of the component. The *hybrid* method was also able to follow the peculiar trend of the $\varphi_{el,avg}$, affected by the fast decline of the SOH and the premature substitution of BESS modules.

Twenty-three configurations were simulated using the most accurate approach (*c20*), testing different electrolyzer sizes, fuel cell sizes, battery sizes, and PV power levels. Then, the same configurations were simulated using the other three approaches (*simplified*, *c1*, and *hybrid*). Finally, the difference between results coming from each of the three previous simulation methods and results from *c20* was analyzed to understand the degree of error that affects the electrolyzer and fuel cells conversion factors, the BESS capacity, and the self-sufficiency that the system can reach using batteries and P2G2P.

Table A8 and Table A9 in Appendix B report the full list of the tested configurations and all the corresponding errors, while Table 8 summarizes the results by reporting the average error that characterizes each simulation approach. For the sake of the comparison, results from simulations that reach 100 % H_2 self-sufficiency were not considered for the average results of such error.

Fig. 18 compares the required computational time to complete 20 years of simulation by using the *simplified*, *c1*, *c20*, and *hybrid* framework. The *simplified* framework only requires 5 s to complete the simulation of one configuration and compute the LCORE. If complete models are employed, the simulation time rises to 71 s with the *c1* method. If all 20 years of operations are simulated, this time becomes 20 times bigger i.e., 1481 s (almost 25 min). The *hybrid* simulation can capture the effects that the degradation of components has on the results but reduces the computational time to 169 s (88.5 % less than the *c20*).

Table 8
Average error on key performance indicators and self-sufficiency assessment from *simplified*, *c1*, and *hybrid* simulations approaches.

Avg. error	Electrolyzer φ [%]	Fuel Cell φ [%]	Battery Capacity [%]	BESS SSd [%]	H_2 SSd [%]
simplified	7.281	1.181	14.862	0.959	0.467
c1	0.384	1.052	14.862	0.911	0.456
hybrid	0.244	0.069	1.466	0.014	0.015

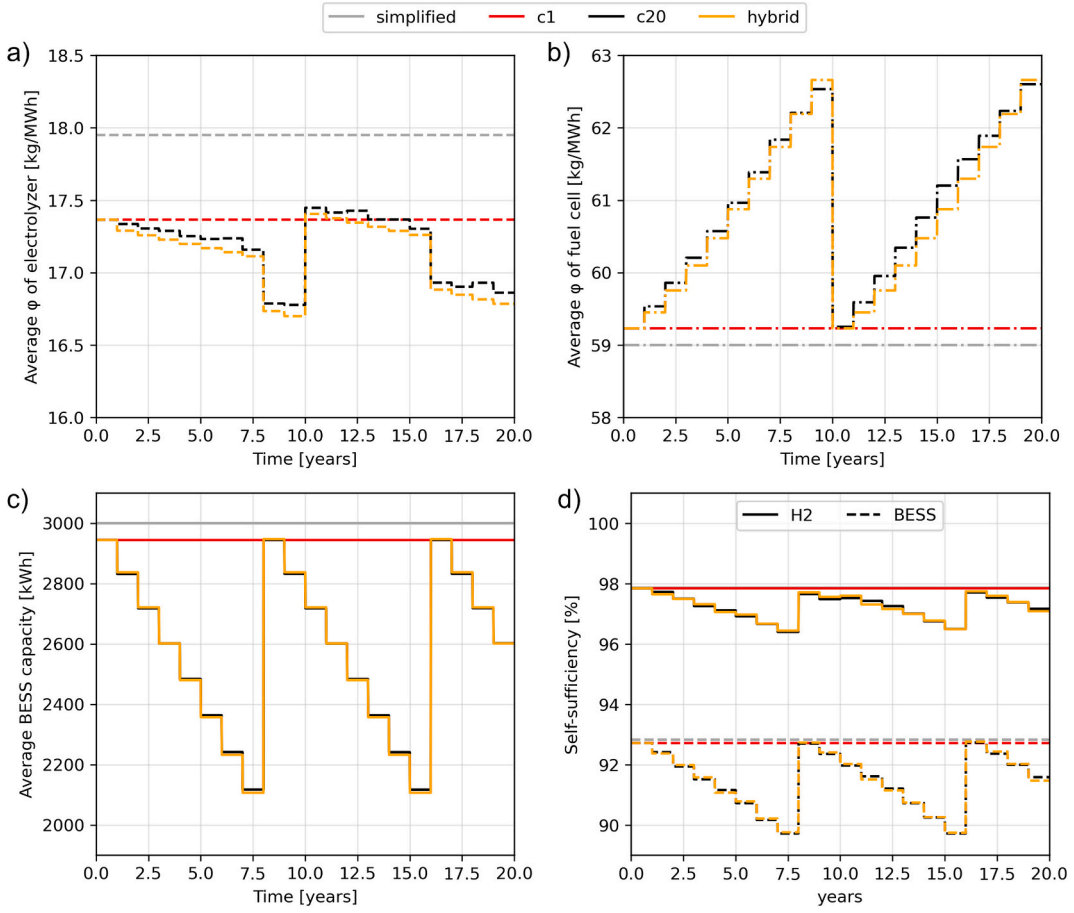

Fig. 17. Comparison between the time variation of a) average electrolyzer conversion factor, b) average fuel cell conversion factor, c) average BESS capacity, d) self-sufficiency due to the battery effect and P2G2P effect.

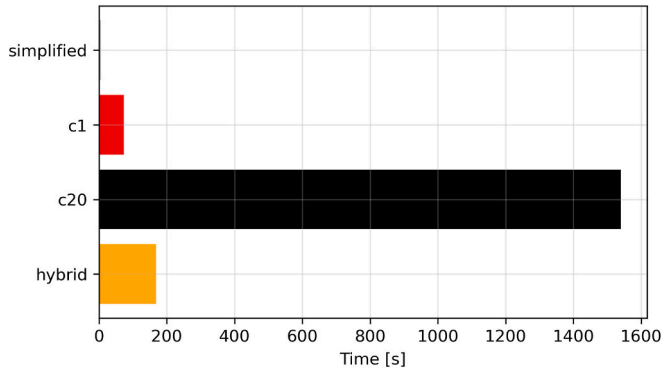

Fig. 18. Comparison between computational times required by *simplified*, *c1*, *c20* and *hybrid* simulation methods.

4.2. Optimization results

After the evaluation of the accuracy of the novel *hybrid* method and the potential time reduction, this section presents results from the application of the proposed optimization framework that involves the new simulation method.

Table 9 summarizes the main technical assumptions made, lists the size range that bounds the global optimization of components, and defines the resolution used to find integer results. As stated in Section 3.5.3, integrality was forced to variables to obtain a realistic solution that involves only commercially reasonable sizes for components.

4.2.1. PV expansion

The analysis presented in this section aims to study the maximum contribution that the upgrade of the PV generation can have. To this end, sizes up to 8 MWp are considered, two times higher than the maximum size limit set for the global optimization (Table 9). Fig. 19 shows the SSd that the system can reach by increasing only the PV installed power. With only the increase in power production, SSd saturates at a value of around 77.5 %.

The SSd trend in Fig. 19 shows that the introduction of a storage system is required. Although the PV production has a higher matching degree with the power consumption with respect to wind generation, the RES generators alone are unable to cover the load demand of the island. Even when capacities fifty times the current one are installed, the SSd cannot reach 100 % in absence of an ESS.

4.2.2. System supported by the lithium-ion BESS – Scenario 1

The first scenario considers only the possibility of expanding the current PV field up to 4 MWp and introducing a Li-ion BESS up to 25 MWh. Table 10 reports results from the size optimization using the differential evolution algorithm considering average component prices listed in Appendix A.

Optimizations required from 1425 to 1650 iterations to converge, with a computational time between 14 and 17 h. Optimal configurations were tested also using the most accurate approach (*c20*) to ensure if the computed LCORE is reasonable.

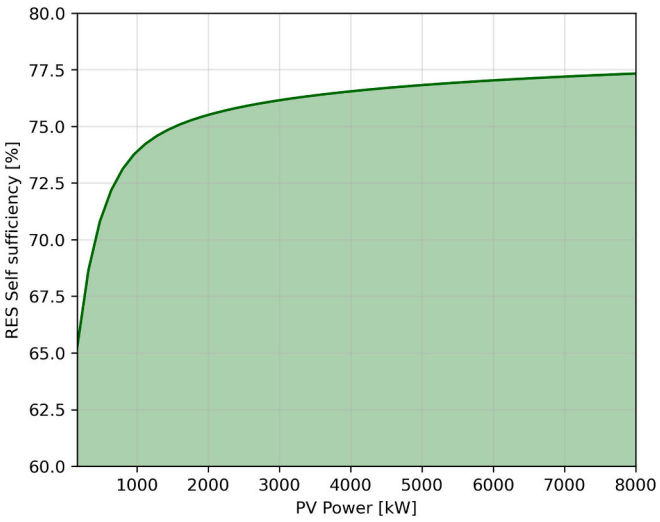

Fig. 19. Self-sufficiency degree of the HPS increasing the PV installed power (no storage means).

Table 10
Results from the size optimization considering the system supported only by BESS.

BESS [MWh]	PV [kWp]	LCORE [€/MWh]	LCORE (*c20*) [€/MWh]	Iter. [−]	Time [h]
15	2610	320.85	319.78	1425	14.4

The minimum LCORE that the system can reach when supported only by a BESS is 320.85 €/MWh. The optimal configuration involves a 15 MWh battery and the increment of the PV peak power to 2610 kWp, 2450 more than the current configuration.

Results presented in Table 10 came from an optimization that poses no limit to the optimal PV power capacity. However, geographical constraints or technical requirements may restrict the maximum power generation capacity that the system can have. Therefore, this section presents results from a sensitivity analysis that aims to investigate the optimal storage combination at different installed PV power levels. Again, this level indicates the PV peak power that adds to the WT generation (800 kW).

Fig. 20 compares the LCORE that a system supported only by BESS can reach varying PV installed power. The analysis considers prices averaged from references listed in Appendix A. Even if the tested PV power levels range from 160 to 4160 kW, with a resolution of 160 kW, Fig. 20 does not show results from configurations that involved a PV power lower than 1440 kW. Low PV power configurations would indeed

Table 9
Technical assumptions of the main components of the system: Wind Turbine, PV field, Li-ion BESS, ALK electrolyzer, PEM fuel cell, H_2 compressor, and H_2 tank.

Component	Characteristics	Technical parameters	Considered size range in global optimization	Resolution in global optimization
Wind Turbine	real prod.	–	800 kW	–
PV field	real prod. (scaled)	–	0–4.16 MW	10 kW
Li-ion BESS	model (ideal)	$\eta_{avg} = 90$ % C-rate$_{charge} = 1$C C-rate$_{discharge} = 3$C	0–25 MWh	50 kWh
ALK electrolyzer	model (comm.)	$\varphi_{EL,init} = 17.95$ kg/MWh $P_{min} = 20$ % P_{nom}	0–700 kW	50 kW (5 cells)
PEM FC	model (comm.)	$\varphi_{fc,init} = 59$ kg/MWh	0–1.2 MW	65 kW (5 stacks)
H_2 compressor	model (ideal)	Es = 1.18 kWh/kg	50 kW	–
H_2 Tank	model (ideal)	–	0–10 t	100

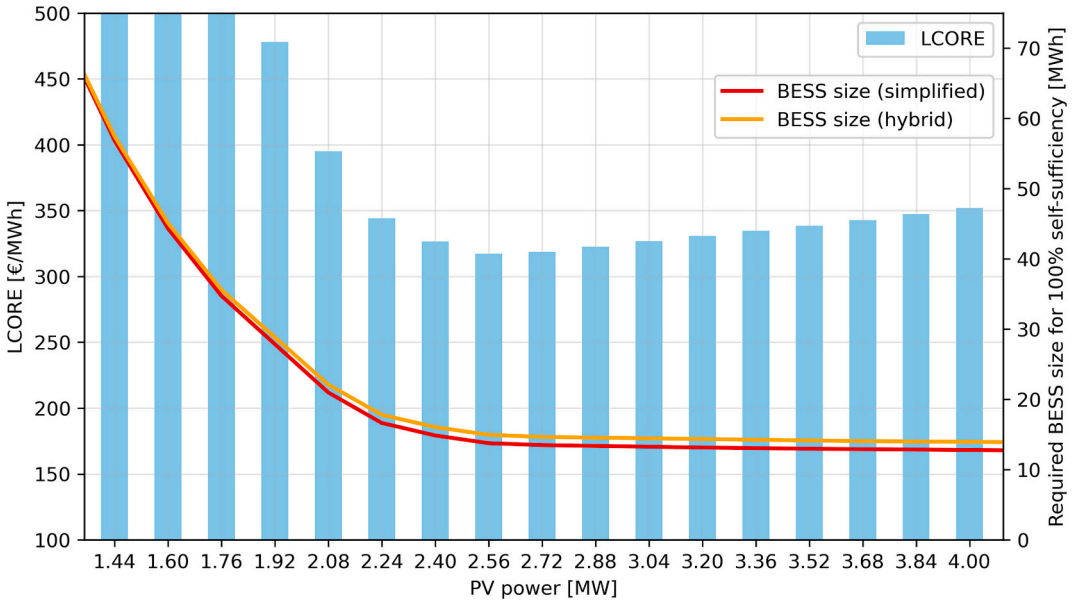

Fig. 20. Minimum LCORE and required BESS size varying the PV installed power.

require an economically unsustainable BESS capacities to reach full SS.

The orange line in Fig. 20 indicates the optimal BESS size at each considered PV power level. Initially, the optimal BESS size strongly decreases with the increase in the PV installed power. However, when the PV power reaches 2.4 MW, the optimal BESS size stabilizes at around 14–15 MWh. This represents the minimum BESS capacity required to support the system in reaching 100 % self-sufficiency. When the contribution of installing additional PV modules stops having a tangible impact on the SSd, the BESS becomes the only way to cover the residual demand. The minimum of the LCORE indeed corresponds to the point at which the optimal BESS size starts saturating. The minimum is reached with a PV size of 2560 kW and a BESS size of 14,950 kWh.

The red line in Fig. 20 indicates instead the optimal BESS size according to the *simplified* simulation. Results show that the *simplified* method inevitably underestimates the required BESS size: by neglecting the BESS degradation, the optimization using the *simplified* method outputs configurations unable to maintain 100 % self-sufficiency in the long run. The *hybrid* simulation, on the other hand, considers that additional capacity is required to maintain the performance in time.

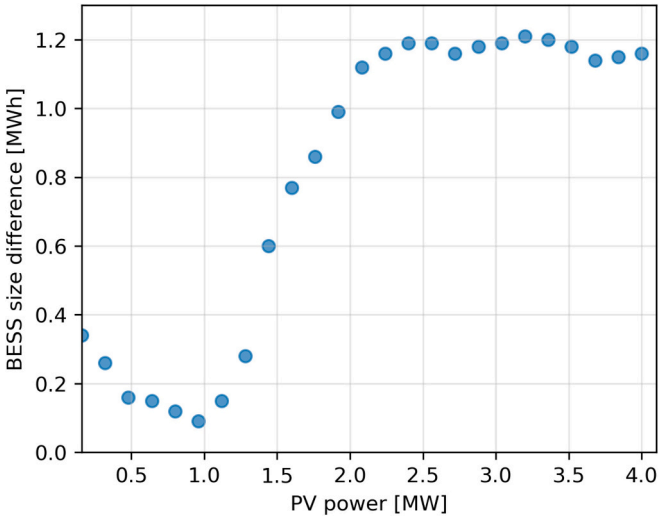

Fig. 21. Difference in optimal BESS size according to optimization results based on *simplified* simulations and *hybrid* simulations.

Fig. 21 shows the scatter of the difference between the two outcomes. When the installed PV is small, both optimizations converge to a similar result. When the PV capacity increases and the BESS size decreases, the error made by the *simplified* method increases. An error of 1.2 MWh on a BESS capacity of around 14.5 MWh means that the required BESS capacity is underestimated by 8 % if the degradation of the component is not considered.

4.2.3. *System supported by BESS and P2G2P – Scenario*

The second scenario considers also the introduction of the P2G2P, along the upgrade of the PV generation and the introduction of the BESS. Table 11 reports results from the size optimization of the system supported by BESS and P2G2P.

Optimizations required from 2275 to 3450 iterations before reaching the target tolerance and, this time, the computational time took from 38 to almost 48 h.

Considering average prices (see Appendix A), the optimal solution consists of the installation of an 1810 kWp PV field, supported by a 6.7 MWh BESS. The P2G2P system produces hydrogen slowly during winter with a 250 kW electrolyzer and stores the gas in a 2000 kg hydrogen tank. Then, a high-power FC of 890 kW is required to cover the load during consumption peaks. With this configuration, the minimum LCORE that the system can reach is 264.55 €/MWh. The same configuration was simulated using the most accurate approach and produced a slightly lower LCORE (263.43 €/MWh).

This study presents a sensitivity analysis to assess the best HES configuration at different installed solar power levels also for the second scenario (BESS and P2G2P). The PV ranges from 800 to 4160 kW, again with a resolution of 160 kW. Similar to the first scenario (only BESS), configurations with a PV capacity lower than 800 kW were excluded due to the proven financial unfeasibility of solutions involving outsized storage capacities.

Fig. 22 presents the results from the economic analysis considering average prices from references in Appendix A. The plot shows the trend of LCORE (light blue line), optimal electrolyzer installed power (red line), hydrogen tank size (blue line), and Li-ion battery capacity (orange line) varying the PV installed power in the second scenario (BESS and P2G2P).

The minimum LCORE (264.29 €/MWh) is next to the one provided by the unbounded optimization. This configuration involves 1760 kW PV power, 200 kW electrolyzer, 890 kW FC, 2800 kg tanks, and a 7.1

Table 11
Results from the size optimization considering the system supported by BESS and P2G2P.

EL [kW]	FC [kW]	BESS [MWh]	Tank [kg]	PV [kWp]	LCORE [€/MWh]	LCORE (*c20*) [€/MWh]	Iter.	Time [h]
250	890	6.7	2000	1810	264.55	263.43	2275	38.3

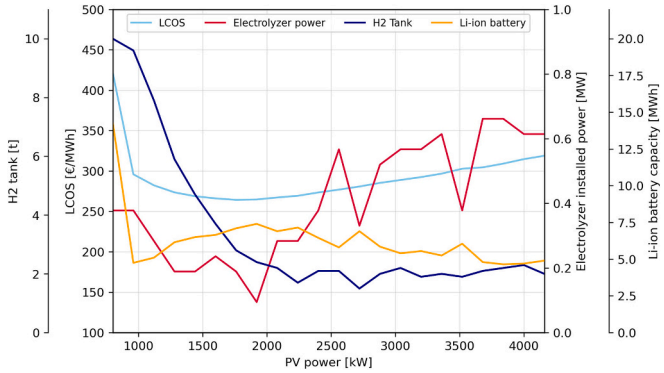

Fig. 22. The trend of LCORE (light blue line), optimal electrolyzer installed power (red line), hydrogen tank size (blue line), and Li-ion battery capacity (orange line) varying the PV installed power in the second scenario (BESS and P2G2P). (For interpretation of the references to colour in this figure legend, the reader is referred to the web version of this article.)

MWh BESS.

When the PV size is limited to 800 kW, the system can reach 100 % self-sufficiency using the combination of a large BESS (14.25 MWh) and a large H_2 tank (10 tons). Hydrogen is produced using a 400 kW electrolyzer, while the optimal fuel cell size is 945 kW. With this configuration, the LCORE is 421.17 €/MWh. The optimal BESS size drops when the PV power can reach 960 kW and, with higher PV power levels the optimal BESS size ranges around smaller sizes between 4.65 MWh and 7.4 MWh. The optimal configuration varies between layouts that rely more on BESS and layouts that use more the P2G2P. Overall, the electrolyzer size increases with the PV size. However, the solution highly varies between only 100 kW to 700 kW, depending on the size of the BESS that supports the operation. The optimal H_2 tank decreases with the PV size since a higher generation during summer reduces the deficit that P2G2P must cover. The decreasing trend of this variable is more pronounced but still presents a degree of variability. The LCORE trend drops to 295 €/MWh as soon as the PV size can reach 960 kW. Then, the cost metric gradually decreases until the optimal PV size is reached (1760–1920 kW). From those sizes on, the LCORE increases again since the overall optimal storage capacity is reached. The solution shifts between configurations that rely more upon BESS and configurations that value more P2G2P, but additional PV power generation is no longer economically convenient.

The left column of Fig. 23 shows the comparison between the optimal size of components according to optimizations based on *simplified* simulation (dashed lines) and *hybrid* simulation (continuous lines). The right column of Fig. 23 shows plots of the percentage error between the two. Even in this case, the *simplified* simulation approach led to an underestimation of the required components sizes to maintain 100 % self-sufficiency and a consequent error on the LCORE estimation.

4.2.4. Comparison between scenarios: "Only BESS" vs "BESS + P2G2P"

Fig. 24 compares the trend of the LCORE varying the PV installed power between the first scenario (only BESS) and the second scenario (BESS and P2G2P. Dots highlight the overall minimum that the price metric can reach in each condition. With each of the considered price combinations of components, the second scenario can reach a lower LCORE than the first scenario.

4.3. Energy flows before and after the application of storage devices

Fig. 25 shows the time variation of the energy deficit and excess before and after the application of the two storage systems: BESS and P2G2P. The analyzed configuration is the optimal result from the *hybrid* optimization when the maximum PV size is limited to 800 kWp, i.e., the lowest PV upgrade considered in the sensitivity analysis presented in section 4.3.1. Even if the BESS can cover most of the winter deficit, there is still a consistent residual demand during the summer season. The electrolyzer consumes most of the winter energy surplus to produce enough green hydrogen for seasonal storage. This H_2 feeds the fuel cell to cover the summer needs. After the introduction of the P2G2P, the energy deficit is reduced to zero (red flat line).

Fig. 26 shows the time variation of the energy flows involved in the optimal configuration when no constraints are applied to the PV size. This configuration involves an 1810 kWp PV field, in addition to the already present 800 kW wind turbine.

Fig. 27 shows the time variation of the SOC of the BESS (a) and the amount of hydrogen stored inside high-pressure tanks (b). As in Fig. 26, this figure refers to the optimal configuration found without constraints to the PV size. Fig. 27 (a) shows that the SOC trend varies between the maximum (15 %) and minimum (95 %) value for most part of the considered year of operation. On the other hand, Fig. 27 (b) shows that amount of H_2 stored in HP tanks continues to rise during winter and suddenly drops during summer.

5. Discussion

This study proposes a novel simulation method able to consider the long-term degradation of components, while limiting the computational cost of simulations. This trade-off allows the adoption of this kind of approach also by stochastic optimization algorithms that require several iterations before reaching the global minimum. Even if presented results are specific to the presented case study, the application allows general comments on the approach, as the computational time required in a real case study, the accuracy of the method, and the evaluation of the error that simulation methods that neglect the degradation effect may induce.

Fig. 16 and Fig. 17 have shown that the *simplified* simulation method and the one-year simulation approach that uses complete components models (*c1*) may attribute the 100 % self-sufficiency that the system can reach in the first year of operation to all the remaining years. However, results from the twenty-years long simulation using complete component models (*c20*) show that the actual behavior differs quite significantly from the ideal case. The decay of the SOH shrinks the available BESS capacity, the electrolyzer becomes less efficient in storing the excess energy in the form of hydrogen, and the fuel cell cannot convert the gas back into electricity with the same effectiveness as a brand-new device. A totally self-sustained system during the first year of operation may fail to reach total autonomy even from the second year on. Only the novel *hybrid* simulation approach can effectively capture the trend highlighted by *c20*.

Compared to results by Pu et al. [57], the resulting average lifetimes of the modeled electrolyzer and fuel cell stacks are longer: the optimization converges on combinations that allow the stack to work until reaching the expected 10 years before replacement (as in Fig. 16 and Fig. 17). The expected lifetime of the stack is closer to results from Le et al. [103]. These results affected by the kind of operation that this analysis considers: being paired with high-capacity BESSs, hydrogen chains work mainly as seasonal storages, diminishing the working hours

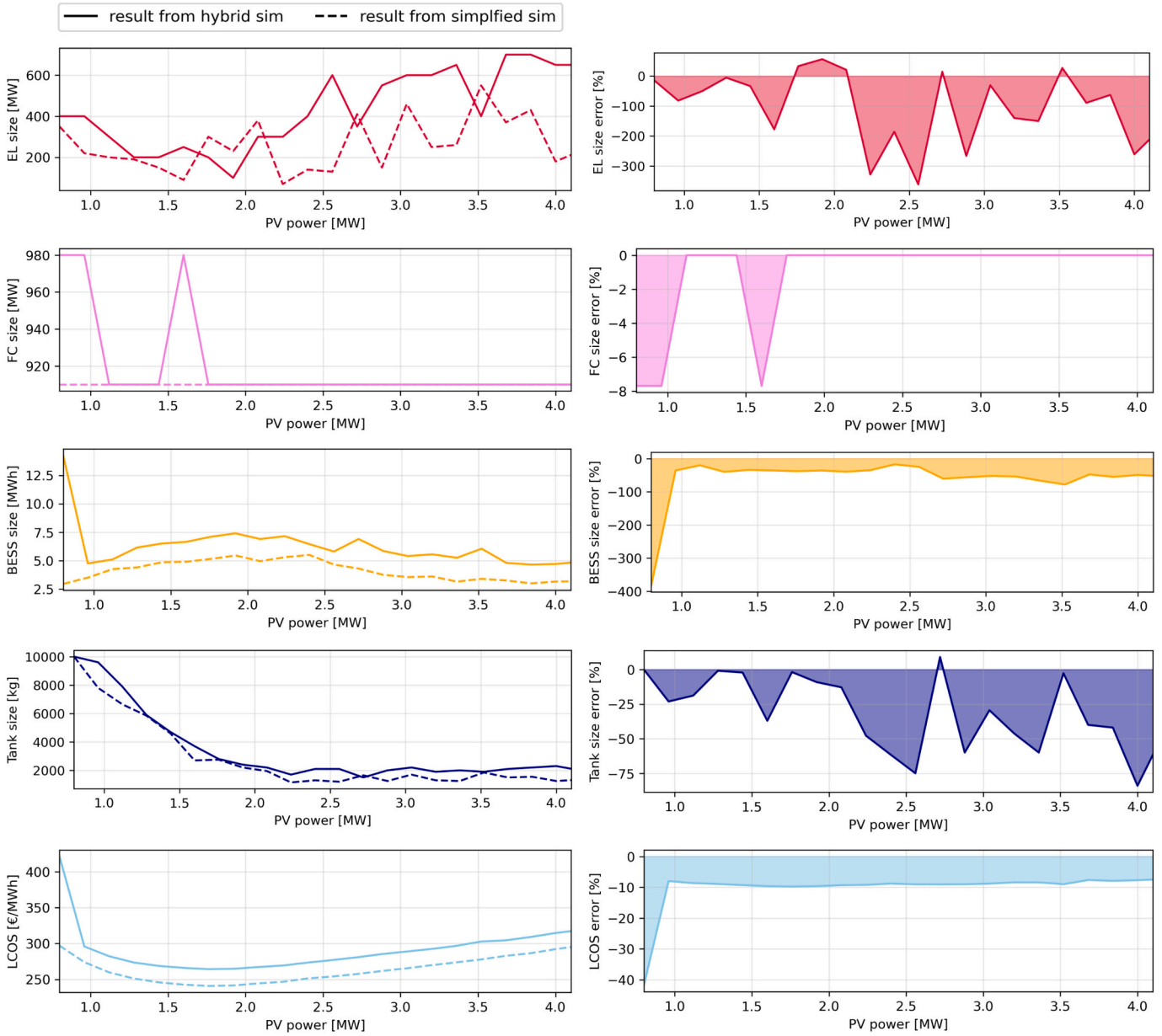

Fig. 23. Comparison between the optimal size of components according to optimizations based on *simplified* simulations and *hybrid* simulation (left column) and plot of the percentage error between the two (right column).

during a year of operation and thus extending the expected lifetime of components.

Results from Section 4.1 have also shown that the average outcome from the *hybrid* simulation is characterized by errors of at least one order of magnitude lower than outcomes from other approaches (Table 8 and Tables A8 - A9 in Appendix B). Both *c1* and *hybrid* performed well in estimating the average conversion factor of the electrolyzer ($\varphi_{el,avg}$), but only the novel approach was able to capture the actual trend of the BESS capacity. Overall, the accuracy of the *hybrid* simulation in estimating the self-sufficiency degree of the system is characterized by an error of only 0.015 %. Moreover, only the novel method was able to correctly evaluate the lifetime of components, crucial when assessing the actual techno-economic outcome of a HES configuration in the long term.

While maintaining a high accuracy, the *hybrid* simulation framework reduces the computational time of 85 % with respect to *c20* (Fig. 18). This reduction is necessary to perform HES sizing optimizations using stochastic methods as the differential evolution. Indeed, results from Table 10 and Table 11 have shown that the algorithm required to explore from 2250 to 3500 different configurations before reaching the selected tolerance.

Results from the application of the *hybrid* simulation method to the case study of the HES of the island of Tilos proved that the proposed approach can be used to evaluate the optimal design of a 100 % self-sustained microgrid. The application proved that the method is compatible with a stochastic optimization algorithm, required to avoid local minima.

The number of iterations required for the optimization algorithm to find the global optimum and the consequent computational time was evaluated both for analyses involving only PV expansion and battery (scenario 1 - Table 10) and analyses including also the hydrogen chain (scenario 2 - Table 11). Results highlighted the importance of reducing computational time: necessitating from 1424 iterations (14 h) to 2275 iterations (38 h on a supercomputer), these types of problems may highly benefit from the newly proposed approach. The comparison in Fig. 18 indicates that the *hybrid* method requires 88.5 % less time to simulate 20 years of operation. This means that, if an approach as *c20* is

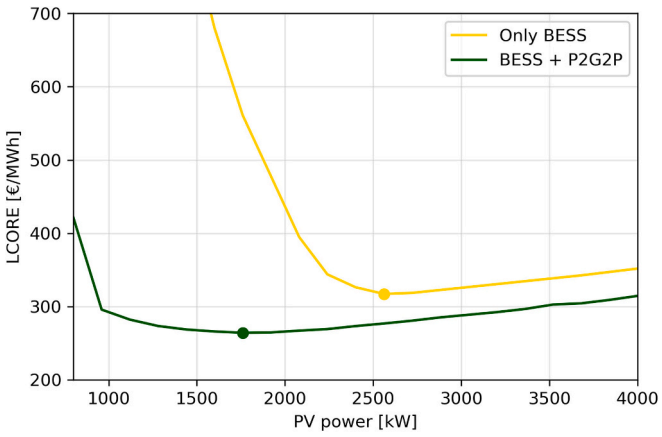

Fig. 24. Comparison between the trend of LCORE varying the PV installed power between the first scenario (only BESS) and the second scenario (BESS and P2G2P).

used to perform the same analysis, it would take up to 330 h on a supercomputer to obtain a solution as the one for the BESS + P2G2P case.

Simplified simulations may reduce the computational cost even more but may also compromise the accuracy of results. The outcome of optimization frameworks using the *hybrid* simulation method was compared to the outcome of optimization frameworks using the *simplified* approach. These comparisons have confirmed that the degradation assessment is crucial to correctly estimate the required size of storage systems. If the degradation is neglected, the optimizations converge to undersized combinations that cannot cover the entire energy request in the long run.

The comparison of results related to the first scenario (Fig. 20 and Fig. 21) clearly shows that the *simplified* framework underestimates the required BESS size by up to 8 %. These results are in line with findings from Omar [161]: comprehending and integrating BESS lifetime and degradation to optimize the economic feasibility of RES systems is crucial.

The comparison made for the second scenario (Fig. 23) have confirmed that, even in this case, the *simplified* simulation clearly tends to underestimate the required BESS capacity and the sizes of components of the hydrogen chain. By neglecting the degradation of cells, *simplified* optimizations converge on undersized storage combinations unable to maintain 100 % self-sufficiency in the long run. The mismatch on the optimal sizing of components in the hydrogen chain is variable. The H_2 tank can be undersized by 31.5 % on average (up to 84 %), while the electrolyzer size can characterized by a remarkable error up to 103.1 % (up to 361.5 %). The fuel cell can be undersized up to 7.7 %, but only 1 % on average. For all the considered PV sizes, the optimal BESS capacity determined by the *simplified* simulation is consistently lower (59.6 % under-sizing error on average). Consequently, the *simplified* simulation always underestimates the optimal LCORE that configurations can reach, committing an error of 10.2 % on average.

The estimated difference in fuel cell size between a simulation considering degradation and a simulation that neglects performance decay was up to 8 %. A considerable difference even if lower than the 25 % obtained by Erdnic and Uzunoglu [55]. Again, this result is case-sensitive and may be affected by several factors, but still remarks the importance of estimating degradation.

Optimal configurations identified by the proposed optimization framework using the *hybrid* method were tested by simulating the same combinations of components using the *c20* approach (Table 10 and Table 11). These comparisons confirmed that resulting combinations can actually maintain 100 % SSd for the whole lifetime of the system and that the computed LCORE is quite accurate. The mismatch between the two results can be caused by the method used to ensure that optimizations do not propose solutions unable to maintain the full SSd, i.e., to the price attributed to the missing energy. Even with infinitesimally small missing quantities, the high price attributed can produce a difference in the computed LCORE.

The comparison between the minimum LCORE from the two considered scenarios (Fig. 24) have shown that *hybrid* storage solutions involving both the Li-ion BESS and the P2G2P are always more convenient that solutions involving only a BESS. Due to the peculiar shape of the load of Tilos, seasonal storage represents a cost-effective way to reach full self-sufficiency. Because of consumption peaks, it is more convenient to use a fuel cell as a backup generator than oversizing the

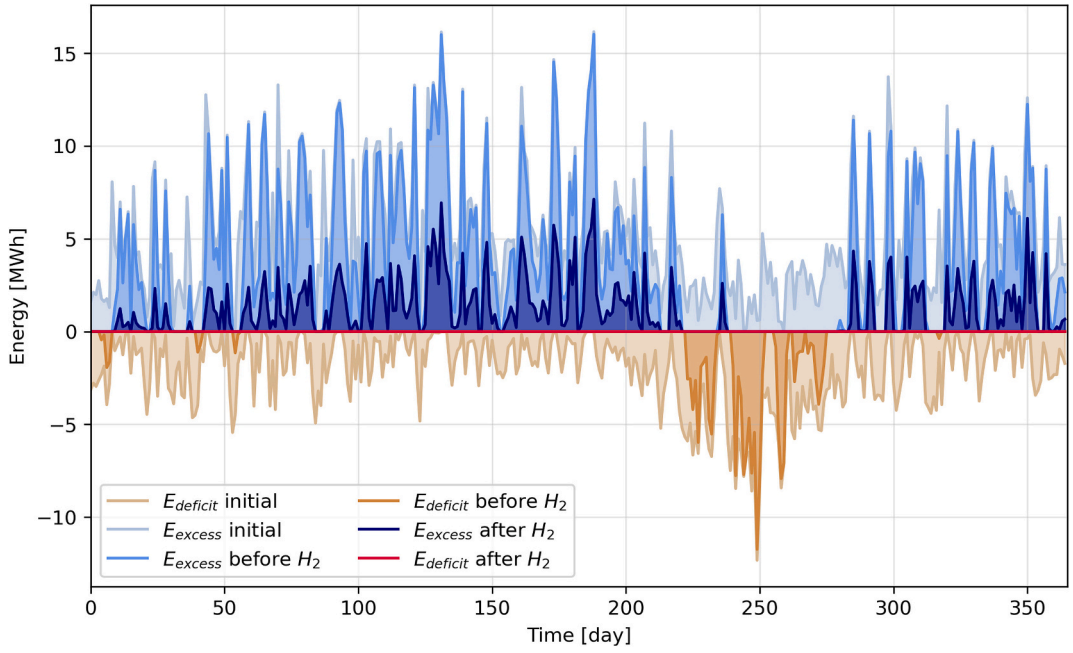

Fig. 25. Time variation of the energy deficit and excess before and after the application of P2G2P. Energy flows referred to the optimal configuration from the second scenario with the maximum PV size equal to 800 kWp.

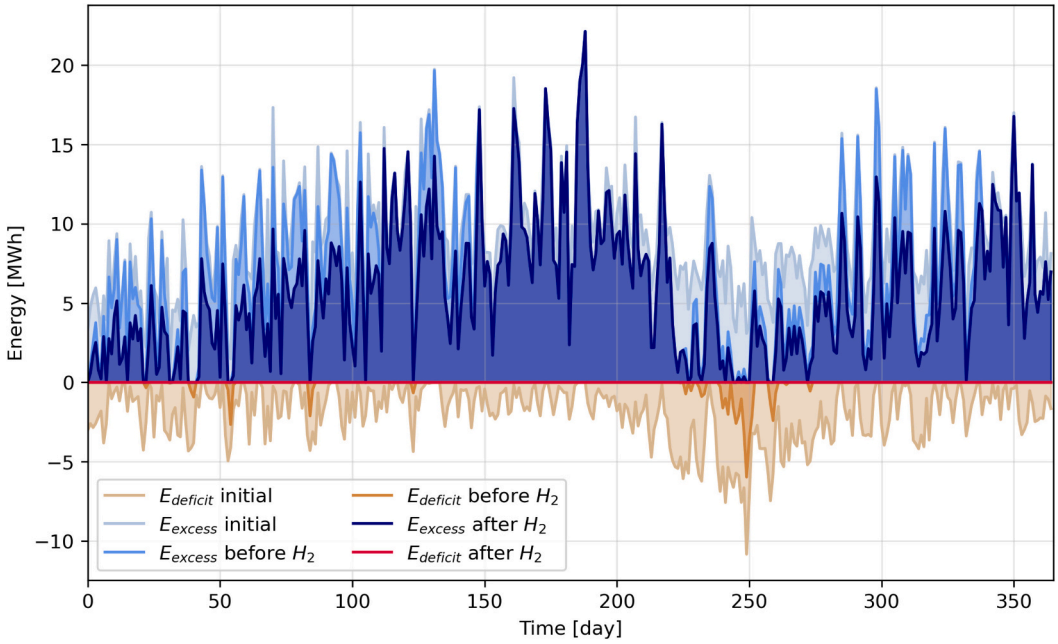

Fig. 26. Time variation of the energy deficit and excess before and after the application of P2G2P. Energy flows referred to the optimal configuration from the second scenario without constraints to the PV size.

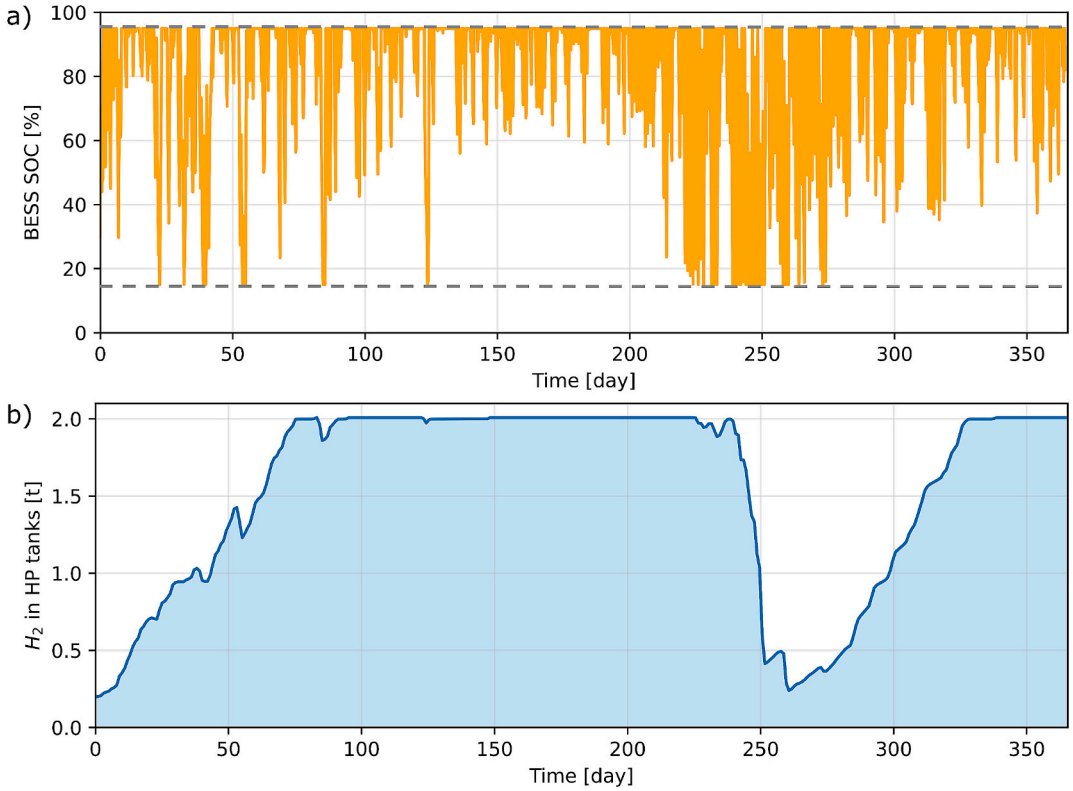

Fig. 27. Time variation of the a) BESS SOC bounded between the allowed minimum (15 %) and maximum (95 %) value and b) H_2 stored in high-pressure tanks. Trend referred to the optimal configuration from the second scenario without constraints to the PV size.

RES generation or only relying on a BESS. The latter, being a closed electrochemical cell, cannot decuple power from energy capacity. These results are in line with the results of Marocco et al. [162], who demonstrated that hydrogen allows the battery and RES not to be oversized in off-grid *hybrid* renewable energy systems.

However, the P2G2P solution comes with the installation of several devices to make the hydrogen chain work. The electrolyzer absorbs power from renewables for the hydrogen production, but also the compressor requires energy to drive the gas transformation and increase the volumetric energy density of the storage. This operation adds 70 kW to the electrical load that the RES generation must cover. Since during winter the total load of the island of Tilos varies between 200 and 600

kW, the compressor may increase the load considerably. On the other hand, this load is stable for a certain amount of time and more predictable than the usual electrical request from the island. Results show that, even if configuration involving P2G2P must add this electrical consumption to the overall energy request, the LCORE is still lower when the hydrogen chain is considered. The ratio between the power absorption from the compressor and the load from the network is close to what was considered by Maestre et al. [152] for a self-sufficient social home (1.5 kW compressor added to a 0.5–6 kW load).

The yearly time variations of the SOC of the BESS and the H_2 stored in high-pressure tanks (Fig. 27) show the complementarity of the two storage means. While the BESS SOC highly varies between the minimum and maximum allowed value, the stored H_2 shows a clear rising trend during winter (high energy excess) and a sudden drop during summer (abrupt peak of consumption and consequent energy deficit). These trends show that the first technology mainly covers hourly and daily power unbalances, while the second technology mainly acts as seasonal storage. The variation of the H_2 contained in storage tanks has a similar shape to what was obtained by Bielmann et al. [113] and Maestre et al. [152] in their seasonal energy storage system based on hydrogen. The BESS SOC trend varies on a daily basis as in results from Le et al. [103] and Yang et al. [163]. As found by Gabrielli et al. [164], the behavior of an H2 storage shifts towards the seasonal role when paired with a battery.

Energy flows from the optimized configurations (Fig. 26) show that the BESS can cover most of the energy deficit that arises from the mismatch between RES production and load request. The residual deficit consists of occasional peaks during winter and a consistent remaining request during summer. After the introduction of the P2G2P, the energy deficit is removed but the residual energy excess is still considerable. This behavior results from the competitive PV prices that make the excessive RES generation still more convenient than the installation of high-capacity storage technologies.

The residual excess of the HES has the potential to be exploited. Energy can be sold to the nearby islands by means of submarine connections, used to power a desalination plant to cover the request for freshwater of the island, or to feed a new fleet of electric vehicles on the island.

Another possibility is to convert this electrical energy excess into green hydrogen, a fuel that can be exported via shipping. Participation in the hydrogen market may be financially beneficial as proved by results from Pavić et al. [58]. A consequent increase in the capacity factor of the electrolyzer would raise the average conversion factor of the machine but would decrease the expected lifetime of the component. A careful analysis would be required to find the optimal trade-off between the two effects.

The methodology proposed in this work to establish the degradation of performance of components aims to capture the main influences that affect their operation. The estimation of degradation of components could be improved by the application of machine learning methods. If a wider sample of complete results is generated, data-driven methods have the potential to extract deeper correlations between the performance trends of components during the first year of operation and their future behavior.

Further developments could also regard the assessment of the performance degradation of generators. This study focused only on the degradation of storage devices because the historical production of renewable generators was available from the SCADA of an actual HPS. A degradation model of the PV field and the wind turbine could be used to forecast the decreasing production and balance sizing errors also in the design of generators.

6. Conclusions

This study proposes an innovative simulation method designed to reduce computational costs while maintaining high accuracy in long-term techno-economic analyses of energy systems. This method is tailored for applications supported by multiple storage technologies (i.e., batteries and hydrogen storage). Even if neglected by most studies, an accurate estimation of the degradation of components is crucial. By hybridizing a detailed simulation for the first year with simplified long-term degradation models, the method reduces computational costs by 88.5 % while accurately estimating component performance and lifespan.

To assess the feasibility of using the novel simulation approach for the robust design of a real HES, an optimization framework involving the proposed method was applied to a real case study: the design of a 100 % self-sufficient microgrid. Results revealed that storage solutions combining BESS with P2G2P are more cost-effective (264 €/MWh) than solutions involving only batteries (320 €/MWh). Furthermore, neglecting degradation can lead to under-sizing errors: 103.1 % on average for electrolyzer, 31.5 % for H_2 tank, 59.6 % for the battery, and up to 7.7 % for the fuel cell. As a result, undersized designs can produce an error in the evaluation of energy cost of 10.2 % on average. The proposed *hybrid* approach to simulation and optimization thus offers a valuable tool for designing robust and sustainable HESs capable of meeting the long-term energy needs of 100 % self-sufficient grids.

The current study described in detail the proposed simulation methodology and results from the application of two concurrent approaches in a real-world case study. A future study will focus on the specific application, considering also the expected drop in price of renewable generators and storage devices, that could be allowed by the application of the method.

CRediT authorship contribution statement

Francesco Superchi: Writing – original draft, Validation, Software, Methodology, Investigation, Formal analysis, Data curation, Conceptualization. **Antonis Moustakis:** Supervision, Software, Data curation. **George Pechlivanoglou:** Supervision, Resources, Project administration, Funding acquisition, Conceptualization. **Alessandro Bianchini:** Writing – review & editing, Supervision, Project administration, Methodology, Funding acquisition, Conceptualization.

Declaration of competing interest

The authors declare that they have no known competing financial interests or personal relationships that could have appeared to influence the work reported in this paper.

Data availability

The data that has been used is confidential.

Acknowledgments

Thanks are due to Eunice Energy Group for providing access to data regarding the Tilos Hybrid Power Station and for the co-financing of the PhD project of Dr. Francesco Superchi.

The authors would like also to thank Prof. Giovanni Ferrara from the University of Florence for the coordination of the PhD project of Dr. Superchi and Dr. Sanders Schepers for his contribution to the creation of the models for hydrogen compression.

Appendix A

Table A1
Li-ion BESS prices.

Study	Ref	Price	Prop	Price [€/kWh]
Mauler (2021)	[165]	234 $/kWh		234
Penisa (2020)	[166]	100 $/kWh		100
Beuse (2020)	[167]	316 $/kWh		316
NREL (2023)	[168]	338 $/kWh	10 h	338
		537 $/kWh	2 h	537

Table A2
PEM fuel cell prices.

Study	Ref	Price	range	Price [€/kW]
IRENA (2020)	[169]	700–1400	Min	700
			Max	1400
Gallardo (2021)	[170]	1000		1000
Baldi (2022)	[6]	730		730

Table A3
ALK electrolyzer prices.

Study	Ref	Price	range	Price [€/kW]
IEA (2019)	[171]	500–1400	Min	500
			Max	1400
IEA (2020)	[172]	1320		1320
NetZero (2021)	[173]	750–1160	Min	750
			Max	1160
IRENA (2020)	[169]	500–1000	Min	500
			Max	1000
Gallardo (2021)	[170]	500–700	Min	500
			Max	700
IRENA (2019)	[174]	840		840
ESCG (2022)	[175]	1320		1320
Bohm (2020)	[176]	1100		1100
Grigoriev (2020)	[177]	500–1400	Min	500
			Max	1400
Roos (2021)	[178]	419–1153	Min	419
			Max	1153

Table A4
Hydrogen tank prices.

Study	Ref	Price	Prop	Price [€/kg]
Leeuwen (2018)	[179]	490 €/kg		490
Kharel (2018)	[180]	430 €/kg		430
Niaz (2015)	[147]	400–530 €/kg		400
Ulleberg (2020)	[181]	250 bar: 550 €/kg	250 bar	550
Parks (2014)	[182]	172 bar: 470 $/kg	172 bar	470
Ikäheimo (2018)	[183]	700 bar: 500 €/kg	700 bar	500
SANDIA (2011)	[184]	500 $/kg		500
Shin (2023)	[185]	350 bar: 400 $/kg	350 bar	400
Villalonga (2021)	[186]	438 USD/kg		438

Table A5
Hydrogen compressor prices.

Study	Ref	Price
ESCG (2022)	[175]	39.30 [€/kW]
		39.30 [€/kW]
Richardson (2015)	[187]	Avg: 50 k–140 k [€/unit]
	[187]	Case study: 54 k€
Ulleberg(2020)	[181]	60 k€/unit

Table A6
PV field prices.

Study	Ref	Price	range	Price [€/kW]
Ozden (2017)	[134]	1600–5000 $/kW	Min	1600
			Max	5000
IRENA (2019)	[188]	1210 USD/kW		1210
IEA (2020)	[189]	667–1321 USD/kW	Avg	1055
			Min	677
			Max	1321
Statista	[190]	876 USD/kW		876
		983 USD/kW		983
		917 USD/kW		917

Appendix B

Table A7
Onshore wind turbine prices.

Study	Ref	Price	range	Price [€/kWh]
Sens (2022)	[191]	1325		1325
IEA (2020)	[189]	1055–2213 USD/kW	Avg	1591
			Min	1055
			Max	2213
IRENA (2022)	[192]	1626 USD/kW	Avg	1626
			Min	990
			Max	1998
		1274 USD/kW		1274

Table A8
Error on BESS SSd and H_2 SSd from *simplified*, *c1* and *hybrid* simulations.

					Error on BESS SSd [%]			Error on H_2 SSd [%]		
	EL [kW]	FC [kW]	BESS [MWh]	PV [kWp]	*simpl.*	*c1*	*hyb.*	*simpl.*	*c1*	*hyb.*
1	300	938	5.27	1440	0.917	0.927	0.005	0.461	0.471	−0.012
2	300	938	5.27	1760	1.083	1.034	−0.009	0.609	0.602	−0.021
3	300	938	5.27	2080	1.158	1.086	0.028	0.377	0.377	0.000
4	300	938	5.27	2400	1.125	1.048	0.003	0.244	0.244	−0.021
5	300	938	5.27	2720	1.135	1.087	0.019	0.172	0.172	−0.023
6	100	938	5.27	1760	1.087	0.998	0.005	0.759	0.679	0.038
7	200	938	5.27	1760	1.064	1.010	0.018	0.657	0.615	0.009
8	300	938	5.27	1760	1.083	1.034	−0.009	0.609	0.602	−0.021
9	400	938	5.27	1760	1.065	1.028	0.019	0.441	0.441	−0.017
10	500	938	5.27	1760	1.082	1.032	0.022	0.331	0.331	−0.001
11	600	938	5.27	1760	1.094	1.021	0.013	0.231	0.231	−0.017
12	300	420	5.27	1760	1.088	1.039	0.006	0.326	0.318	−0.004
13	300	560	5.27	1760	1.084	1.035	−0.006	0.483	0.480	−0.014
14	300	700	5.27	1760	1.084	1.035	−0.009	0.574	0.574	−0.020
15	300	840	5.27	1760	1.083	1.034	−0.009	0.602	0.602	−0.021
16	300	560	5.27	1760	1.084	1.035	−0.006	0.483	0.480	−0.014
17	300	938	3	1760	1.486	1.364	0.009	0.640	0.623	0.003
18	300	938	4	1760	1.484	1.349	0.031	0.685	0.628	0.020
19	300	938	6	1760	0.760	0.736	0.004	0.185	0.185	−0.006
20	300	938	7	1760	0.527	0.505	−0.004	0.001	0.001	0.001
21	300	938	8	1760	0.254	0.267	−0.028	4E-04	4E-04	3E-04
22	300	938	9	1760	0.136	0.138	−0.035	2E-04	2E-04	2E-04
23	300	938	10	1760	0.093	0.108	−0.026	2E-04	1E-04	2E-04

Table A9
Error on Electrolyzer φ, Fuel Cell φ and Battery Capacity from *simplified*, *c1* and *hybrid* simulations.

	Error on Electrolyzer φ [%]			Error on Fuel Cell φ [%]			Error on Battery Capacity [%]		
	simpl.	*c1*	*hyb.*	*simpl.*	*c1*	*hyb.*	*simpl.*	*c1*	*hyb.*
1	6.698	0.682	0.054	−1.528	−1.170	−0.101	15.792	15.792	−1.424
2	7.156	0.233	−0.306	−1.239	−1.131	−0.059	16.080	16.080	−1.508

(*continued on next page*)

Table A9 (*continued*)

	Error on Electrolyzer φ [%]			Error on Fuel Cell φ [%]			Error on Battery Capacity [%]		
	simpl.	*c1*	*hyb.*	*simpl.*	*c1*	*hyb.*	*simpl.*	*c1*	*hyb.*
3	7.423	0.125	−0.353	−1.110	−1.015	0.058	16.035	16.035	−1.520
4	7.633	0.198	−0.284	−1.025	−0.938	0.137	15.953	15.953	−1.458
5	7.771	−0.105	−0.518	−0.972	−0.892	0.184	15.846	15.846	−1.490
6	3.183	1.798	−0.055	−1.200	−0.992	0.081	16.109	16.109	−1.451
7	5.659	0.985	−0.069	−1.217	−1.061	0.011	16.069	16.069	−1.468
8	7.156	0.233	−0.306	−1.239	−1.131	−0.059	16.080	16.080	−1.508
9	7.785	0.285	−0.065	−1.251	−1.144	−0.072	16.052	16.052	−1.519
10	8.037	0.177	−0.037	−1.255	−1.147	−0.076	16.030	16.030	−1.458
11	8.091	−0.067	−0.169	−1.256	−1.148	−0.077	16.031	16.031	−1.498
12	7.178	−0.196	−0.620	−1.261	−1.153	−0.082	16.060	16.060	−1.518
13	7.130	0.145	−0.369	−1.245	−1.137	−0.066	16.080	16.080	−1.508
14	7.127	0.173	−0.353	−1.242	−1.134	−0.062	16.079	16.079	−1.509
15	7.156	0.233	−0.306	−1.238	−1.130	−0.059	16.080	16.080	−1.508
16	7.130	0.145	−0.369	−1.245	−1.137	−0.066	16.080	16.080	−1.508
17	4.472	1.071	−0.342	−3.067	−2.687	−0.180	14.667	14.667	−2.235
18	5.822	0.675	−0.299	−2.036	−1.755	−0.025	15.357	15.357	−1.903
19	7.664	0.218	−0.246	−0.963	−0.877	−0.065	14.290	14.290	−1.288
20	8.528	0.021	−0.291	−0.630	−0.571	−0.016	12.329	12.329	−1.215
21	9.129	0.308	−0.015	−0.415	−0.374	0.004	10.790	10.790	−1.092
22	9.603	0.481	0.159	−0.303	−0.270	−0.013	9.470	9.470	−1.061
23	9.929	0.289	0.031	−0.237	−0.209	−0.034	8.466	8.466	−1.071

References

[1] Renewables 2023 – Analysis. IEA; 2024. https://www.iea.org/reports/renewables-2023. accessed May 21, 2024.

[2] Jain A, Yamujala S, Gaur A, Das P, Bhakar R, Mathur J. Power sector decarbonization planning considering renewable resource variability and system operational constraints. Appl Energy 2023;331:120404. https://doi.org/10.1016/j.apenergy.2022.120404.

[3] Danieli P, Carraro G, Volpato G, Cin ED, Lazzaretto A, Masi M. Guidelines for minimum cost transition planning to a 100% renewable multi-regional energy system. Appl Energy 2024;357:122497. https://doi.org/10.1016/j.apenergy.2023.122497.

[4] Gray N, O'Shea R, Smyth B, Lens PNL, Murphy JD. An assessment of decarbonisation pathways for intercontinental deep-sea shipping using power-to-X fuels. Appl Energy 2024;376:124163. https://doi.org/10.1016/j.apenergy.2024.124163.

[5] Liang Z, Liang Y, Luo X, Yu Z, Chen J, Chen Y. Multi-objective optimization of proton exchange membrane fuel cell based methanol-solar-to-X hybrid energy systems. Appl Energy 2024;373:123828. https://doi.org/10.1016/j.apenergy.2024.123828.

[6] Baldi F, Coraddu A, Kalikatzarakis M, Jeleňová D, Collu M, Race J, et al. Optimisation-based system designs for deep offshore wind farms including power to gas technologies. Appl Energy 2022;310:118540. https://doi.org/10.1016/j.apenergy.2022.118540.

[7] Lehner M, Tichler R, Steinmüller H, Koppe M. Power-to-gas: Technology and business models. Cham: Springer International Publishing; 2014. https://doi.org/10.1007/978-3-319-03995-4.

[8] Liu H, Høgh J, Blennow P, Sun X, Zong Y, Chen M. Assessing fluctuating wind to hydrogen production via long-term testing of solid oxide electrolysis stacks. Appl Energy 2024;361:122938. https://doi.org/10.1016/j.apenergy.2024.122938.

[9] Tian C, Tan Q, Fang G, Wen X. Hydrogen production to combat power surpluses in hybrid hydro–wind–photovoltaic power systems. Appl Energy 2024;371:123627. https://doi.org/10.1016/j.apenergy.2024.123627.

[10] Rezaei M, Akimov A, Gray EMA. Techno-economics of offshore wind-based dynamic hydrogen production. Appl Energy 2024;374:124030. https://doi.org/10.1016/j.apenergy.2024.124030.

[11] Maluenda M, Córdova S, Lorca Á, Negrete-Pincetic M. Optimal operation scheduling of a PV-BESS-Electrolyzer system for hydrogen production and frequency regulation. Appl Energy 2023;344:121243. https://doi.org/10.1016/j.apenergy.2023.121243.

[12] Park J, Kang S, Kim S, Kim H, Kim S-K, Lee JH. Optimizing green hydrogen systems: balancing economic viability and reliability in the face of supply-demand volatility. Appl Energy 2024;368:123492. https://doi.org/10.1016/j.apenergy.2024.123492.

[13] Weiss R, Ikäheimo J. Flexible industrial power-to-X production enabling large-scale wind power integration: a case study of future hydrogen direct reduction iron production in Finland. Appl Energy 2024;365:123230. https://doi.org/10.1016/j.apenergy.2024.123230.

[14] Svendsmark E, Straus J, Crespo del Granado P. Developing hydrogen energy hubs: the role of H2 prices, wind power and infrastructure investments in northern Norway. Appl Energy 2024;376:124130. https://doi.org/10.1016/j.apenergy.2024.124130.

[15] Veenstra AT, Mulder M. Profitability of hydrogen production: assessment of investments in electrolysers under various market circumstances. Appl Energy 2024;375:124111. https://doi.org/10.1016/j.apenergy.2024.124111.

[16] Fang J, Yang M, Sui J, Luo T, Yu Y, Ao Y, et al. Enhancing solar-powered hydrogen production efficiency by spectral beam splitting and integrated chemical energy storage. Appl Energy 2024;372:123833. https://doi.org/10.1016/j.apenergy.2024.123833.

[17] Gong Y, Liu T, Liu P, Duan L. Deriving joint operating rule curves for hydro–hydrogen–wind–photovoltaic hybrid power systems. Appl Energy 2024;375:124084. https://doi.org/10.1016/j.apenergy.2024.124084.

[18] Rezaei M, Akimov A, Gray Emac A. Techno-economics of renewable hydrogen export: a case study for Australia-Japan. Appl Energy 2024;374:124015. https://doi.org/10.1016/j.apenergy.2024.124015.

[19] Sui Q, Zhang J, Li J, Li Z, Su C, Liu C. Optimal scheduling for renewable power grid and vessel-based hydrogen chain integrated systems considering flexible energy transfer. Appl Energy 2024;367:123401. https://doi.org/10.1016/j.apenergy.2024.123401.

[20] Anoune K, Bouya M, Astito A, Abdellah AB. Sizing methods and optimization techniques for PV-wind based hybrid renewable energy system: a review. Renew Sust Energ Rev 2018;93:652–73. https://doi.org/10.1016/j.rser.2018.05.032.

[21] Klyve ØS, Grab R, Olkkonen V, Marstein ES. Influence of high-resolution data on accurate curtailment loss estimation and optimal design of hybrid PV–wind power plants. Appl Energy 2024;372:123784. https://doi.org/10.1016/j.apenergy.2024.123784.

[22] Basnet MR, Bryan JA, Dana SJ, Meek AS, Wang H, Talbot P. Stochastic optimization and uncertainty quantification of Natrium-based nuclear-renewable energy Systems for Flexible Power Applications in deregulated markets. Appl Energy 2024;375:124105. https://doi.org/10.1016/j.apenergy.2024.124105.

[23] Bechlenberg A, Luning EA, Saltık MB, Szirbik NB, Jayawardhana B, Vakis AI. Renewable energy system sizing with power generation and storage functions accounting for its optimized activity on multiple electricity markets. Appl Energy 2024;360:122742. https://doi.org/10.1016/j.apenergy.2024.122742.

[24] Silvestri L, De Santis M. Renewable-based load shifting system for demand response to enhance energy-economic-environmental performance of industrial enterprises. Appl Energy 2024;358:122562. https://doi.org/10.1016/j.apenergy.2023.122562.

[25] Kim YS, Park GH, Kim SW, Kim D. Incentive design for hybrid energy storage system investment to PV owners considering value of grid services. Appl Energy 2024;373:123772. https://doi.org/10.1016/j.apenergy.2024.123772.

[26] Hull C, Wust J, Booysen MJ, McCulloch MD. Techno-economic optimization and assessment of solar-battery charging station under grid constraints with varying levels of fleet EV penetration. Appl Energy 2024;374:123990. https://doi.org/10.1016/j.apenergy.2024.123990.

[27] Nketiah E, Song H, Adjei M, Adu-Gyamfi G, Obuobi B, Cudjoe D. Assessment of energy generation potential and mitigating greenhouse gas emissions from biogas from food waste: Insights from Jiangsu Province. Appl Energy 2024;371:123717. https://doi.org/10.1016/j.apenergy.2024.123717.

[28] Jouttijärvi S, Karttunen L, Ranta S, Miettunen K. Techno-economic analysis on optimizing the value of photovoltaic electricity in a high-latitude location. Appl Energy 2024;361:122924. https://doi.org/10.1016/j.apenergy.2024.122924.

[29] Jung J, Song C-O, Lee D-J, Yoon K. Optimal energy procurement with long-term photovoltaic energy contracts considering generation uncertainty: a two-dimensional auction approach. Appl Energy 2024;356:122383. https://doi.org/10.1016/j.apenergy.2023.122383.

[30] Dinçer AE, Demir A, Yılmaz K. Multi-objective turbine allocation on a wind farm site. Appl Energy 2024;355:122346. https://doi.org/10.1016/j.apenergy.2023.122346.

[31] Mariuzzo I, Fina B, Stroemer S, Raugi M. Economic assessment of multiple energy community participation. Appl Energy 2024;353:122060. https://doi.org/10.1016/j.apenergy.2023.122060.

[32] Tafone A, Raj Thangavelu S, Morita S, Romagnoli A. Design optimization of a novel cryo-polygeneration demonstrator developed in Singapore – techno-economic feasibility study for a cooling dominated tropical climate. Appl Energy 2023;330:119916. https://doi.org/10.1016/j.apenergy.2022.119916.

[33] Pagnini L, Bracco S, Delfino F, De-Simón-Martín M. Levelized cost of electricity in renewable energy communities: uncertainty propagation analysis. Appl Energy 2024;366:123278. https://doi.org/10.1016/j.apenergy.2024.123278.

[34] Rathod AA. S. B. Optimization of stand-alone hybrid renewable energy system based on techno-socio-enviro-financial perspective using improved red-tailed hawk algorithm. Appl Energy 2024;376:124137. https://doi.org/10.1016/j.apenergy.2024.124137.

[35] Đukan M, Gut D, Gumber A, Steffen B. Harnessing solar power in the Alps: a study on the financial viability of mountain PV systems. Appl Energy 2024;375:124019. https://doi.org/10.1016/j.apenergy.2024.124019.

[36] Behzadi A, Duwig C, Ploskic A, Holmberg S, Sadrizadeh S. Application to novel smart techniques for decarbonization of commercial building heating and cooling through optimal energy management. Appl Energy 2024;376:124224. https://doi.org/10.1016/j.apenergy.2024.124224.

[37] Ren Y, Sun K, Zhang K, Han Y, Zhang H, Wang M, et al. Optimization of the capacity configuration of an abandoned mine pumped storage/wind/photovoltaic integrated system. Appl Energy 2024;374:124089. https://doi.org/10.1016/j.apenergy.2024.124089.

[38] Danieli P, Lazzaretto A, Al-Zaili J, Sayma A, Masi M, Carraro G. The potential of the natural gas grid to accommodate hydrogen as an energy vector in transition towards a fully renewable energy system. Appl Energy 2022;313:118843. https://doi.org/10.1016/j.apenergy.2022.118843.

[39] Mehr AS, Gandiglio M, MosayebNezhad M, Lanzini A, Mahmoudi SMS, Yari M, et al. Solar-assisted integrated biogas solid oxide fuel cell (SOFC) installation in wastewater treatment plant: energy and economic analysis. Appl Energy 2017;191:620–38. https://doi.org/10.1016/j.apenergy.2017.01.070.

[40] Bompard E, Botterud A, Corgnati S, Huang T, Jafari M, Leone P, et al. An electricity triangle for energy transition: application to Italy. Appl Energy 2020;277:115525. https://doi.org/10.1016/j.apenergy.2020.115525.

[41] Cremoncini D, Di Lorenzo G, Frate GF, Bischi A, Baccioli A, Ferrari L. Techno-economic analysis of aqueous organic redox flow batteries: stochastic investigation of capital cost and levelized cost of storage. Appl Energy 2024;360:122738. https://doi.org/10.1016/j.apenergy.2024.122738.

[42] Chi Y, Lin J, Li P, Yu Z, Mu S, Li X, et al. Elevating the acceptable cost threshold for solid oxide cells: a case study on refinery decarbonization. Appl Energy 2024;373:123829. https://doi.org/10.1016/j.apenergy.2024.123829.

[43] Zhou Y, Zhang H, Ji S, Sun M, Ding X, Zheng N, et al. Whole process dynamic performance analysis of a solar-aided liquid air energy storage system: from single cycle to multi-cycle. Appl Energy 2024;373:123938. https://doi.org/10.1016/j.apenergy.2024.123938.

[44] Poli N, Bonaldo C, Moretto M, Guarnieri M. Techno-economic assessment of future vanadium flow batteries based on real device/market parameters. Appl Energy 2024;362:122954. https://doi.org/10.1016/j.apenergy.2024.122954.

[45] Vazquez-Sanchez H, Nagaraja SS, Cross NR, Hall DM, Mani Sarathy S. A techno-economic analysis of a thermally regenerative ammonia-based battery. Appl Energy 2023;347:121501. https://doi.org/10.1016/j.apenergy.2023.121501.

[46] Blaabjerg F, Ionel DM, Yang Y, Wang H. Renewable energy systems: Technology overview and perspectives. In: Renew. Energy devices Syst. Simul. MATLAB® ANSYS®. CRC Press; 2017.

[47] Geleta D, Manshahia M. Optimization of renewable energy systems: a review. Int J Sci Res Sci Technol 2017;3:769–95.

[48] Forough AB, Roshandel R. Lifetime optimization framework for a hybrid renewable energy system based on receding horizon optimization. Energy 2018;150:617–30. https://doi.org/10.1016/j.energy.2018.02.158.

[49] Mielcarek A, Ceran B, Jurasz J. The impact of degradation of PV/battery-independent system components on technical and economic indicators and sizing process. Energies 2023;16:6642. https://doi.org/10.3390/en16186642.

[50] Angenendt G, Zurmühlen S, Axelsen H, Sauer DU. Comparison of different operation strategies for PV battery home storage systems including forecast-based operation strategies. Appl Energy 2018;229:884–99. https://doi.org/10.1016/j.apenergy.2018.08.058.

[51] Lubello P, Papi F, Bianchini A, Carcasci C. Considerations on the impact of battery ageing estimation in the optimal sizing of solar home battery systems. J Clean Prod 2021;329:129753. https://doi.org/10.1016/j.jclepro.2021.129753.

[52] Fowler MW, Mann RF, Amphlett JC, Peppley BA, Roberge PR. Incorporation of voltage degradation into a generalised steady state electrochemical model for a PEM fuel cell. J Power Sources 2002;106:274–83. https://doi.org/10.1016/S0378-7753(01)01029-1.

[53] Kuckshinrichs W, Ketelaer T, Koj JC. Economic analysis of improved alkaline water electrolysis. Front Energy Res 2017:5. https://doi.org/10.3389/fenrg.2017.00001.

[54] Franco AA, Doublet ML, Bessler WG, editors. Physical multiscale modeling and numerical simulation of electrochemical devices for energy conversion and storage: From theory to engineering to practice. London: Springer; 2016. https://doi.org/10.1007/978-1-4471-5677-2.

[55] Erdinc O, Uzunoglu M. A new perspective in optimum sizing of hybrid renewable energy systems: consideration of component performance degradation issue. Int J Hydrog Energy 2012;37:10479–88. https://doi.org/10.1016/j.ijhydene.2012.04.071.

[56] Sufyan M, Rahim NA, Tan C, Muhammad MA, Raihan SRS. Optimal sizing and energy scheduling of isolated microgrid considering the battery lifetime degradation. PLoS One 2019;14:e0211642. https://doi.org/10.1371/journal.pone.0211642.

[57] Pu Y, Li Q, Zou X, Li R, Li L, Chen W, et al. Optimal sizing for an integrated energy system considering degradation and seasonal hydrogen storage. Appl Energy 2021;302:117542. https://doi.org/10.1016/j.apenergy.2021.117542.

[58] Pavić I, Čović N, Pandžić H. PV–battery-hydrogen plant: cutting green hydrogen costs through multi-market positioning. Appl Energy 2022;328:120103. https://doi.org/10.1016/j.apenergy.2022.120103.

[59] Go J, Byun J, Orehounig K, Heo Y. Battery-H2 storage system for self-sufficiency in residential buildings under different electric heating system scenarios. Appl Energy 2023;337:120742. https://doi.org/10.1016/j.apenergy.2023.120742.

[60] Essayeh C, Morstyn T. Optimal sizing for microgrids integrating distributed flexibility with the Perth west smart city as a case study. Appl Energy 2023;336:120846. https://doi.org/10.1016/j.apenergy.2023.120846.

[61] Modu B, Abdullah MP, Bukar AL, Hamza MF. A systematic review of hybrid renewable energy systems with hydrogen storage: sizing, optimization, and energy management strategy. Int J Hydrog Energy 2023;48:38354–73. https://doi.org/10.1016/j.ijhydene.2023.06.126.

[62] Basnet S, Deschinkel K, Le Moyne L, Cécile Péra M. A review on recent standalone and grid integrated hybrid renewable energy systems: system optimization and energy management strategies. Renew Energy Focus 2023;46:103–25. https://doi.org/10.1016/j.ref.2023.06.001.

[63] Ceran B, Mielcarek A, Hassan Q, Teneta J, Jaszczur M. Aging effects on modelling and operation of a photovoltaic system with hydrogen storage. Appl Energy 2021;297:117161. https://doi.org/10.1016/j.apenergy.2021.117161.

[64] Ceran B, Orłowska A. The impact of power source performance decrease in a PV/WT/FC hybrid power generation system on the result of a multi-criteria analysis of load distribution. Energies 2019;12:3453. https://doi.org/10.3390/en12183453.

[65] Jurasz J, Ceran B, Orłowska A. Component degradation in small-scale off-grid PV-battery systems operation in terms of reliability, environmental impact and economic performance. Sustain Energy Technol Assess 2020;38:100647. https://doi.org/10.1016/j.seta.2020.100647.

[66] Parhizkar T, Hafeznezami S. Degradation based operational optimization model to improve the productivity of energy systems, case study: solid oxide fuel cell stacks. Energy Convers Manag 2018;158:81–91. https://doi.org/10.1016/j.enconman.2017.12.045.

[67] Bordin C, Anuta HO, Crossland A, Gutierrez IL, Dent CJ, Vigo D. A linear programming approach for battery degradation analysis and optimization in offgrid power systems with solar energy integration. Renew Energy 2017;101:417–30. https://doi.org/10.1016/j.renene.2016.08.066.

[68] Qin D, He K, Liu F, Wang T, Chen J. Online lifecycle operating costs minimization strategy for fuel cell buses considering power sources degradation. Energ Technol 2024;12:2301115. https://doi.org/10.1002/ente.202301115.

[69] Abdelghany MB, Al-Durra A, Daming Z, Gao F. Optimal multi-layer economical schedule for coordinated multiple mode operation of wind–solar microgrids with hybrid energy storage systems. J Power Sources 2024;591:233844. https://doi.org/10.1016/j.jpowsour.2023.233844.

[70] Shen W, Zeng B, Zeng M. Multi-timescale rolling optimization dispatch method for integrated energy system with hybrid energy storage system. Energy 2023;283:129006. https://doi.org/10.1016/j.energy.2023.129006.

[71] Liu H, Ren H, Gu Y, Lin Y, Hu W, Song J, et al. Design and on-site implementation of an off-grid marine current powered hydrogen production system. Appl Energy 2023;330:120374. https://doi.org/10.1016/j.apenergy.2022.120374.

[72] Huang J, An Q, Zhou M, Tang R, Dong Z, Lai J, et al. A self-adaptive joint optimization framework for marine hybrid energy storage system design considering load fluctuation characteristics. Appl Energy 2024;361:122973. https://doi.org/10.1016/j.apenergy.2024.122973.

[73] Fan F, Aditya V, Xu Y, Cheong B, Gupta AK. Robustly coordinated operation of a ship microgird with hybrid propulsion systems and hydrogen fuel cells. Appl Energy 2022;312:118738. https://doi.org/10.1016/j.apenergy.2022.118738.

[74] Sheng C, Guo Z, Lei J, Zhang S, Zhang W, Chen W, et al. Optimal energy management strategies for hybrid power systems considering Pt degradation. Appl Energy 2024;360:122764. https://doi.org/10.1016/j.apenergy.2024.122764.

[75] He Y, Zhou Y, Wang Z, Liu J, Liu Z, Zhang G. Quantification on fuel cell degradation and techno-economic analysis of a hydrogen-based grid-interactive residential energy sharing network with fuel-cell-powered vehicles. Appl Energy 2021;303:117444. https://doi.org/10.1016/j.apenergy.2021.117444.

[76] Zhang Z, Guan C, Liu Z. Real-time optimization energy management strategy for fuel cell hybrid ships considering power sources degradation. IEEE Access 2020;8:87046–59. https://doi.org/10.1109/ACCESS.2020.2991519.

[77] Yue M, Jemei S, Gouriveau R, Zerhouni N. Review on health-conscious energy management strategies for fuel cell hybrid electric vehicles: degradation models and strategies. Int J Hydrog Energy 2019;44:6844–61. https://doi.org/10.1016/j.ijhydene.2019.01.190.

[78] Fletcher T, Thring R, Watkinson M. An energy management strategy to concurrently optimise fuel consumption & PEM fuel cell lifetime in a hybrid vehicle. Int J Hydrog Energy 2016;41:21503–15. https://doi.org/10.1016/j.ijhydene.2016.08.157.

[79] Balestra L, Schjølberg I. Modelling and simulation of a zero-emission hybrid power plant for a domestic ferry. Int J Hydrog Energy 2021;46:10924–38. https://doi.org/10.1016/j.ijhydene.2020.12.187.

[80] Amini M, Khorsandi A, Vahidi B, Hosseinian SH, Malakmahmoudi A. Optimal sizing of battery energy storage in a microgrid considering capacity degradation and replacement year. Electr Power Syst Res 2021;195:107170. https://doi.org/10.1016/j.epsr.2021.107170.

[81] Terlouw T, AlSkaif T, Bauer C, van Sark W. Multi-objective optimization of energy arbitrage in community energy storage systems using different battery technologies. Appl Energy 2019;239:356–72. https://doi.org/10.1016/j.apenergy.2019.01.227.

[82] Schmidt TS, Beuse M, Zhang X, Steffen B, Schneider SF, Pena-Bello A, et al. Additional emissions and cost from storing Electricity in Stationary Battery Systems. Environ Sci Technol 2019;53:3379–90. https://doi.org/10.1021/acs.est.8b05313.

[83] Wang B, Yu X, Xu H, Wu Q, Wang L, Huang R, et al. Scenario analysis, management, and optimization of a new vehicle-to-Micro-grid (V2μG) network based on off-grid renewable building energy systems. Appl Energy 2022;325:119873. https://doi.org/10.1016/j.apenergy.2022.119873.

[84] Ur Rehman W, Bo R, Mehdipourpicha H, Kimball JW. Sizing battery energy storage and PV system in an extreme fast charging station considering uncertainties and battery degradation. Appl Energy 2022;313:118745. https://doi.org/10.1016/j.apenergy.2022.118745.

[85] Fioriti D, Pellegrino L, Lutzemberger G, Micolano E, Poli D. Optimal sizing of residential battery systems with multi-year dynamics and a novel rainflow-based model of storage degradation: An extensive Italian case study. Electr Power Syst Res 2022;203:107675. https://doi.org/10.1016/j.epsr.2021.107675.

[86] Shin H, Roh JH. Framework for sizing of energy storage system supplementing photovoltaic generation in consideration of battery degradation. IEEE Access 2020;8:60246–58. https://doi.org/10.1109/ACCESS.2020.2977985.

[87] Liu Y, Wu X, Du J, Song Z, Wu G. Optimal sizing of a wind-energy storage system considering battery life. Renew Energy 2020;147:2470–83. https://doi.org/10.1016/j.renene.2019.09.123.

[88] Castillejo-Cuberos A, Cardemil JM, Escobar R. Techno-economic assessment of photovoltaic plants considering high temporal resolution and non-linear dynamics of battery storage. Appl Energy 2023;334:120712. https://doi.org/10.1016/j.apenergy.2023.120712.

[89] Liu J, Wu H, Huang H, Yang H. Renewable energy design and optimization for a net-zero energy building integrating electric vehicles and battery storage considering grid flexibility. Energy Convers Manag 2023;298:117768. https://doi.org/10.1016/j.enconman.2023.117768.

[90] Dall'Armi C, Pivetta D, Taccani R. Uncertainty analysis of the optimal health-conscious operation of a hybrid PEMFC coastal ferry. Int J Hydrog Energy 2022;47:11428–40. https://doi.org/10.1016/j.ijhydene.2021.10.271.

[91] Dall'Armi C, Pivetta D, Taccani R. Health-conscious optimization of long-term operation for hybrid PEMFC ship propulsion systems. Energies 2021;14:3813. https://doi.org/10.3390/en14133813.

[92] Pivetta D, Dall'Armi C, Taccani R. Multi-objective optimization of hybrid PEMFC/Li-ion battery propulsion systems for small and medium size ferries. Int J Hydrog. Energy 2021;46:35949–60. https://doi.org/10.1016/j.ijhydene.2021.02.124.

[93] Zhang W, He Y, Wu N, Zhang F, Lu D, Liu Z, et al. Assessment of cruise ship decarbonization potential with alternative fuels based on MILP model and cabin space limitation. J Clean Prod 2023;425:138667. https://doi.org/10.1016/j.jclepro.2023.138667.

[94] Rezaei M, Akimov A, Gray EMA. Levelised cost of dynamic green hydrogen production: a case study for Australia's hydrogen hubs. Appl Energy 2024;370:123645. https://doi.org/10.1016/j.apenergy.2024.123645.

[95] Nicita A, Maggio G, Andaloro APF, Squadrito G. Green hydrogen as feedstock: financial analysis of a photovoltaic-powered electrolysis plant. Int J Hydrog Energy 2020;45:11395–408. https://doi.org/10.1016/j.ijhydene.2020.02.062.

[96] Liu T, Li J, Yang Z, Duan Y. Evaluation of the short- and long-duration energy storage requirements in solar-wind hybrid systems. Energy Convers Manag 2024;314:118635. https://doi.org/10.1016/j.enconman.2024.118635.

[97] Zhai R, Liu H, Chen Y, Wu H, Yang Y. The daily and annual technical-economic analysis of the thermal storage PV-CSP system in two dispatch strategies. Energy Convers Manag 2017;154:56–67. https://doi.org/10.1016/j.enconman.2017.10.040.

[98] Zhang H, Yuan T. Optimization and economic evaluation of a PEM electrolysis system considering its degradation in variable-power operations. Appl Energy 2022;324:119760. https://doi.org/10.1016/j.apenergy.2022.119760.

[99] Roshandel R, Parhizkar T. Degradation based optimization framework for long term applications of energy systems, case study: solid oxide fuel cell stacks. Energy 2016;107:172–81. https://doi.org/10.1016/j.energy.2016.04.007.

[100] Guinot B, Champel B, Montignac F, Lemaire E, Vannucci D, Sailler S, et al. Techno-economic study of a PV-hydrogen-battery hybrid system for off-grid power supply: impact of performances' ageing on optimal system sizing and competitiveness. Int J Hydrog Energy 2015;40:623–32. https://doi.org/10.1016/j.ijhydene.2014.11.007.

[101] Li B, Roche R, Paire D, Miraoui A. Sizing of a stand-alone microgrid considering electric power, cooling/heating, hydrogen loads and hydrogen storage degradation. Appl Energy 2017;205:1244–59. https://doi.org/10.1016/j.apenergy.2017.08.142.

[102] Li Z, Xia Y, Bo Y, Wei W. Optimal planning for electricity-hydrogen integrated energy system considering multiple timescale operations and representative time-period selection. Appl Energy 2024;362:122965. https://doi.org/10.1016/j.apenergy.2024.122965.

[103] Le TS, Nguyen TN, Bui D-K, Ngo TD. Optimal sizing of renewable energy storage: a techno-economic analysis of hydrogen, battery and hybrid systems considering degradation and seasonal storage. Appl Energy 2023;336:120817. https://doi.org/10.1016/j.apenergy.2023.120817.

[104] Tzanes G, Zafeiraki E, Papapostolou C, Zafirakis D, Konstantinos M, Kavadias K, et al. Assessing the status of electricity generation in the non-Interconnected Islands of the Aegean Sea region. Energy Procedia 2019;159:424–9. https://doi.org/10.1016/j.egypro.2018.12.065.

[105] Skopetou N, Zestanakis PA, Rotas R, Iliadis P, Papadopoulos C, Nikolopoulos N, et al. Energy analysis and environmental impact assessment for self-sufficient non-interconnected islands: the case of Nisyros island. J Clean Prod 2024;447:141647. https://doi.org/10.1016/j.jclepro.2024.141647.

[106] Żołądek M, Figaj R, Kafetzis A, Panopoulos K. Energy-economic assessment of self-sufficient microgrid based on wind turbine, photovoltaic field, wood gasifier, battery, and hydrogen energy storage. Int J Hydrog Energy 2024;52:728–44. https://doi.org/10.1016/j.ijhydene.2023.04.327.

[107] Kougias I, Szabó S, Nikitas A, Theodossiou N. Sustainable energy modelling of non-interconnected Mediterranean islands. Renew Energy 2019;133:930–40. https://doi.org/10.1016/j.renene.2018.10.090.

[108] Superchi F, Schepers S, Moustakis A, Pechivanoglou G, Bianchini A. Towards the introduction of green hydrogen in the energy mix of Mediterranean islands through the integration of wind and solar power: a techno-economic case study. 2023. p. 3351–61. https://doi.org/10.52202/069564-0301.

[109] Notton G, Nivet M-L, Zafirakis D, Motte F, Voyant C, Fouilloy A. Tilos, the first autonomous renewable green island in Mediterranean: A horizon 2020 project. 2024.

[110] Superchi F, Giovannini N, Moustakis A, Pechlivanoglou G, Bianchini A. Optimization of the power output scheduling of a renewables-based hybrid power station using MILP approach: the case of Tilos island. Renew Energy 2024;220:119685. https://doi.org/10.1016/j.renene.2023.119685.

[111] ENERCON wind turbines for all wind classes | Build your wind farm with ENERCON turbines. https://www.enercon.de/en/wind-turbines/product-portfolio. [Accessed 18 June 2024].

[112] Li K, Tseng KJ. Energy efficiency of lithium-ion battery used as energy storage devices in micro-grid. IECON 2015 - 41st Annu. Conf IEEE Ind Electron Soc. 2015. p. 005235–40. https://doi.org/10.1109/IECON.2015.7392923.

[113] Bielmann M, Vogt UF, Zimmermann M, Züttel A. Seasonal energy storage system based on hydrogen for self sufficient living. J Power Sources 2011;196:4054–60. https://doi.org/10.1016/j.jpowsour.2010.11.096.

[114] Elberry AM, Thakur J, Santasalo-Aarnio A, Larmi M. Large-scale compressed hydrogen storage as part of renewable electricity storage systems. Int J Hydrog Energy 2021;46:15671–90. https://doi.org/10.1016/j.ijhydene.2021.02.080.

[115] Haug P, Kreitz B, Koj M, Turek T. Process modelling of an alkaline water electrolyzer. Int J Hydrog Energy 2017;42:15689–707. https://doi.org/10.1016/j.ijhydene.2017.05.031.

[116] Hu K, Fang J, Ai X, Huang D, Zhong Z, Yang X, et al. Comparative study of alkaline water electrolysis, proton exchange membrane water electrolysis and solid oxide electrolysis through multiphysics modeling. Appl Energy 2022;312:118788. https://doi.org/10.1016/j.apenergy.2022.118788.

[117] Superchi F, Papi F, Mannelli A, Balduzzi F, Ferro FM, Bianchini A. Development of a reliable simulation framework for techno-economic analyses on green hydrogen production from wind farms using alkaline electrolyzers. Renew Energy 2023;207:731–42. https://doi.org/10.1016/j.renene.2023.03.077.

[118] Kotowicz J, Uchman W, Jurczyk M, Sekret R. Evaluation of the potential for distributed generation of green hydrogen using metal-hydride storage methods. Appl Energy 2023;344:121269. https://doi.org/10.1016/j.apenergy.2023.121269.

[119] Zakaria Z, Kamarudin SK. A review of alkaline solid polymer membrane in the application of AEM electrolyzer: materials and characterization. Int J Energy Res 2021;45:18337–54. https://doi.org/10.1002/er.6983.

[120] Hu S, Guo B, Ding S, Yang F, Dang J, Liu B, et al. A comprehensive review of alkaline water electrolysis mathematical modeling. Appl Energy 2022;327:120099. https://doi.org/10.1016/j.apenergy.2022.120099.

[121] Superchi F, Mati A, Carcasci C, Bianchini A. Techno-economic analysis of wind-powered green hydrogen production to facilitate the decarbonization of hard-to-abate sectors: a case study on steelmaking. Appl Energy 2023;342:121198. https://doi.org/10.1016/j.apenergy.2023.121198.

[122] Alberto L, Riascos LAM. Controlling operating temperature in PEM fuel cells. ABCM Symp Ser Mechatron 2010:4.

[123] Banasiak D, Kienberger T. A comparative analysis of the economic feasibility of reversible hydrogen systems based on time-resolved operation optimisation. Appl Energy 2024;371:123639. https://doi.org/10.1016/j.apenergy.2024.123639.

[124] Pastore LM, Groppi D, Feijoo F, Lo Basso G, Astiaso Garcia D, de Santoli L. Optimal decarbonisation pathways for the Italian energy system: modelling a long-term energy transition to achieve zero emission by 2050. Appl Energy 2024;367:123358. https://doi.org/10.1016/j.apenergy.2024.123358.

[125] del Pozo Gonzalez H, Bernadet L, Torrell M, Bianchi FD, Tarancón A, Gomis-Bellmunt O, et al. Power transition cycles of reversible solid oxide cells and its impacts on microgrids. Appl Energy 2023;352:121887. https://doi.org/10.1016/j.apenergy.2023.121887.

[126] Wang M, Pei P, Xu Y, Ren P, Wang H. Novel methods for fault diagnosis and enhancing CO tolerance in PEM fuel cells fueled with impure hydrogen. Appl Energy 2024;375:124021. https://doi.org/10.1016/j.apenergy.2024.124021.

[127] Bharti A, Natarajan R. Chapter 7 - Proton exchange membrane testing and diagnostics. In: Kaur G, editor. PEM Fuel Cells. Elsevier; 2022. p. 137–71. https://doi.org/10.1016/B978-0-12-823708-3.00007-9.

[128] Barbir F. Chapter one - introduction. In: Barbir F, editor. PEM Fuel Cells. 2nd ed. Boston: Academic Press; 2013. p. 1–16. https://doi.org/10.1016/B978-0-12-387710-9.00001-1.
[129] Linares R, Raël S, Berger K, Hinaje M, Lévêque J. PEM single fuel cell as a dedicated power source for high-inductive superconducting coils. Int J Hydrog Energy 2018;43:5913–21. https://doi.org/10.1016/j.ijhydene.2017.09.013.
[130] PRODUCT DATA SHEET FCS 13-XXL Gen 2.9 n.d. 2024.
[131] Stropnik R, Mlakar N, Lotrič A, Sekavčnik M, Mori M. The influence of degradation effects in proton exchange membrane fuel cells on life cycle assessment modelling and environmental impact indicators. Int J Hydrog Energy 2022;47:24223–41. https://doi.org/10.1016/j.ijhydene.2022.04.011.
[132] Chen H, Pei P, Song M. Lifetime prediction and the economic lifetime of proton exchange membrane fuel cells. Appl Energy 2015;142:154–63. https://doi.org/10.1016/j.apenergy.2014.12.062.
[133] Yu Y, Yu Q, Luo R, Chen S, Yang J, Yan F. Degradation and polarization curve prediction of proton exchange membrane fuel cells: An interpretable model perspective. Appl Energy 2024;365:123289. https://doi.org/10.1016/j.apenergy.2024.123289.
[134] Ozden E, Tari I. PEM fuel cell degradation effects on the performance of a stand-alone solar energy system. Int J Hydrog Energy 2017;42:13217–25. https://doi.org/10.1016/j.ijhydene.2017.04.017.
[135] Nelson DB, Nehrir MH, Wang C. Unit sizing and cost analysis of stand-alone hybrid wind/PV/fuel cell power generation systems. Renew Energy 2006;31:1641–56. https://doi.org/10.1016/j.renene.2005.08.031.
[136] Lu X, Du B, Zhou S, Zhu W, Li Y, Yang Y, et al. Optimization of power allocation for wind-hydrogen system multi-stack PEM water electrolyzer considering degradation conditions. Int J Hydrog Energy 2023;48:5850–72. https://doi.org/10.1016/j.ijhydene.2022.11.092.
[137] Bharath KVS, Blaabjerg F, Haque A, Khan MA. Model-based data driven approach for fault identification in proton exchange membrane fuel cell. Energies 2020;13:3144. https://doi.org/10.3390/en13123144.
[138] Dimian AC, Bildea CS, Kiss AA. Chapter 20 - Equipment Selection and Design. In: Dimian AC, Bildea CS, Kiss AA, editors. Comput. Aided Chem. Eng. 35. Elsevier; 2014. p. 757–88. https://doi.org/10.1016/B978-0-444-62700-1.00020-6.
[139] Baroutaji A, Carton J, Sajjia M, Olabi AG. Materials in PEM fuel cells. Ref Module Mater Sci Mater Eng 2015. https://doi.org/10.1016/B978-0-12-803581-8.04006-6.
[140] Burheim OS, Su H, Hauge HH, Pasupathi S, Pollet BG. Study of thermal conductivity of PEM fuel cell catalyst layers. Int J Hydrog Energy 2014;39:9397–408. https://doi.org/10.1016/j.ijhydene.2014.03.206.
[141] Atan R, WAN WM. Temperature profiles of an air-cooled Pem fuel cell stack under active and passive cooling operation. Procedia Eng 2012;41:1735–42. https://doi.org/10.1016/j.proeng.2012.07.376.
[142] Dicks A, Rand D. Fuel Cell Systems Explained 2018. https://doi.org/10.1002/9781118706992.
[143] Tashie-Lewis BC, Nnabuife SG. Hydrogen production, distribution, storage and power conversion in a hydrogen economy - a technology review. Chem Eng J Adv 2021;8:100172. https://doi.org/10.1016/j.ceja.2021.100172.
[144] Hydrogen Production & Distribution. IEA-ETSAP. 2014.
[145] Ho Nguyen D, Hoon Kim J, To Nguyen Vo T, Kim N, Seon Ahn H. Design of portable hydrogen tank using adsorption material as storage media: An alternative to type IV compressed tank. Appl Energy 2022;310:118552. https://doi.org/10.1016/j.apenergy.2022.118552.
[146] AlZohbi G, Almoaikel A, AlShuhail L. An overview on the technologies used to store hydrogen. Energy Rep 2023;9:28–34. https://doi.org/10.1016/j.egyr.2023.08.072.
[147] Niaz S, Manzoor T, Pandith AH. Hydrogen storage: materials, methods and perspectives. Renew Sust Energ Rev 2015;50:457–69. https://doi.org/10.1016/j.rser.2015.05.011.
[148] Lahnaoui A, Wulf C, Heinrichs H, Dalmazzone D. Optimizing hydrogen transportation system for mobility by minimizing the cost of transportation via compressed gas truck in North Rhine-Westphalia. Appl Energy 2018;223:317–28. https://doi.org/10.1016/j.apenergy.2018.03.099.
[149] Galassi MC, Acosta-Iborra B, Baraldi D, Bonato C, Harskamp F, Frischauf N, et al. Onboard compressed hydrogen storage: fast filling experiments and simulations. Energy Procedia 2012;29:192–200. https://doi.org/10.1016/j.egypro.2012.09.024.
[150] María Villarreal Vives A, Wang R, Roy S, Smallbone A. Techno-economic analysis of large-scale green hydrogen production and storage. Appl Energy 2023;346:121333. https://doi.org/10.1016/j.apenergy.2023.121333.
[151] Čović N, Pavić I, Pandžić H. Multi-energy balancing services provision from a hybrid power plant: PV, battery, and hydrogen technologies. Appl Energy 2024;374:123966. https://doi.org/10.1016/j.apenergy.2024.123966.
[152] Maestre VM, Ortiz A, Ortiz I. Sustainable and self-sufficient social home through a combined PV-hydrogen pilot. Appl Energy 2024;363:123061. https://doi.org/10.1016/j.apenergy.2024.123061.
[153] Pivetta D, Volpato G, Carraro G, Dall'Armi C, Da Lio L, Lazzaretto A, et al. Optimal decarbonization strategies for an industrial port area by using hydrogen as energy carrier. Int J Hydrog Energy 2024;52:1084–103. https://doi.org/10.1016/j.ijhydene.2023.07.008.
[154] Bell IH, Wronski J, Quoilin S, Lemort V. Pure and Pseudo-pure fluid Thermophysical property evaluation and the open-source Thermophysical property library CoolProp. Ind Eng Chem Res 2014;53:2498–508. https://doi.org/10.1021/ie4033999.
[155] Mannelli A, Papi F, Pechlivanoglou G, Ferrara G, Bianchini A. Discrete wavelet transform for the real-time smoothing of wind turbine power using Li-ion batteries. Energies 2021. https://doi.org/10.3390/en14082184.
[156] Fisher M, Apt J, Whitacre JF. Can flow batteries scale in the behind-the-meter commercial and industrial market? A techno-economic comparison of storage technologies in California. J Power Sources 2019;420:1–8. https://doi.org/10.1016/j.jpowsour.2019.02.051.
[157] Gonzalez-Castellanos AJ, Pozo D, Bischi A. Non-ideal linear operation model for Li-ion batteries. IEEE Trans Power Syst 2020;35:672–82. https://doi.org/10.1109/TPWRS.2019.2930450.
[158] Eras-Almeida AA, Egido-Aguilera MA. Hybrid renewable mini-grids on non-interconnected small islands: review of case studies. Renew Sust Energ Rev 2019;116:109417. https://doi.org/10.1016/j.rser.2019.109417.
[159] scipy.optimize.differential_evolution — SciPy v1.13.0 Manual n.d. https://docs.scipy.org/doc/scipy/reference/generated/scipy.optimize.differential_evolution.html; 2024 (accessed May 22, 2024).
[160] Virtanen P, Gommers R, Oliphant TE, Haberland M, Reddy T, Cournapeau D, et al. SciPy 1.0: fundamental algorithms for scientific computing in Python. Nat Methods 2020;17:261–72. https://doi.org/10.1038/s41592-019-0686-2.
[161] Omar MA. The significance of considering battery service-lifetime for correctly sizing hybrid PV–diesel energy systems. Energies 2024;17:103. https://doi.org/10.3390/en17010103.
[162] Marocco P, Ferrero D, Lanzini A, Santarelli M. The role of hydrogen in the optimal design of off-grid hybrid renewable energy systems. J Energy Storage 2022;46:103893. https://doi.org/10.1016/j.est.2021.103893.
[163] Yang G, Yang D, Liu B, Zhang H. The role of short- and long-duration energy storage in reducing the cost of firm photovoltaic generation. Appl Energy 2024;374:123914. https://doi.org/10.1016/j.apenergy.2024.123914.
[164] Gabrielli P, Poluzzi A, Kramer GJ, Spiers C, Mazzotti M, Gazzani M. Seasonal energy storage for zero-emissions multi-energy systems via underground hydrogen storage. Renew Sust Energ Rev 2020;121:109629. https://doi.org/10.1016/j.rser.2019.109629.
[165] Mauler L, Duffner F, Zeier WG, Leker J. Battery cost forecasting: a review of methods and results with an outlook to 2050. Energy Environ Sci 2021;14:4712–39. https://doi.org/10.1039/D1EE01530C.
[166] Penisa XN, Castro MT, Pascasio JDA, Esparcia EA, Schmidt O, Ocon JD. Projecting the Price of Lithium-ion NMC battery packs using a multifactor learning curve model. Energies 2020;13:5276. https://doi.org/10.3390/en13205276.
[167] Beuse M, Steffen B, Schmidt TS. Projecting the competition between energy-storage Technologies in the Electricity Sector. Joule 2020;4:2162–84. https://doi.org/10.1016/j.joule.2020.07.017.
[168] Utility-Scale Battery Storage. NREL; 2023. https://public.tableau.com/views/2023CAPEX/Inclusions?:embed=y&:toolbar=no&Technology=All,Utility-Scale%20Battery%20Storage&:embed=y&:showVizHome=n&:bootstrapWhenNotified=y&:apiID=handler2 (accessed January 19, 2024).
[169] Green hydrogen cost reduction. IRENA; 2020.
[170] Gallardo FI, Monforti Ferrario A, Lamagna M, Bocci E, Astiaso Garcia D, Baeza-Jeria TE. A techno-economic analysis of solar hydrogen production by electrolysis in the north of Chile and the case of exportation from Atacama Desert to Japan. Int J Hydrog Energy 2021;46:13709–28. https://doi.org/10.1016/j.ijhydene.2020.07.050.
[171] IEA. The Future of Hydrogen – Analysis. 2019.
[172] World energy outlook 2021 – Analysis. IEA; n.d.
[173] Net zero by 2050 – Analysis. IEA; n.d.
[174] Hydrogen: a renewable energy perspective. IRENA 2019:5. https://www.irena.org/-/media/Files/IRENA/Agency/Publication/2019/Sep/IRENA_Hydrogen_2019.pdf.
[175] 2022 Grid Energy Storage Technology Cost and Performance Assessment. 2022.
[176] Böhm H, Zauner A, Rosenfeld DC, Tichler R. Projecting cost development for future large-scale power-to-gas implementations by scaling effects. Appl Energy 2020;264:114780. https://doi.org/10.1016/j.apenergy.2020.114780.
[177] Grigoriev SA, Fateev VN, Bessarabov DG, Millet P. Current status, research trends, and challenges in water electrolysis science and technology. Int J Hydrog Energy 2020;45:26036–58. https://doi.org/10.1016/j.ijhydene.2020.03.109.
[178] Roos TH. The cost of production and storage of renewable hydrogen in South Africa and transport to Japan and EU up to 2050 under different scenarios. Int J Hydrog Energy 2021;46:35814–30. https://doi.org/10.1016/j.ijhydene.2021.08.193.
[179] van Leeuwen C, Mulder M. Power-to-gas in electricity markets dominated by renewables. Appl Energy 2018;232:258–72. https://doi.org/10.1016/j.apenergy.2018.09.217.
[180] Kharel S, Shabani B. Hydrogen as a long-term large-scale energy storage solution to support renewables. Energies 2018;11:2825. https://doi.org/10.3390/en11102825.
[181] Ulleberg Ø, Hancke R. Techno-economic calculations of small-scale hydrogen supply systems for zero emission transport in Norway. Int J Hydrog Energy 2020;45:1201–11. https://doi.org/10.1016/j.ijhydene.2019.05.170.
[182] Parks G, Boyd R, Cornish J, Remick R. Hydrogen Station Compression, Storage, and Dispensing Technical Status and Costs: Systems Integration. Golden, CO (United States): National Renewable Energy Lab. (NREL); 2014. https://doi.org/10.2172/1130621.
[183] Ikäheimo J, Kiviluoma J, Weiss R, Holttinen H. Power-to-ammonia in future north European 100% renewable power and heat system. Int J Hydrog Energy 2018;43:17295–308. https://doi.org/10.1016/j.ijhydene.2018.06.121.

[184] Schoenung SM. Economic analysis of large-scale hydrogen storage for renewable utility applications. Albuquerque, NM, and Livermore, CA (United States): Sandia National Laboratories (SNL); 2011. https://doi.org/10.2172/1029796.
[185] Shin HK, Ha SK. A review on the cost analysis of hydrogen gas storage tanks for fuel cell vehicles. Energies 2023;16:5233. https://doi.org/10.3390/en16135233.
[186] Villalonga S, Laguionie T, Toulc'Hoat J, Desprez B, Baudry G, Ramage M, et al. On board 70 MPA hydrogen composite pressure vessel safety factor. 2021.
[187] Richardson IA, Fisher JT, Frome PE, Smith BO, Guo S, Chanda S, et al. Low-cost, transportable hydrogen fueling station for early market adoption of fuel cell electric vehicles. Int J Hydrog Energy 2015;40:8122–7. https://doi.org/10.1016/j.ijhydene.2015.04.066.
[188] Future of photovoltaic. IRENA; 2019.
[189] Attracting private investment to fund sustainable recoveries: The case of Indonesia's power sector – Analysis. IEA; n.d.
[190] Solar PV installation cost worldwide. Statista n.d; 2022. https://www.statista.com/statistics/809796/global-solar-power-installation-cost-per-kilowatt/. [Accessed 17 January 2024].
[191] Sens L, Neuling U, Kaltschmitt M. Capital expenditure and levelized cost of electricity of photovoltaic plants and wind turbines – development by 2050. Renew Energy 2022;185:525–37. https://doi.org/10.1016/j.renene.2021.12.042.
[192] Renewable power generation costs in 2022. IRENA; 2023.